Climate4you update August 2021

Summary of observations until August 2021:

1: Observed average global air temperature change last 30 years is about +0.17°C per decade.
If unchanged, additional average global air temperature increase by year 2100 will be about +1.3°C.

2: Tide gauges along coasts indicate a typical global sea level increase of about 1-2 mm/yr.
Coastal sea level change rate last 100 year has essential been stable, without recent acceleration.
If unchanged, global sea level at coasts will typically increase 8-16 cm by year 2100, although many locations in regions affected by glaciation 20,000 years ago, will experience a relative sea level drop.

3: *S*ince 2004 the global oceans above 1900 m depth on average have warmed about 0.07°C.
The maximum warming (about 0.2°C, 0-100 m depth) mainly affects oceans near Equator, where the incoming solar radiation is at maximum.

4: Changes in atmospheric CO_2 follow changes in global air temperature.
Changes in global air temperature follow changes in ocean surface temperature.

5: There is no perceptible effect on atmospheric CO_2 due to the COVID-related drop in GHG emissions. Natural sinks and sources for atmospheric CO_2 far outweigh human contributions.

Contents:

August 2021 global surface air temperature overview

General: This newsletter contains graphs and diagrams showing a selection of key meteorological variables, if possible updated to the most recent past month. All temperatures are given in degrees Celsius.

In the maps on pages 4-5, showing the geographical pattern of surface air temperature anomalies, the last previous 10 years are used as reference period.

The rationale for comparing with this recent period instead of various 'normal' periods defined for parts of the past century, is that such reference periods often will be affected by past cold periods, like, e.g., 1945-1980. Most modern comparisons with such reference periods will inevitably appear as warm, and it will be difficult to decide if modern temperatures are increasing or decreasing. Comparing instead with the last previous 10 years overcomes this problem and clearer displays the modern dynamics of ongoing change. This decadal approach also corresponds well to the typical memory horizon for many people and is now also adopted as reference period by other institutions, e.g., the Danish Meteorological Institute (DMI).

In addition, most temperature databases display temporal instability for past data (see, e.g., p. 9). Any comparison with such reference periods will therefore be influenced by ongoing monthly changes of mainly administrative nature. A fluctuating value is clearly not suited as reference value. Simply comparing with the last previous 10 years is more useful as reference for modern changes. Please see also additional reflections on page 47-48.

The different air temperature records have been divided into three quality classes, QC1, QC2 and QC3, respectively, as described on page 9.

In many diagrams shown in the present newsletter the thin line represents the monthly global average value, and the thick line indicate a simple running average, in most cases a simple moving 37-month average, nearly corresponding to a three-year average. The 37-month average is calculated from values covering a range from 18 months before to 18 months after, with equal weight given to all individual months.

The year 1979 has been chosen as starting point in many diagrams, as this roughly corresponds to both the beginning of satellite observations and the onset of the late 20th century warming period. However, several of the data series have a much longer record length, which may be inspected in greater detail on www.climate4you.com.

August 2021 surface air temperature

General: For August 2021, the GISS portal supplied 16200 AIRS interpolated surface air data points, based on satellite observations, and visualised here on pages 4-5. According to most global surface temperature databases, the August 2021 global average air temperature anomaly was a little lower than in the previous month (July). According to AIRS August 2021 was somewhat cooler than August 2020.

The Northern Hemisphere surface temperature anomality pattern for the last 10 years (p.4) was characterised by marked regional contrasts, primarily controlled by the dominant jet stream configuration. Eastern Siberia, most of North America and Europe were relatively cold. In contrast, in between these regions relatively warm regions existed in most of Greenland and most of Russia. Ocean wise, the North Atlantic south of 20°N was below average conditions, while regions between 20°N and 60°N were relatively warm. The North Pacific was generally below average surface conditions, although a relatively warm region existed south of Alaska. In the Arctic, relatively cold conditions characterised the East Siberia-Canada-Alaska and the Atlantic sectors, while the remaining regions (including Greenland) were relatively warm.

Near the Equator temperatures were mostly below (especially in the Pacific Ocean) the 10-year average.

The Southern Hemisphere temperatures were largely below or near the average for the previous 10 years. Much of South America and Australia were, however, a little above average. Ocean wise, surface temperatures conditions were near average or below. Parts of the South Atlantic were very cold. Most of the Antarctic was relatively cold, although a large part of East Antarctica was relatively warm.

August 2021 global surface air temperature overview versus average August last 10 years

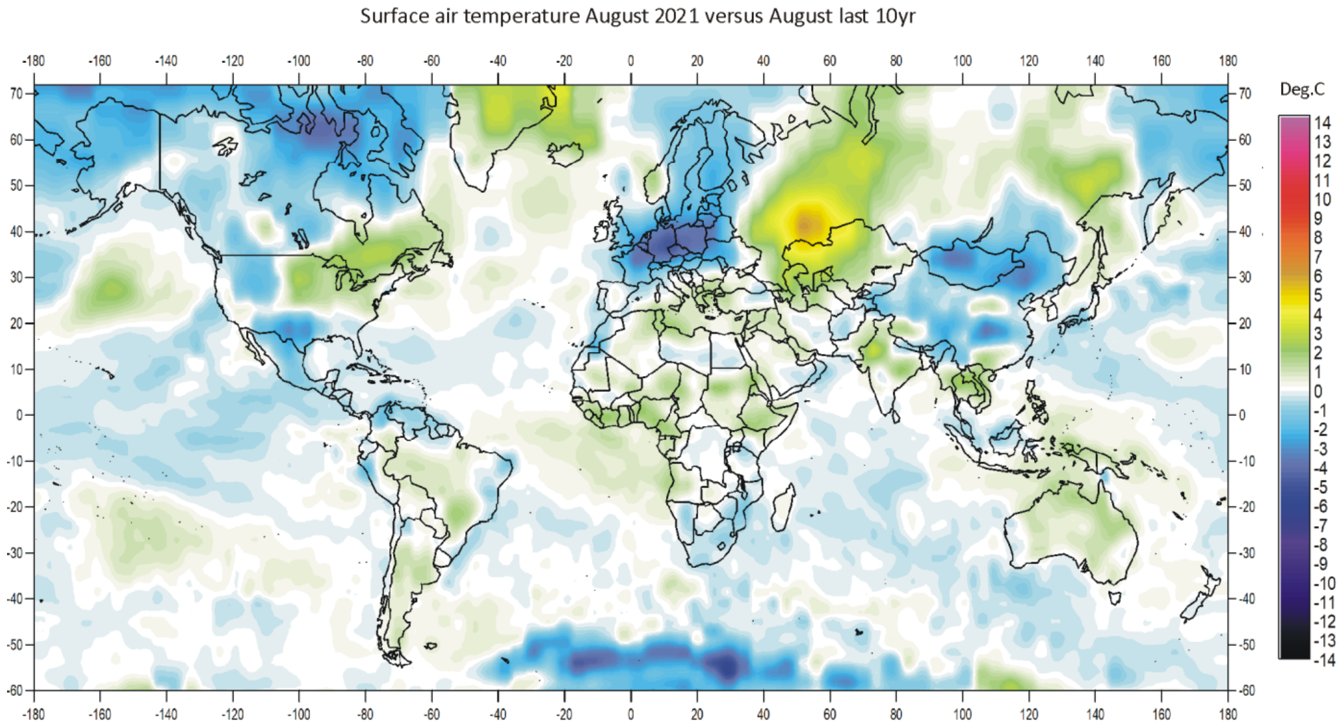

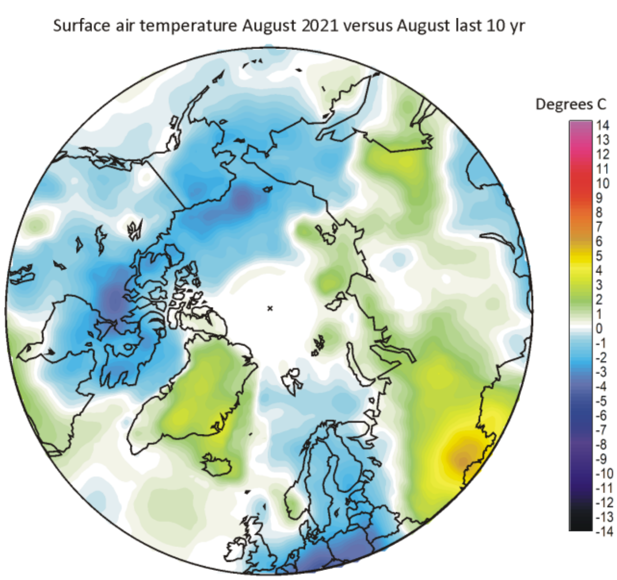

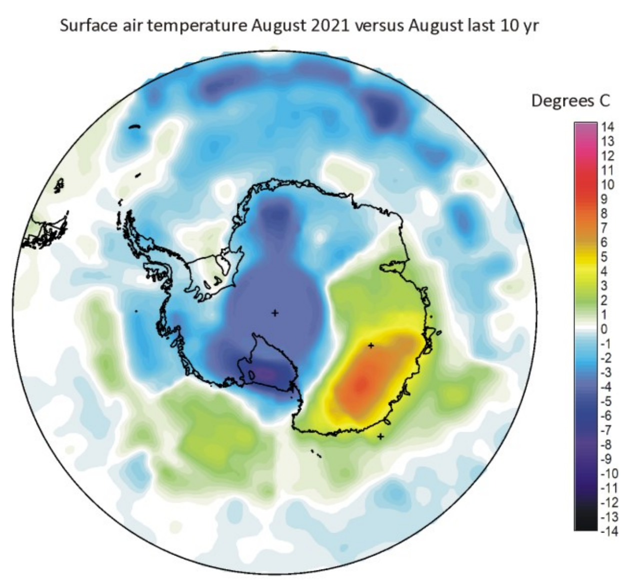

August 2021 surface air temperature compared to the average of August over the last 10 years. Green-yellow-red colours indicate areas with higher temperature than the 10-year average, while blue colours indicate lower than average temperatures. Data source: Remote Sensed Surface Temperature Anomaly, AIRS/Aqua L3 Monthly Standard Physical Retrieval 1-degree x 1-degree V007 (https://airs.jpl.nasa.gov/), obtained from the GISS data portal (https://data.giss.nasa.gov/gistemp/maps/index_v4.html).

August 2021 global surface air temperature compared to August 2020

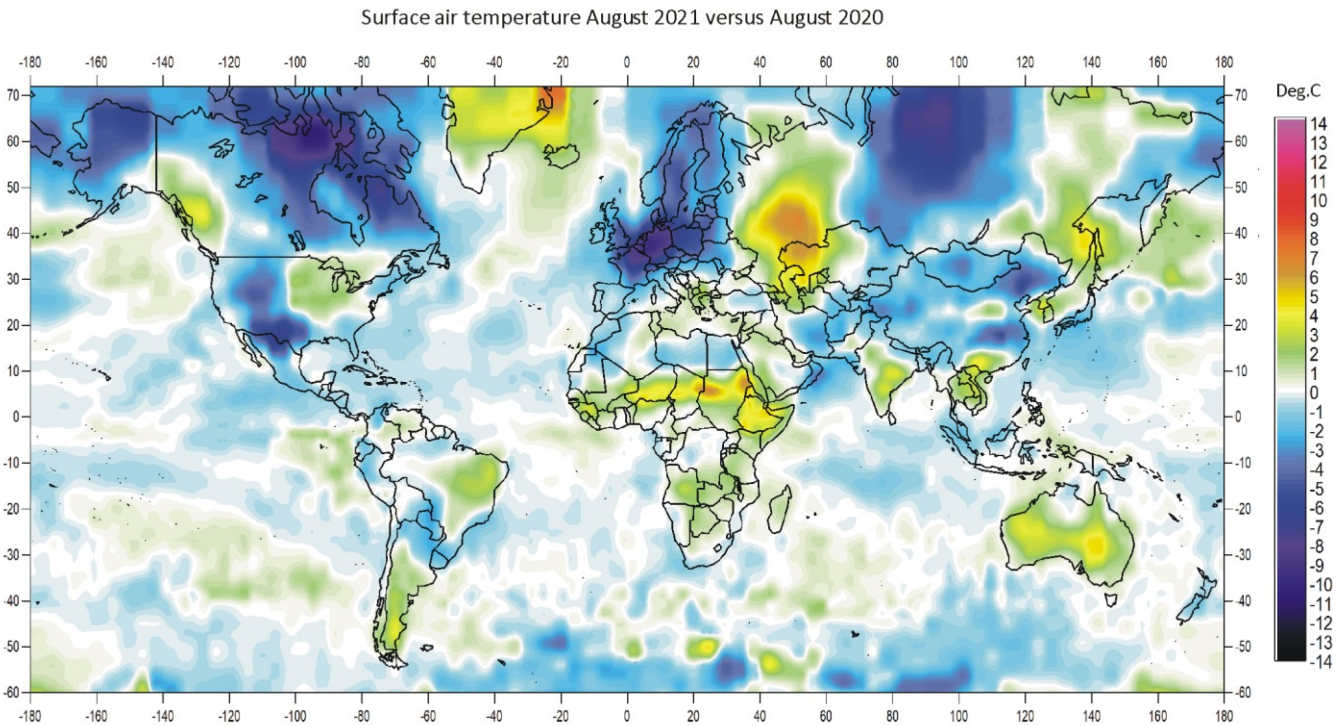

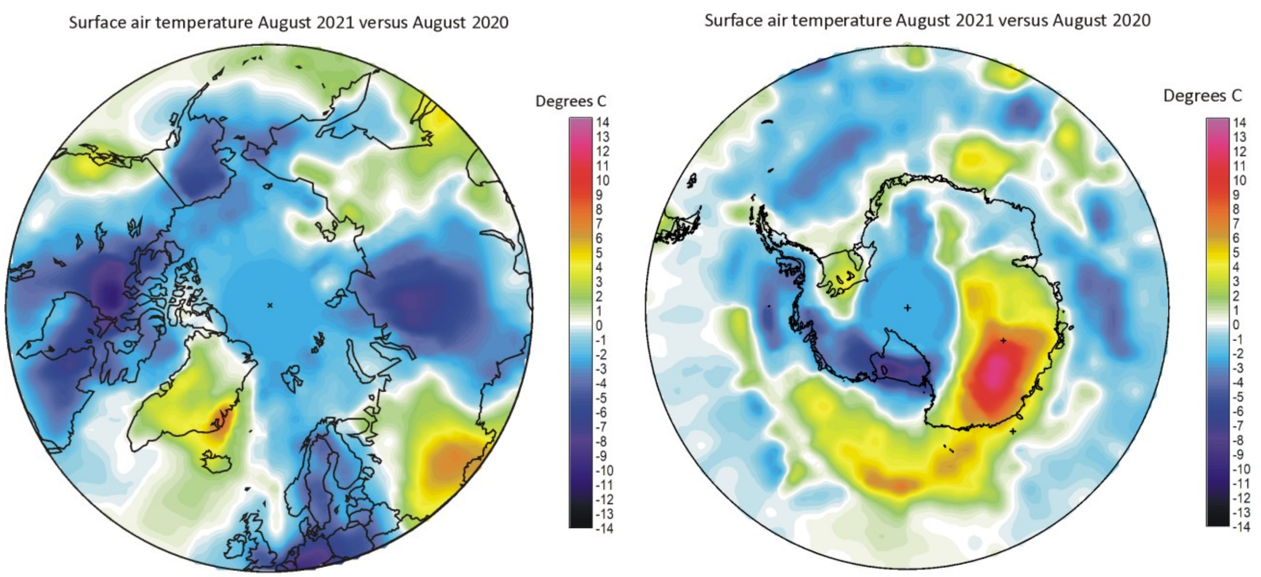

August 2021 surface air temperature compared to August 2020. Green-yellow-red colours indicate regions where the present month was warmer than last year, while blue colours indicate regions where the present month was cooler than last year. Variations in monthly temperature from one year to the next has no tangible climatic importance but may nevertheless be interesting to study. Data source: Remote Sensed Surface Temperature Anomaly, AIRS/Aqua L3 Monthly Standard Physical Retrieval 1-degree x 1-degree V007 (https://airs.jpl.nasa.gov/), obtained from the GISS data portal (https://data.giss.nasa.gov/gistemp/maps/index_v4.html).

Temperature quality class 1: Lower troposphere temperature from satellites, updated to August 2021 *(see page 9 for definition of classes)*

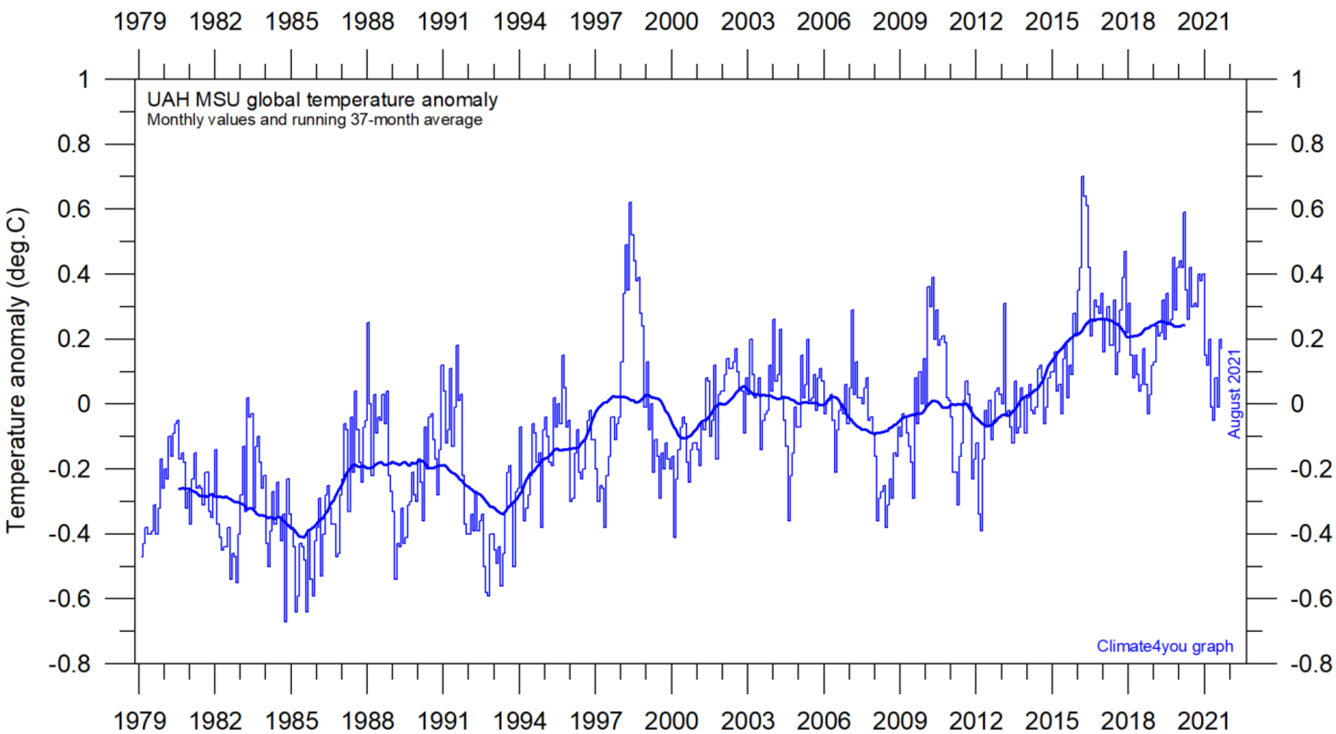

Global monthly average lower troposphere temperature (thin line) since 1979 according to University of Alabama at Huntsville, USA. The thick line is the simple running 37-month average. Reference period 1991-2020.

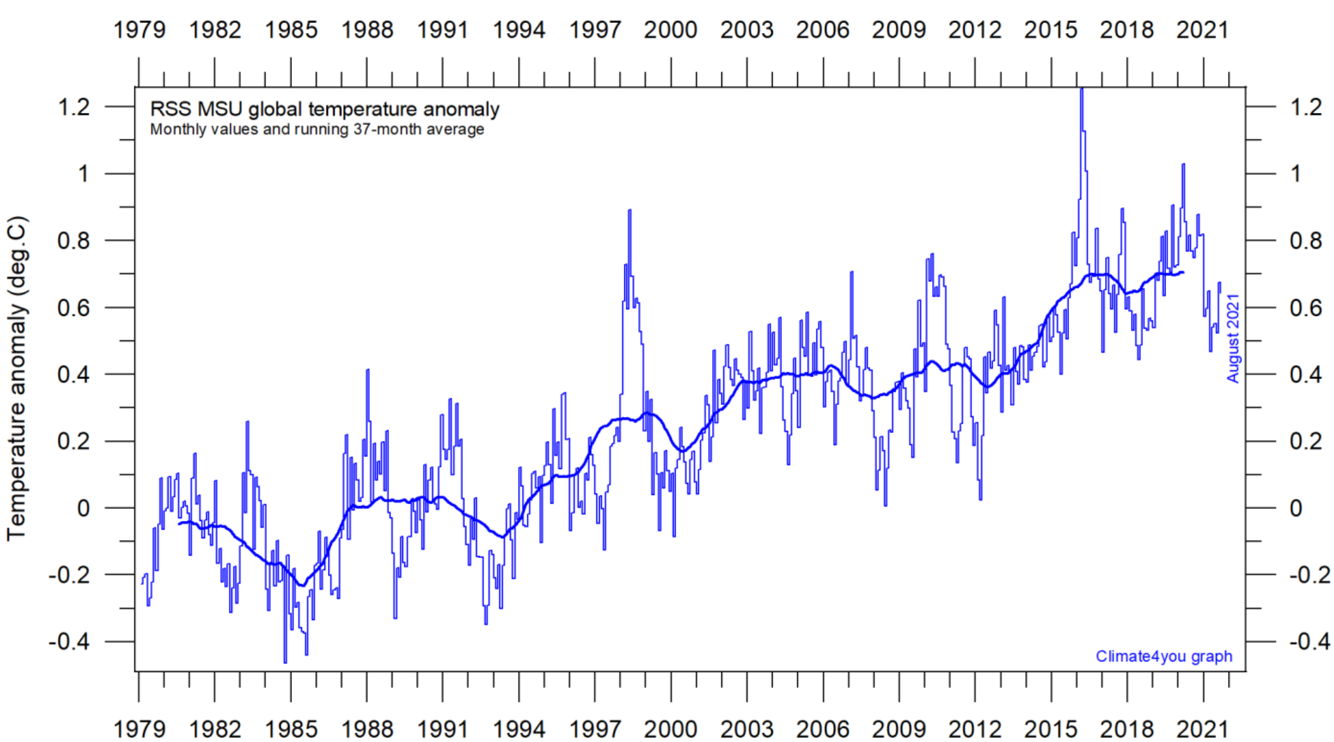

Global monthly average lower troposphere temperature (thin line) since 1979 according to according to Remote Sensing Systems (RSS), USA. The thick line is the simple running 37-month average.

Temperature quality class 2: HadCRUT global surface air temperature, updated to June 2021

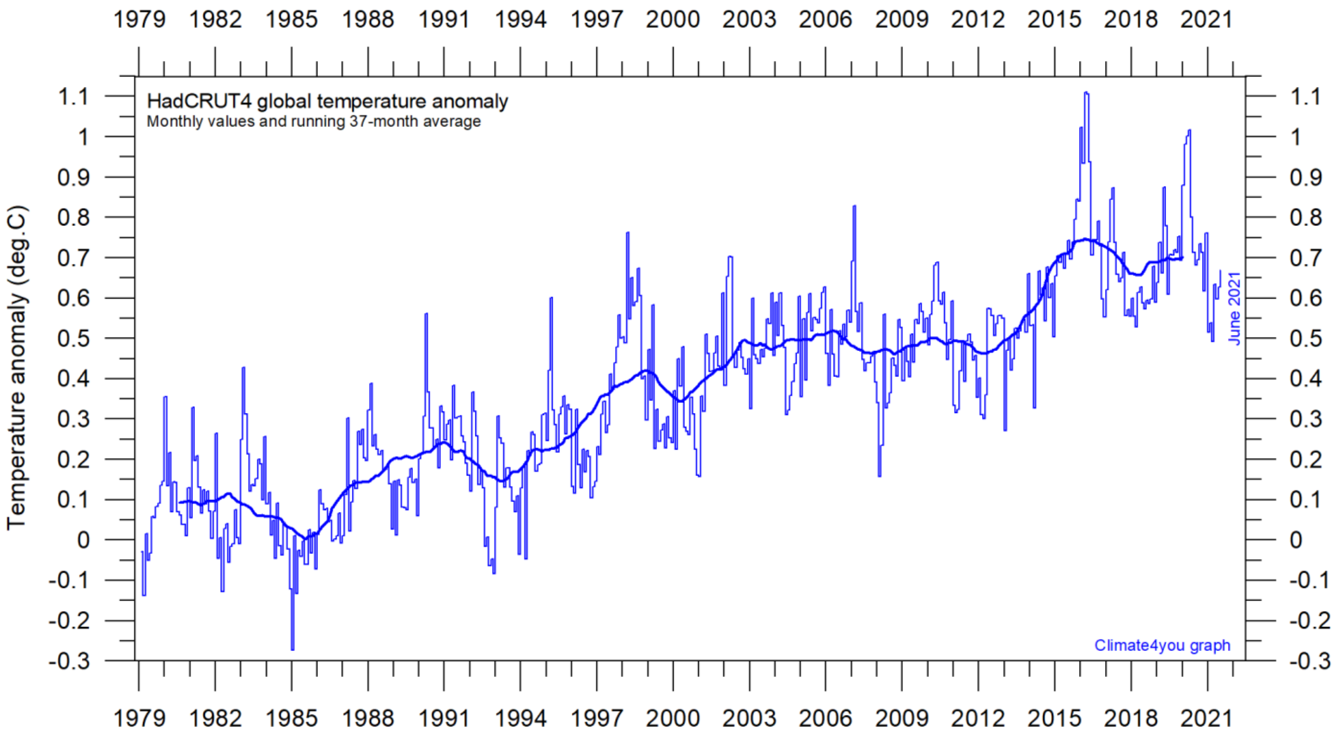

Global monthly average surface air temperature (thin line) since 1979 according to according to the Hadley Centre for Climate Prediction and Research and the University of East Anglia's Climatic Research Unit (CRU), UK. The thick line is the simple running 37-month average. Please note that HadCRUT4 is not yet updated beyond January 2021.

Temperature quality class 3: GISS and NCDC global surface air temperature, updated to August 2021

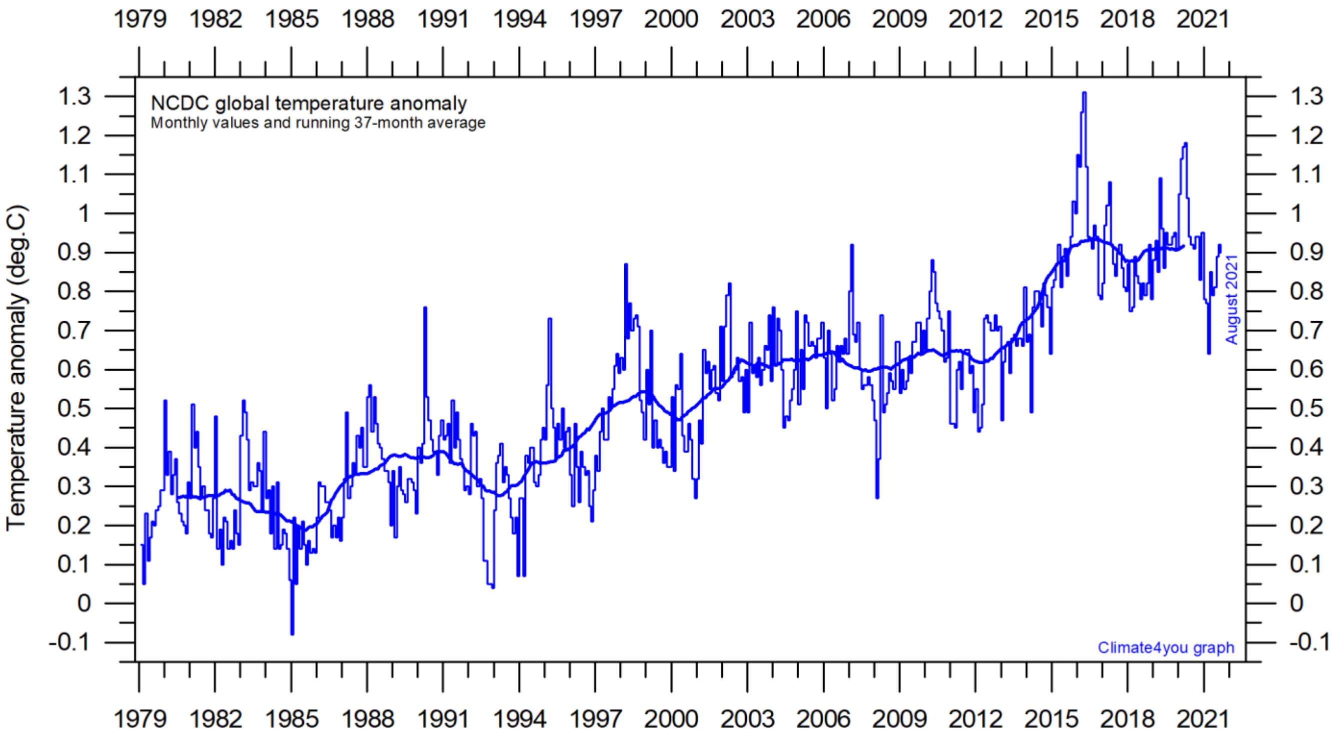

Global monthly average surface air temperature since 1979 according to according to the National Climatic Data Center (NCDC), USA. The thick line is the simple running 37-month average.

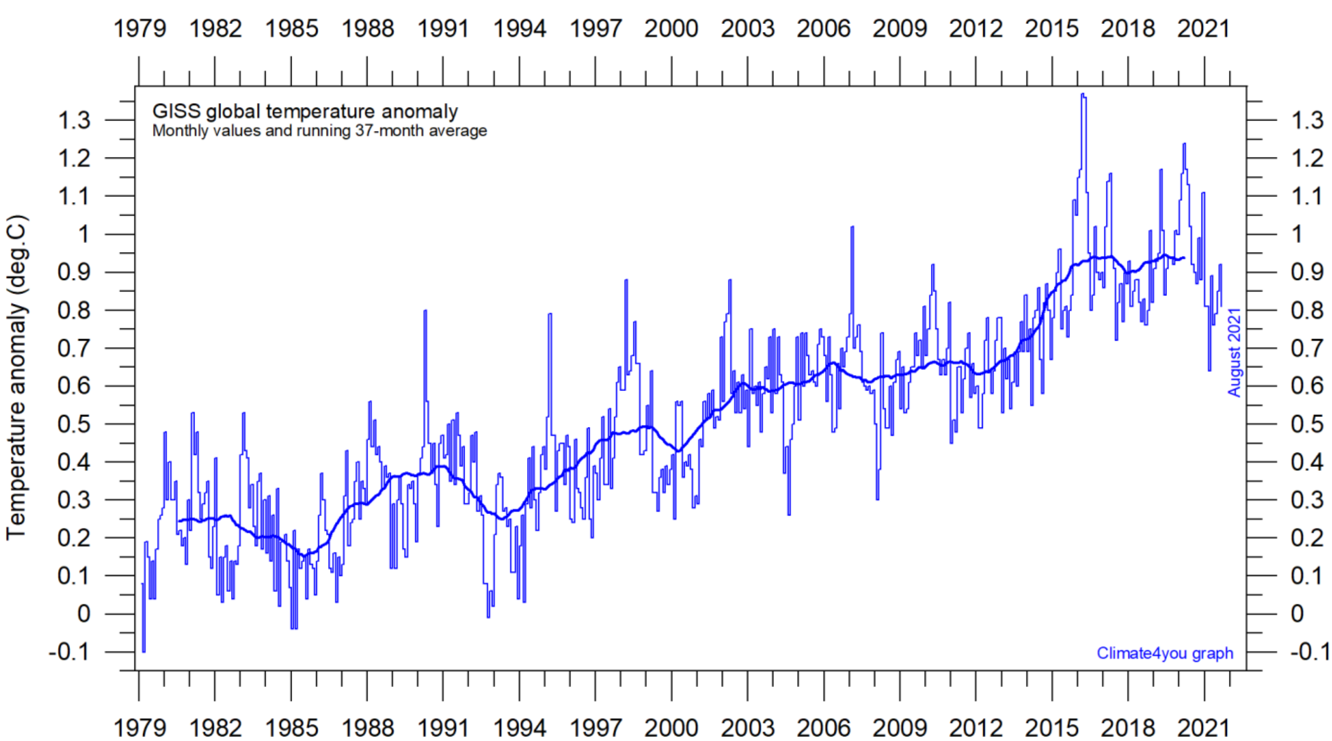

Global monthly average surface air temperature (thin line) since 1979 according to according to the Goddard Institute for Space Studies (GISS), at Columbia University, New York City, USA, using ERSST_v4 ocean surface temperatures. The thick line is the simple running 37-month average.

A note on data record stability and -quality:

The temperature diagrams shown above all have 1979 as starting year. This roughly marks the beginning of the recent episode of global warming, after termination of the previous episode of global cooling from about 1940. In addition, the year 1979 also represents the starting date for the satellite-based global temperature estimates (UAH and RSS). For the three surface air temperature records (HadCRUT, NCDC and GISS), they begin much earlier (in 1850 and 1880, respectively), as can be inspected on www.climate4you.com.

For all three surface air temperature records, but especially NCDC and GISS, administrative changes to anomaly values are quite often introduced, even affecting observations many years back in time. Some changes from the recent past may be due to the delayed addition of new station data or change of station location, while others probably have their origin in changes of the technique implemented to calculate average values from the raw data. It is clearly impossible to evaluate the validity of such administrative changes for the outside user of these records; it is only possible to note that such changes quite often are introduced (se example diagram next page).

In addition, the three surface records represent a blend of sea surface data collected by moving ships or by other means, plus data from land stations of partly unknown quality and unknown degree of representativeness for their region. Many of the land stations also has been moved geographically during their period of operation, instrumentation have been changed, and they are influenced by changes in their near surroundings (vegetation, buildings, etc.).

The satellite temperature records also have their problems, but these are generally of a more technical nature and probably therefore better correctable. In addition, the temperature sampling by satellites is more regular and complete on a global basis than that represented by the surface records. It is also important that the sensors on satellites measure temperature directly by emitted radiation, while most modern surface temperature measurements are indirect, using electronic resistance.

Everybody interested in climate science should gratefully acknowledge the big efforts put into maintaining the different temperature databases referred to in the present newsletter. At the same time, however, it is also important to realise that all temperature records cannot be of equal scientific quality. The simple fact that they to some degree differ shows that they cannot all be correct.

On this background, and for practical reasons, Climate4you therefore operates with three quality classes (1-3) for global temperature records, with 1 representing the highest quality level:

Quality class 1: The satellite records (UAH and RSS).

Quality class 2: The HadCRUT surface record.

Quality class 3: The NCDC and GISS surface records.

The main reason for discriminating between the three surface records is the following:

While both NCDC and GISS often experience quite large administrative changes (see example on p.10), and therefore essentially must be considered as unstable records, the changes introduced to HadCRUT are fewer and smaller. For obvious reasons, as the past does not change, any record undergoing continuing changes cannot describe the past correctly all the time. Frequent and large corrections in a database inevitably signal a fundamental uncertainty about what is likely to represent the correct values.

You can find more on the issue of lack of temporal stability on www.climate4you.com (go to: *Global Temperature*, and then proceed to *Temporal Stability*).

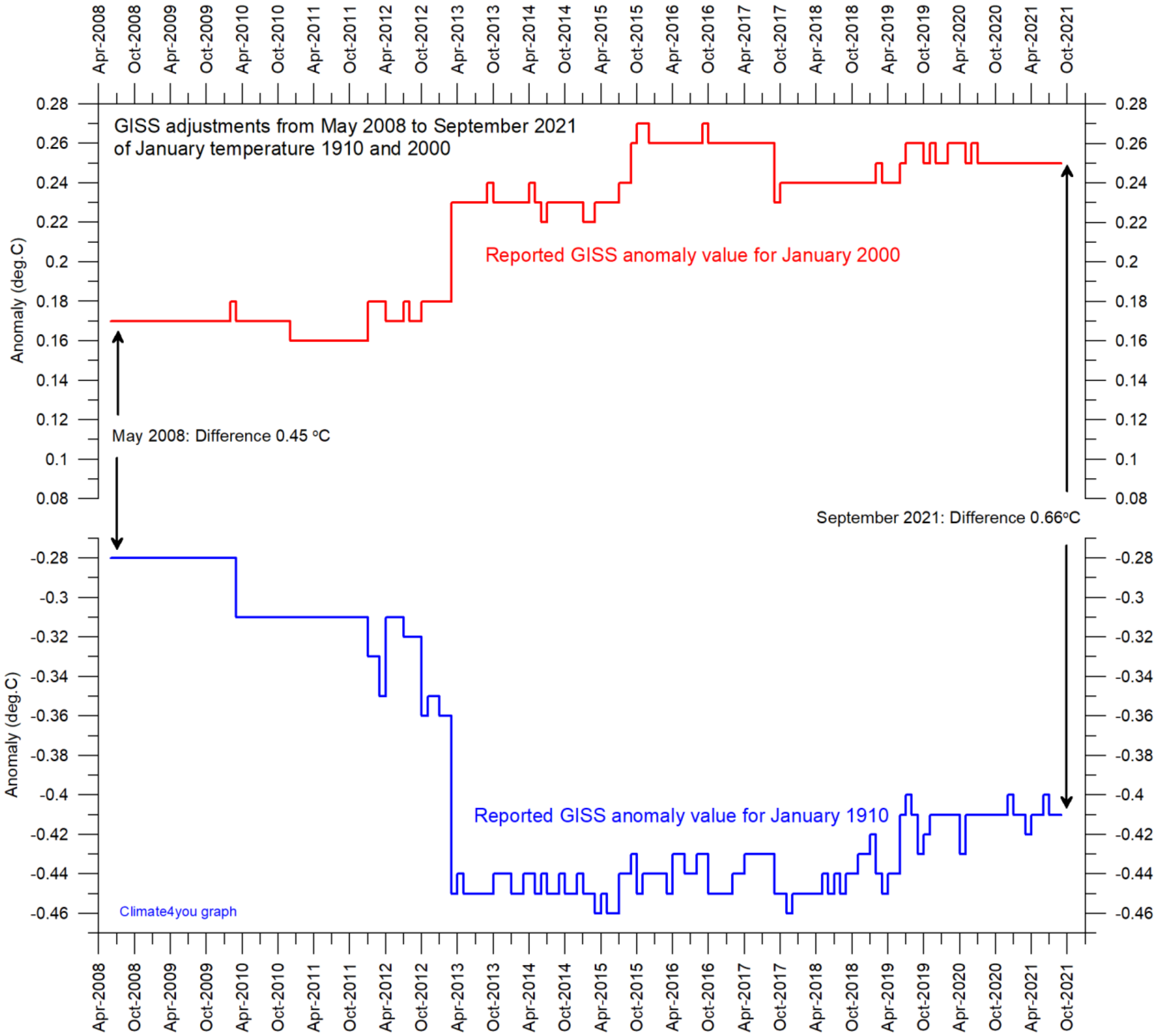

Diagram showing the monthly adjustments made since May 2008 by the [Goddard Institute for Space Studies](#) (GISS), USA, as recorded by published anomaly values for the two months January 1910 and January 2000.

The administrative upsurge of the temperature increase from January 1915 to January 2000 has grown from 0.45 (reported May 2008) to 0.66°C (reported September 2021). This represents an about 47% administrative temperature increase over this period, meaning that nearly half of the apparent global temperature increases from January 1910 to January 2000 (as reported by GISS) is due to administrative changes of the original data since May 2008.

Comparing global surface air temperature and lower troposphere satellite temperatures; updated to June 2021

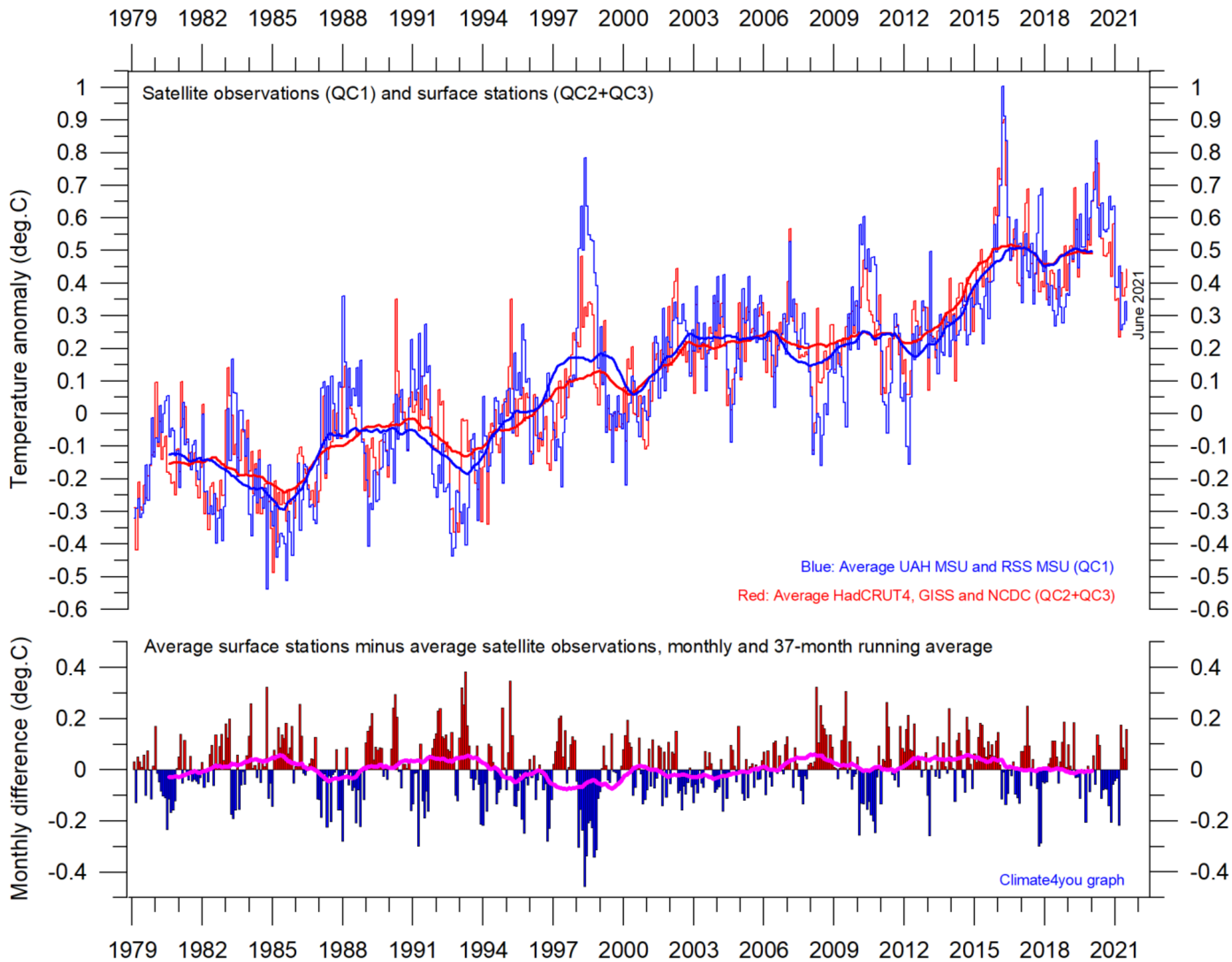

Plot showing the average of monthly global surface air temperature estimates (HadCRUT4, GISS and NCDC) and satellite-based temperature estimates (RSS MSU and UAH MSU). The thin lines indicate the monthly value, while the thick lines represent the simple running 37-month average, nearly corresponding to a running 3-yr average. The lower panel shows the monthly difference between average surface air temperature and satellite temperatures. As the base period differs for the different temperature estimates, they have all been normalised by comparing to the average value of 30 years from January 1979 to December 2008.

Global air temperature linear trends updated to June 2021

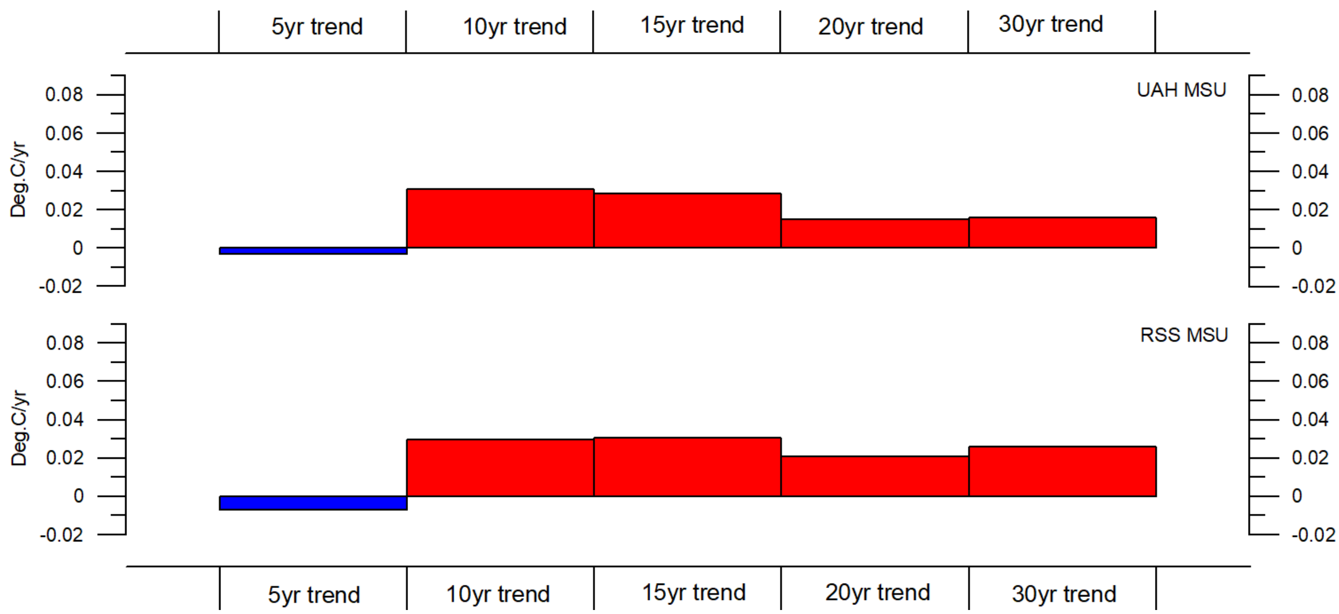

Diagram showing the latest 5, 10, 20 and 30-yr linear annual global temperature trend, calculated as the slope of the linear regression line through the data points, for two satellite-based temperature estimates (UAH MSU and RSS MSU).

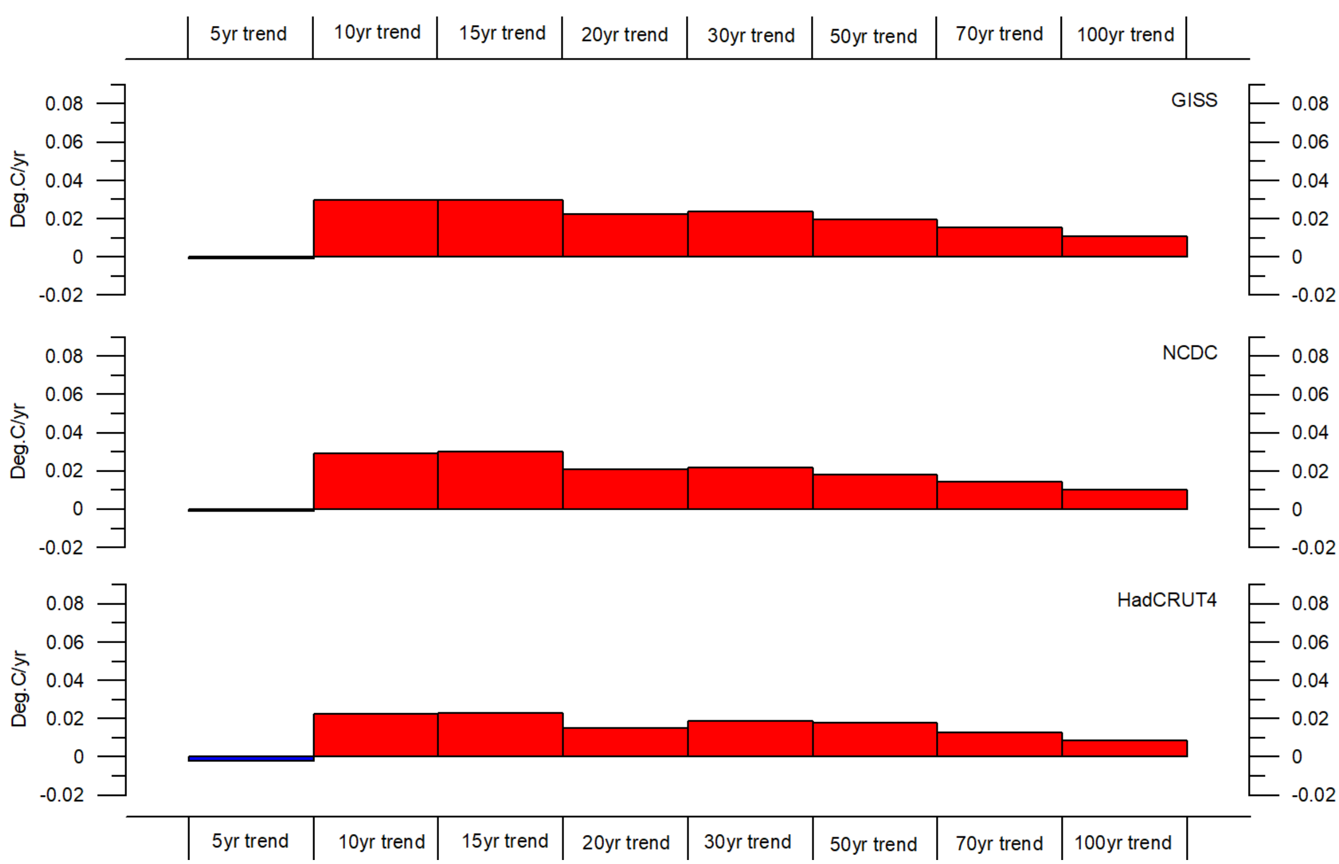

Diagram showing the latest 5, 10, 20, 30, 50, 70 and 100-year linear annual global temperature trend, calculated as the slope of the linear regression line through the data points, for three surface-based temperature estimates (GISS, NCDC and HadCRUT4).

All in one, Quality Class 1, 2 and 3; updated to June 2021

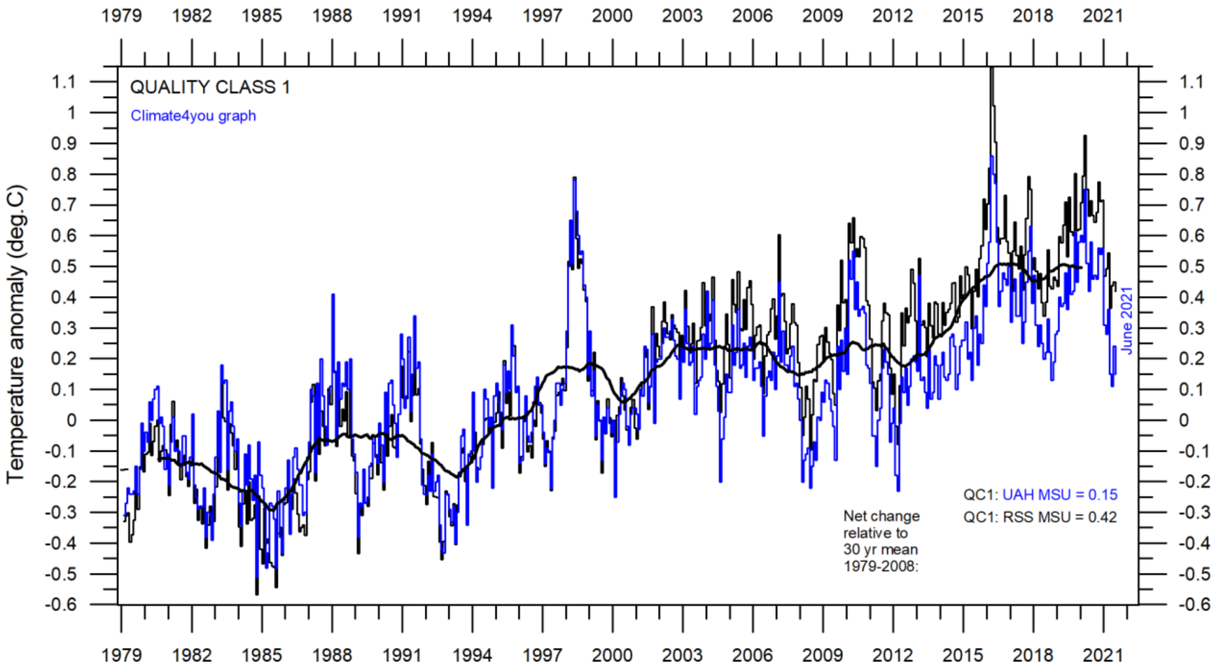

Superimposed plot of Quality Class 1 (UAH and RSS) global monthly temperature estimates. As the base period differs for the individual temperature estimates, they have all been normalised by comparing with the average value of the initial 120 months (30 years) from January 1979 to December 2008. The heavy black line represents the simple running 37 month (c. 3 year) mean of the average of both temperature records. The numbers shown in the lower right corner represent the temperature anomaly relative to the individual 1979-2008 averages.

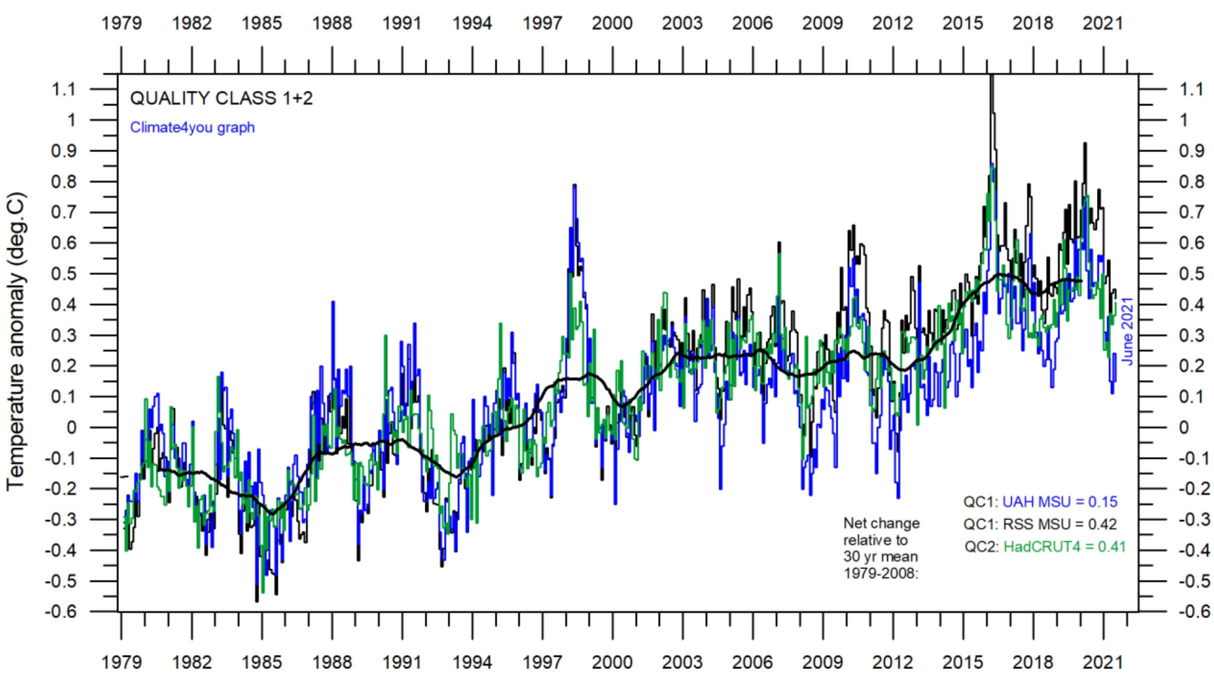

Superimposed plot of Quality Class 1 and 2 (UAH, RSS and HadCRUT4) global monthly temperature estimates. As the base period differs for the individual temperature estimates, they have all been normalised by comparing with the average value of the initial 120 months (30 years) from January 1979 to December 2008. The heavy black line represents the simple running 37 month (c. 3 year) mean of the average of all three temperature records. The numbers shown in the lower right corner represent the temperature anomaly relative to the individual 1979-2008 averages.

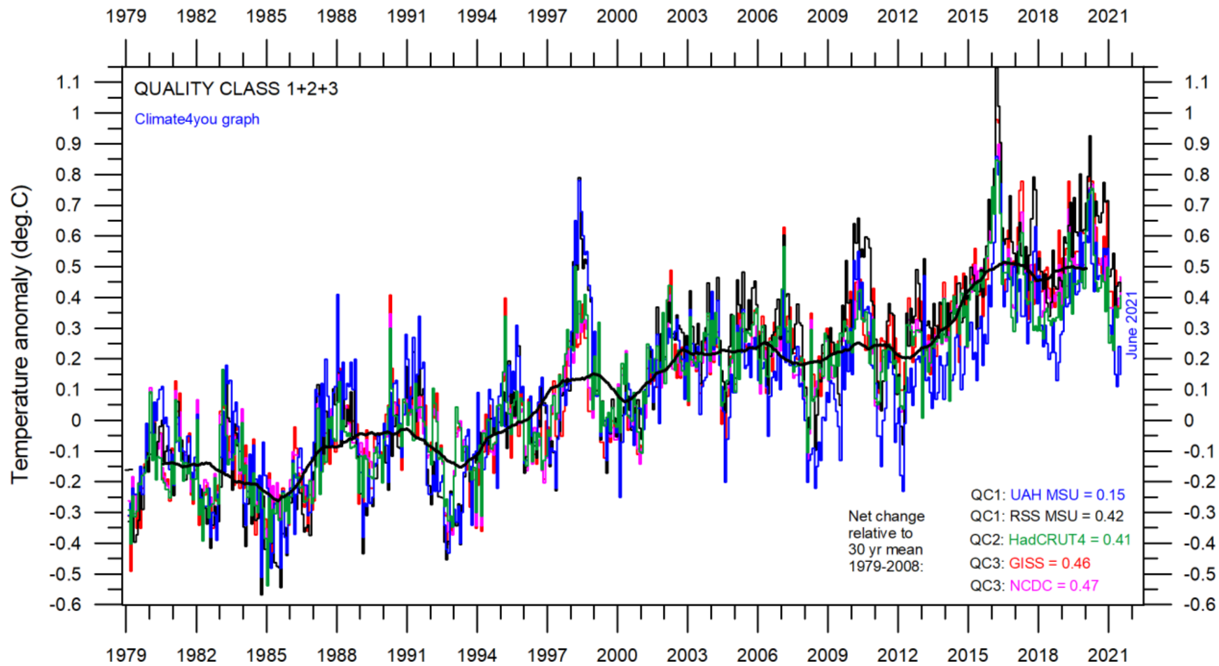

Superimposed plot of Quality Class 1, 2 and 3 global monthly temperature estimates (UAH, RSS, HadCRUT4, GISS and NCDC). As the base period differs for the individual temperature estimates, they have all been normalised by comparing with the average value of the initial 120 months (30 years) from January 1979 to December 2008. The heavy black line represents the simple running 37 month (c. 3 year) mean of the average of all five temperature records. The numbers shown in the lower right corner represent the temperature anomaly relative to the individual 1979-2008 averages.

Please see reflections on page 9 relating to the above three quality classes.

Satellite- and surface-based temperature estimates are derived from different types of measurements and comparing them directly as in the above diagrams therefore may be somewhat ambiguous.

However, as both types of estimates often are discussed together in various news media, the above composite diagrams may nevertheless be of some interest.

In fact, the different types of temperature estimates appear to agree as to the overall temperature variations on a 2-3-year scale, although on a shorter time scale there are often considerable differences between the individual records. However, since about 2003 the surface records used to be drifting towards higher temperatures than the combined satellite record, but this overall tendency was much removed by the major adjustment of the RSS satellite series in 2015 (see lower diagram on page 6).

The combined records (diagram above) suggest a modest global air temperature increase over the last 30 years, about 0.15°C per decade. It should be noted that the apparent temperature increases since about 2003 at least partly is the result of ongoing administrative adjustments (page 9-10). At the same time, the temperature records considered here do not indicate any general temperature decrease during the last 20 years.

The present temperature development does not exclude the possibility that global temperatures may begin to increase significantly later. On the other hand, it also remains a possibility that Earth just now is passing an overall temperature peak, and that global temperatures may begin to decrease during the coming years.

As always, time will show which of these possibilities is correct.

Global sea surface temperature, updated to August 2021

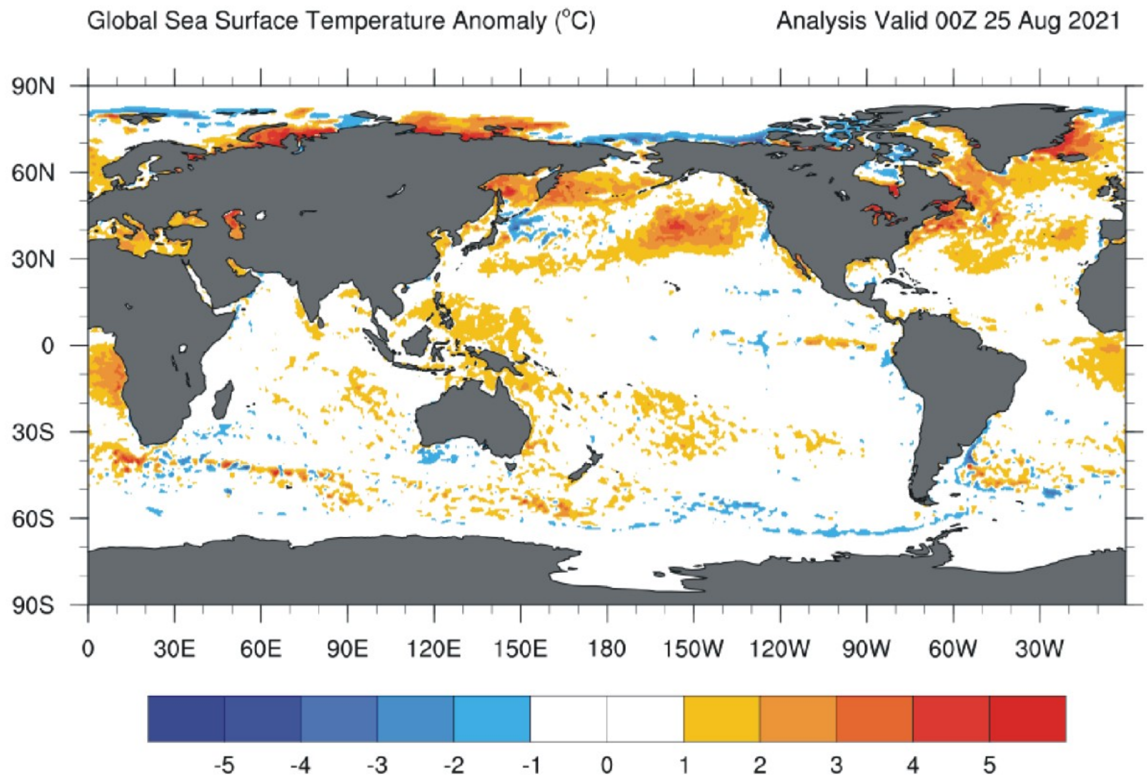

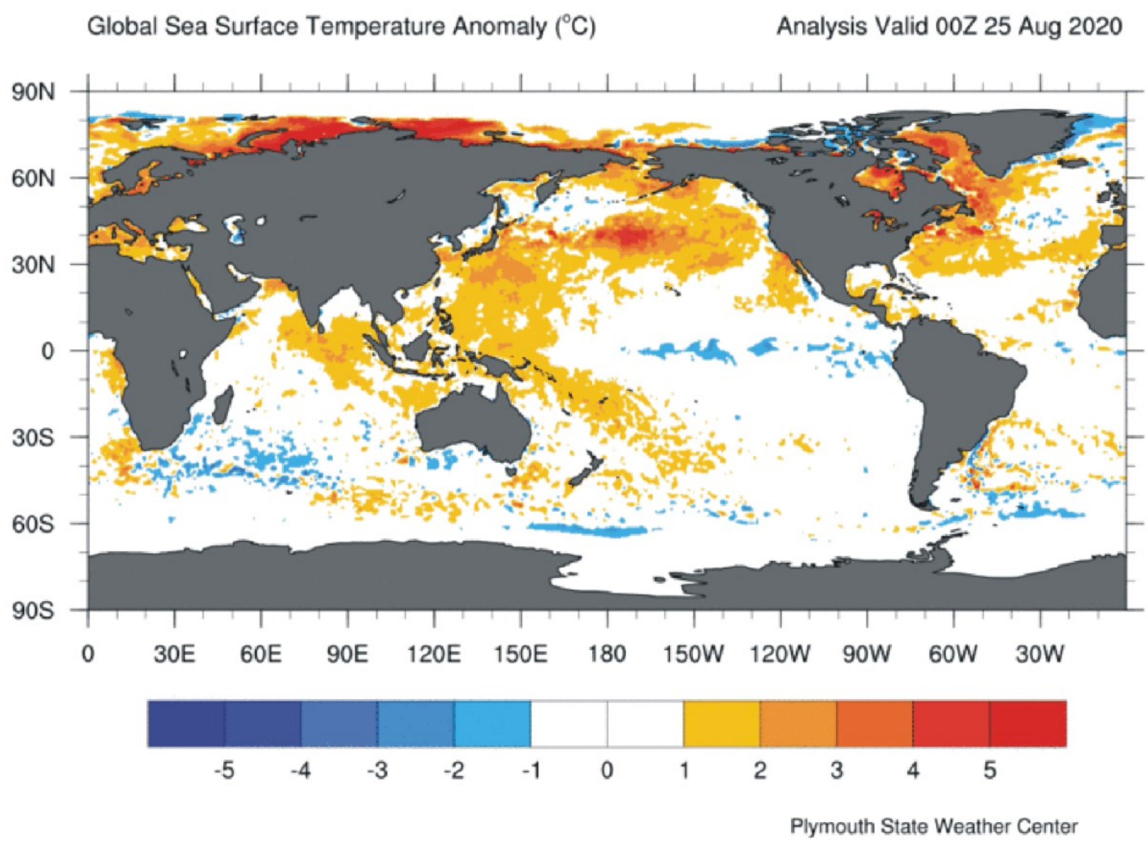

Sea surface temperature anomaly on 25 August 2021 (upper map) and 2020 (lower map). Map source: Plymouth State Weather Center. Reference period: 1977-1991.

Because of the large surface areas near Equator, the temperature of the surface water in these regions is especially important for the global atmospheric temperature (p. 6-8). In fact, no less than 50% of planet Earth's surface area is located within 30°N and 30°S.

A mixture of relatively warm and cold water dominates much of the ocean surface, but with notable differences from month to month. All such ocean surface temperature changes will be influencing global air temperatures in the months to come. Now a cold new La Niña episode is ending in the Pacific Ocean (see p. 24). Relatively warm surface water is found a band in the northern hemisphere, between 30°N and 60°N.

The significance of any short-term cooling or warming reflected in air temperatures should not be overstated. Whenever Earth experiences cold La Niña or warm El Niño episodes major heat exchanges take place between the Pacific Ocean and the atmosphere above, sooner or later showing up in estimates of the global air temperature.

However, this does not necessarily reflect similar changes in the total heat content of the atmosphere-ocean system. In fact, global net changes can be small and such heat exchanges may mainly reflect redistribution of energy between ocean and atmosphere. What matters is the overall temperature development when seen over several years.

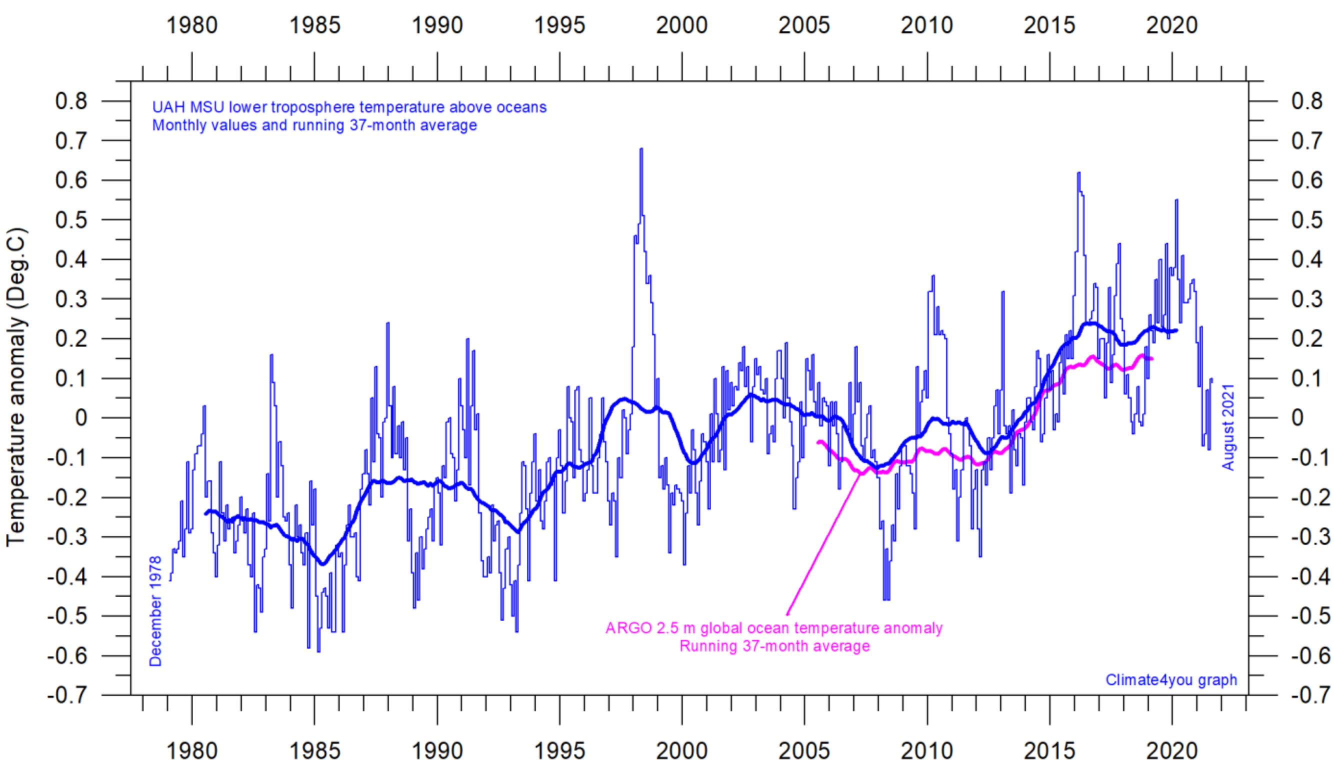

Global monthly average lower troposphere temperature over oceans (thin line) since 1979 according to University of Alabama at Huntsville, USA. The thick line is the simple running 37-month average. Insert: Argo global ocean temperature anomaly from floats, displaced vertically to make visual comparison easier. UAH reference period: 1991-2020.

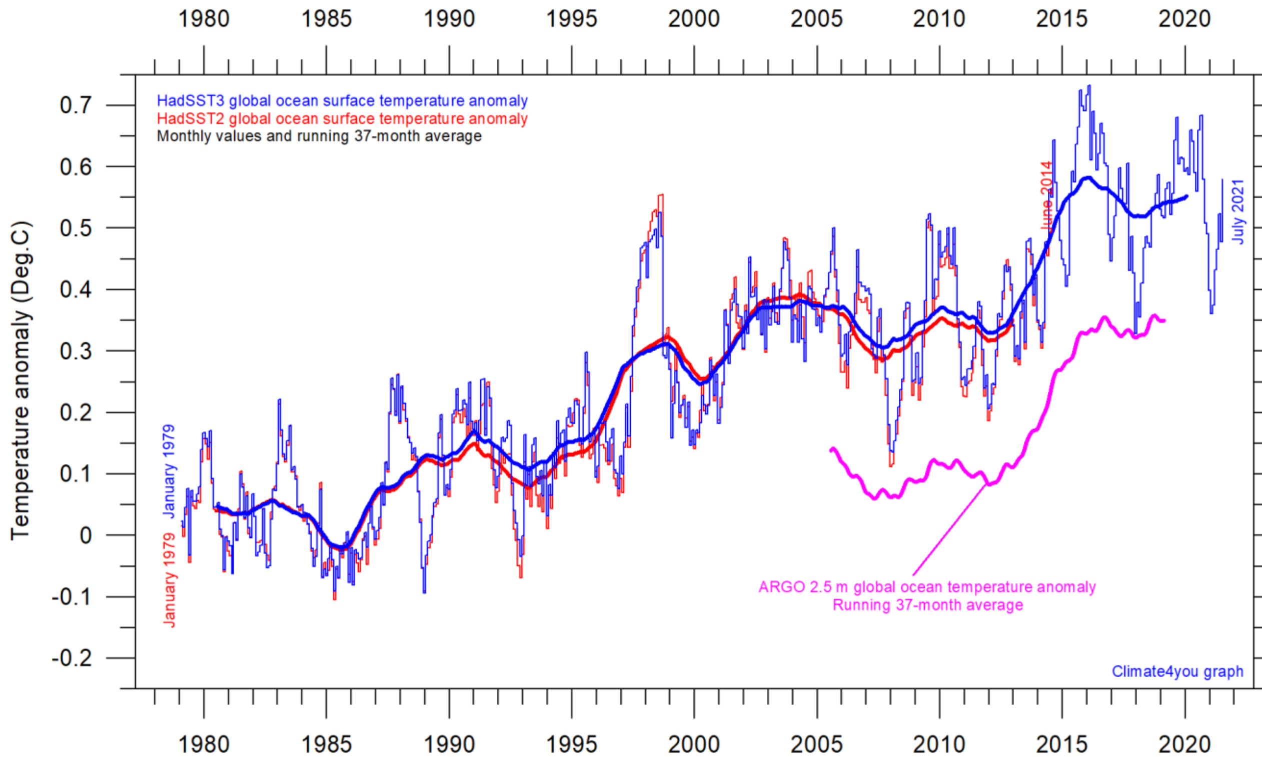

Global monthly average sea surface temperature since 1979 according to University of East Anglia's [Climatic Research Unit](#) ([CRU](#)), UK. Base period: 1961-1990. The thick line is the simple running 37-month average. Insert: Argo global ocean temperature anomaly from floats, displaced vertically to make visual comparison easier.

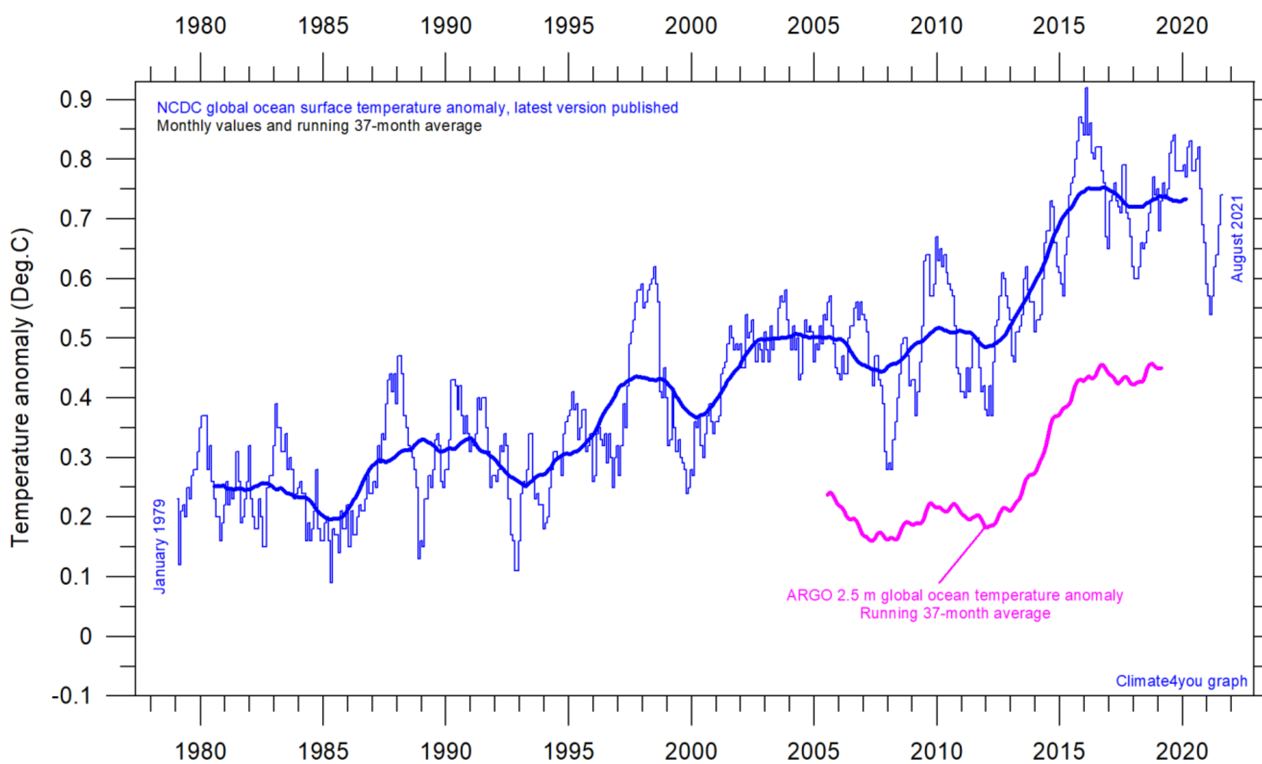

Global monthly average sea surface temperature since 1979 according to the [National Climatic Data Center](#) (NCDC), USA. Base period: 1901-2000. The thick line is the simple running 37-month average. Insert: Argo global ocean temperature anomaly from floats, displaced vertically to make visual comparison easier.

Ocean temperature in uppermost 100 m, updated to March 2021

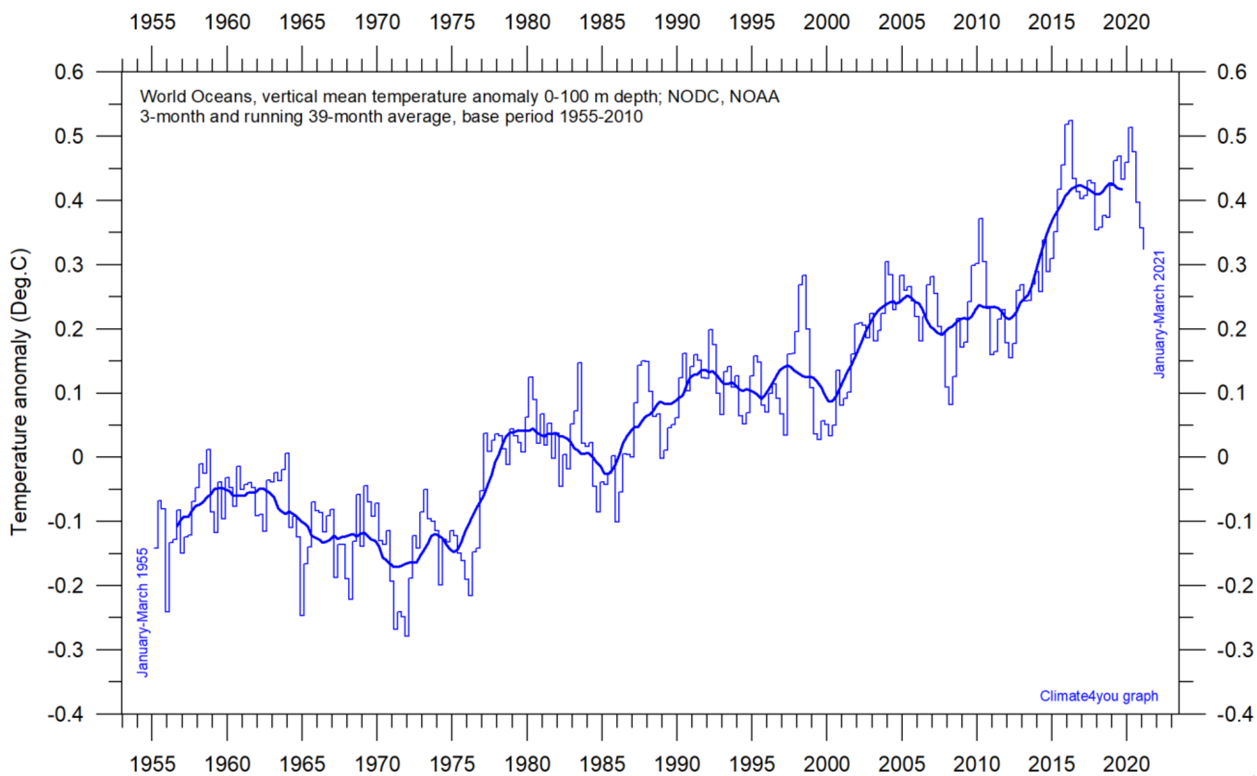

World Oceans vertical average temperature 0-100 m depth since 1955. The thin line indicates 3-month values, and the thick line represents the simple running 39-month (c. 3 year) average. Data source: [NOAA National Oceanographic Data Center](#) (NODC). Base period 1955-2010.

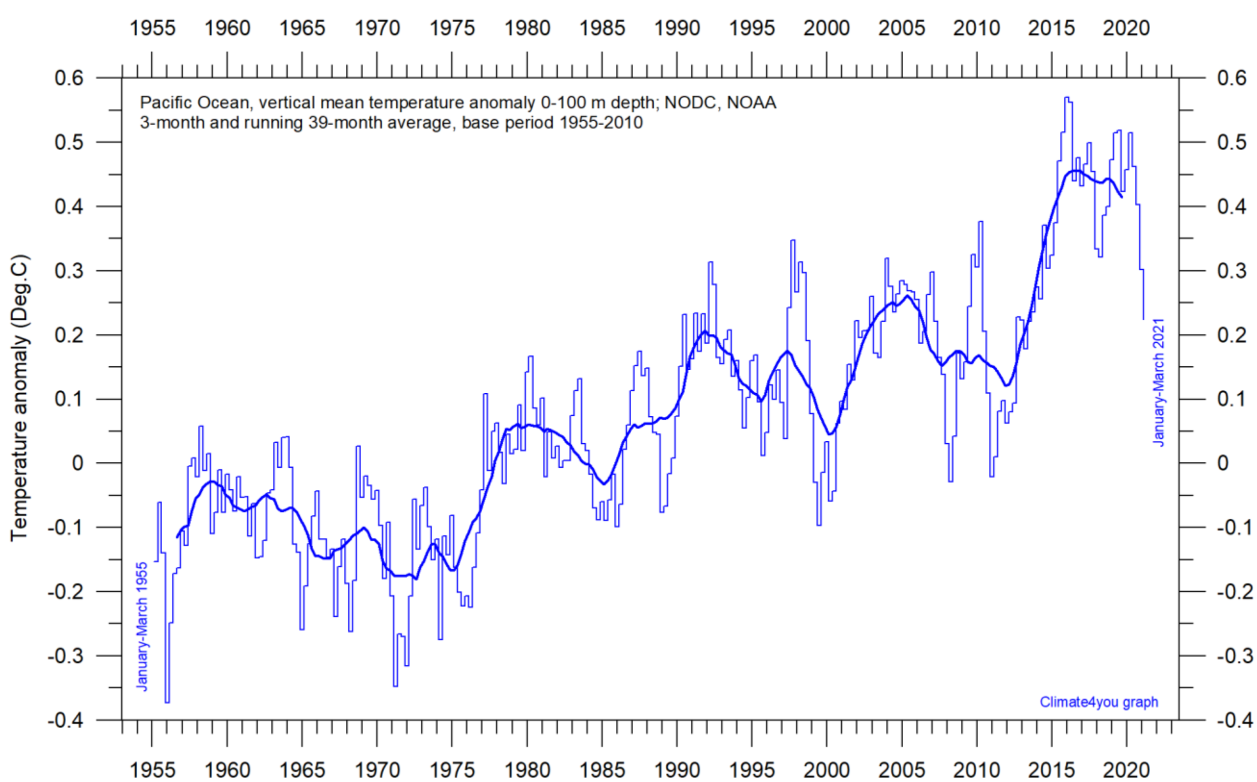

Pacific Ocean vertical average temperature 0-100 m depth since 1955. The thin line indicates 3-month values, and the thick line represents the simple running 39-month (c. 3 year) average. Data source: [NOAA National Oceanographic Data Center](#) (NODC). Base period 1955-2010.

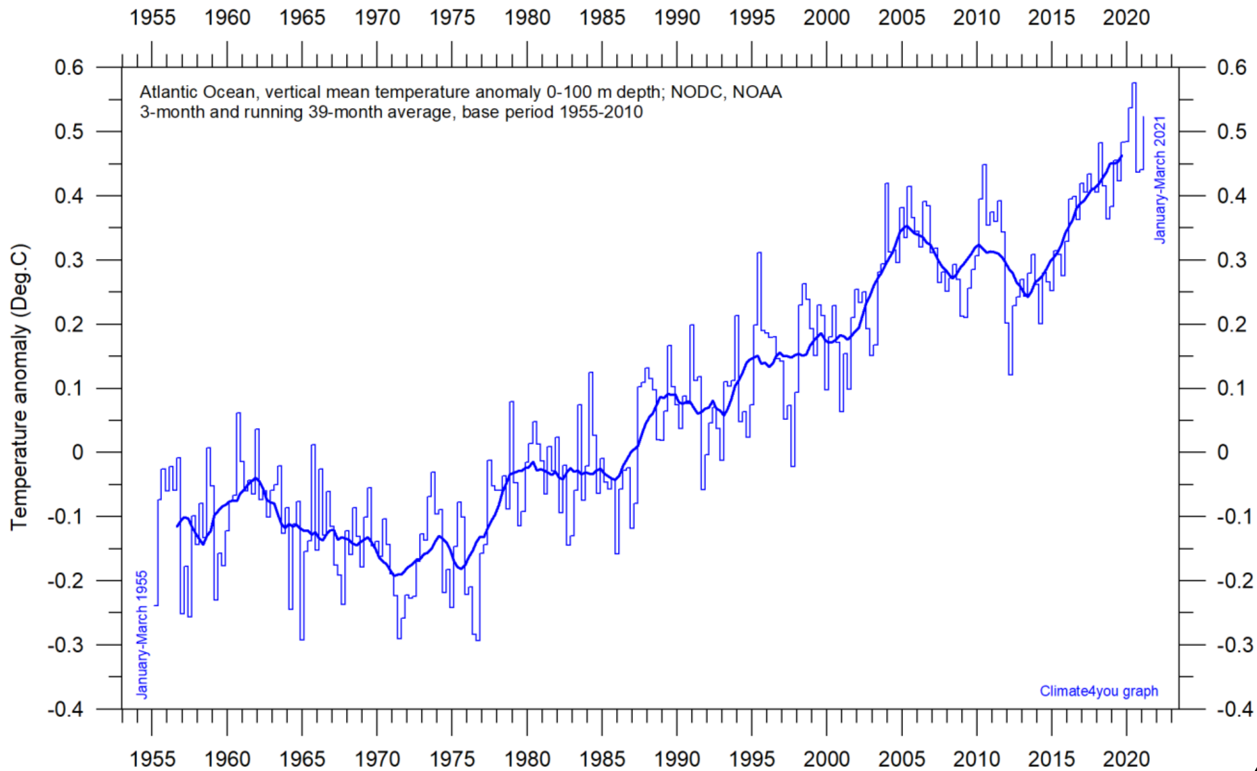

Atlantic Ocean vertical average temperature 0-100 m depth since 1955. The thin line indicates 3-month values, and the thick line represents the simple running 39-month (c. 3 year) average. Data source: [NOAA National Oceanographic Data Center] (NODC). Base period 1955-2010.

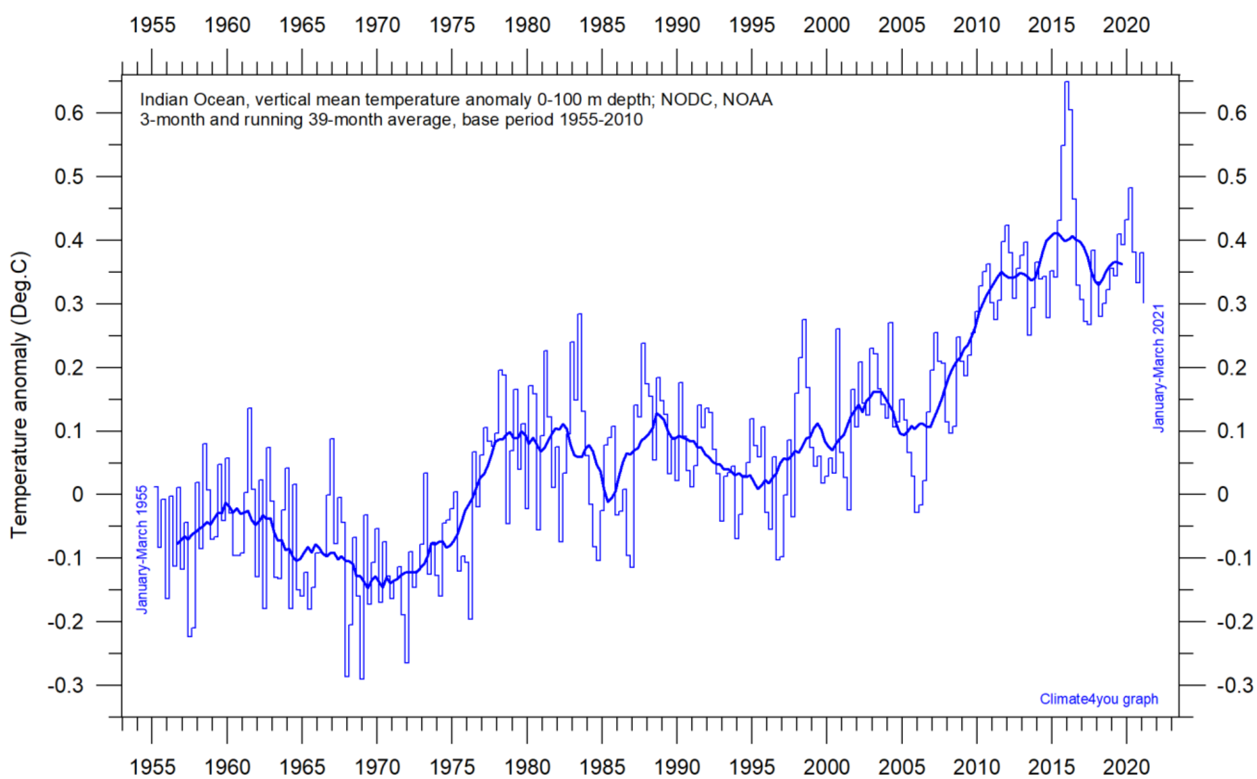

Indian Ocean vertical average temperature 0-100 m depth since 1955. The thin line indicates 3-month values, and the thick line represents the simple running 39-month (c. 3 year) average. Data source: [NOAA National Oceanographic Data Center] (NODC). Base period 1955-2010.

North Atlantic heat content uppermost 700 m, updated to March 2021

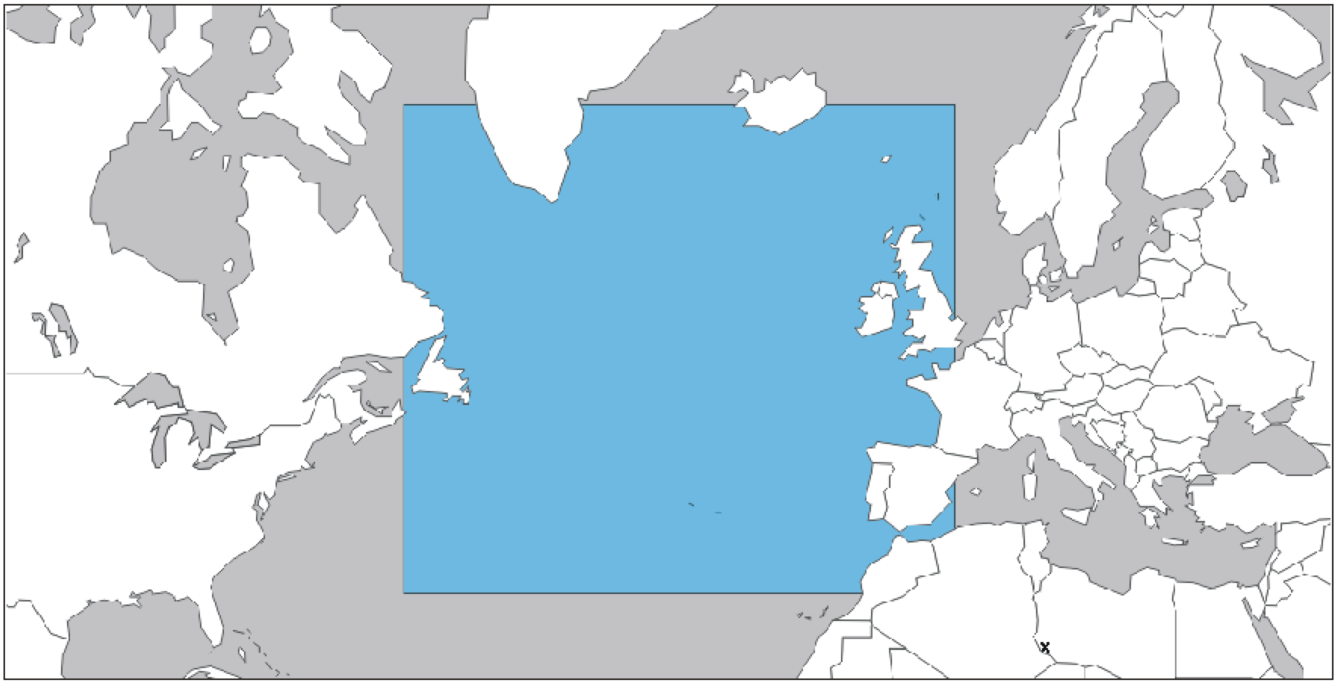

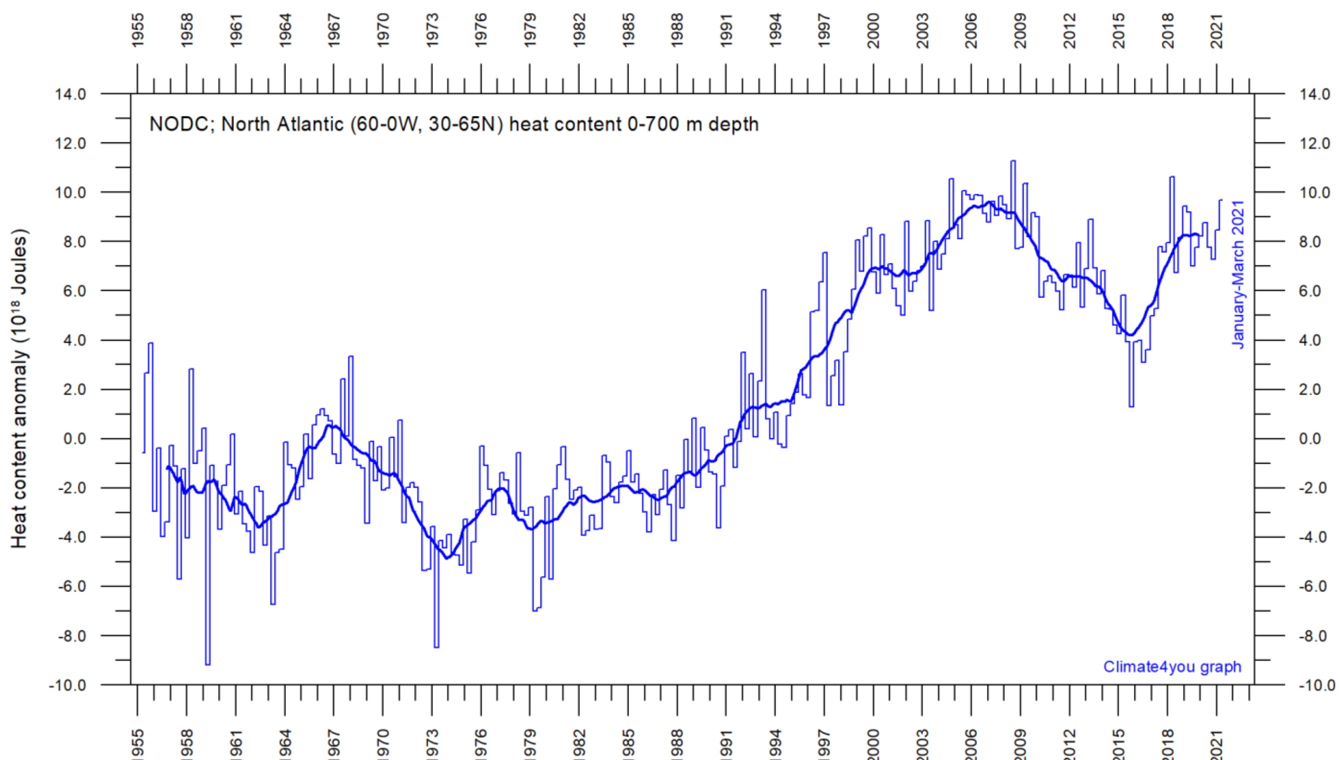

Global monthly heat content anomaly (10[18] Joules) in the uppermost 700 m of the North Atlantic (60-0W, 30-65N; see map above) *ocean since January 1955. The thin line indicates monthly values, and the thick line represents the simple running 37-month (c. 3 year) average. Data source:* [*National Oceanographic Data Center*]() *(NODC).*

North Atlantic temperatures 0-800 m depth along 59°N, 30-0W, updated to August 2020

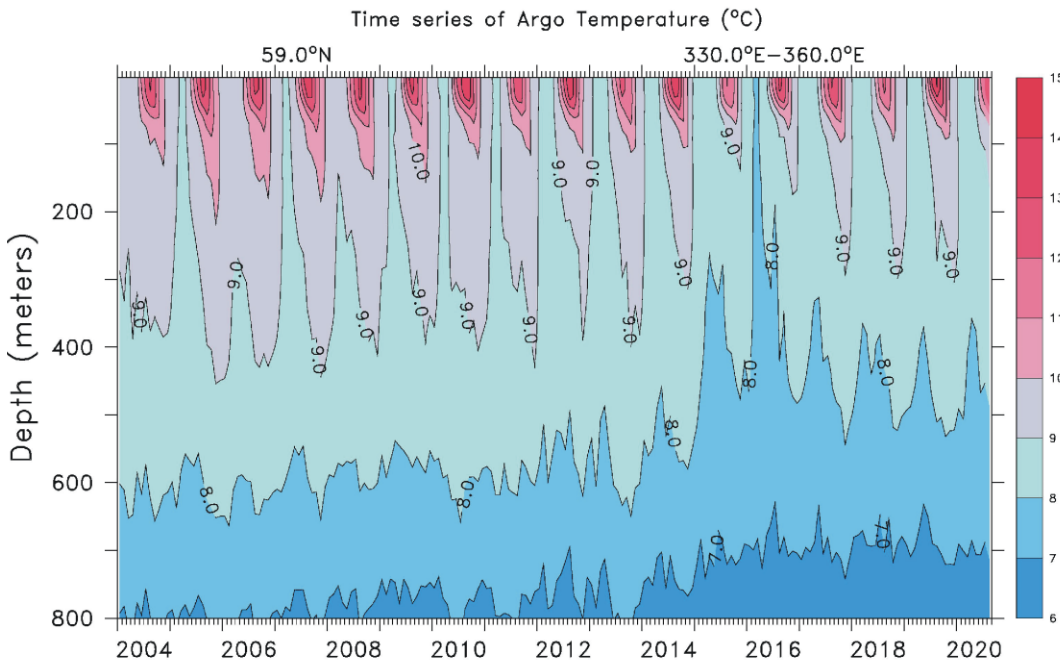

Time series depth-temperature diagram along 59 N across the North Atlantic Current from 30°W to 0°W, from surface to 800 m depth. Source: Global Marine Argo Atlas. See also the diagram below.

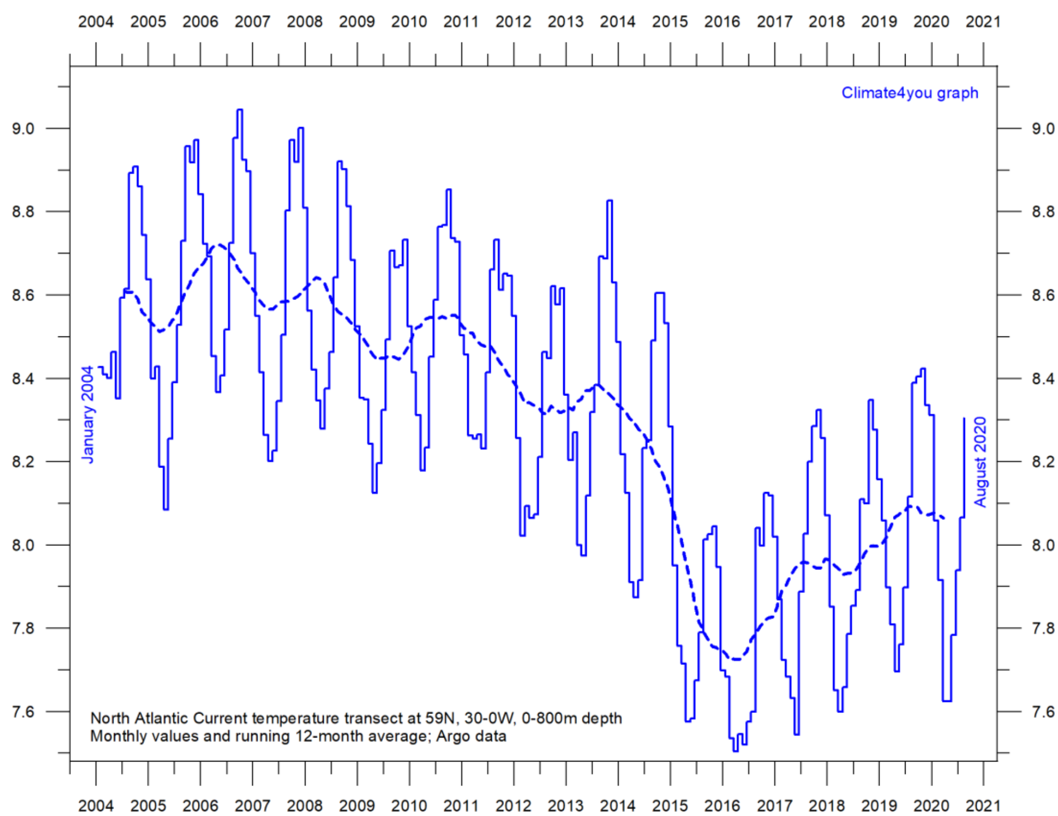

Average temperature along 59 N, 30-0W, 0-800m depth, corresponding to the main part of the North Atlantic Current, using Argo-data. Source: Global Marine Argo Atlas. Additional information can be found in: Roemmich, D. and J. Gilson, 2009. The 2004-2008 mean and annual cycle of temperature, salinity, and steric height in the global ocean from the Argo Program. Progress in Oceanography, 82, 81-100.

[Global ocean temperature 0-1900 m depth summary, updated to August 2020]

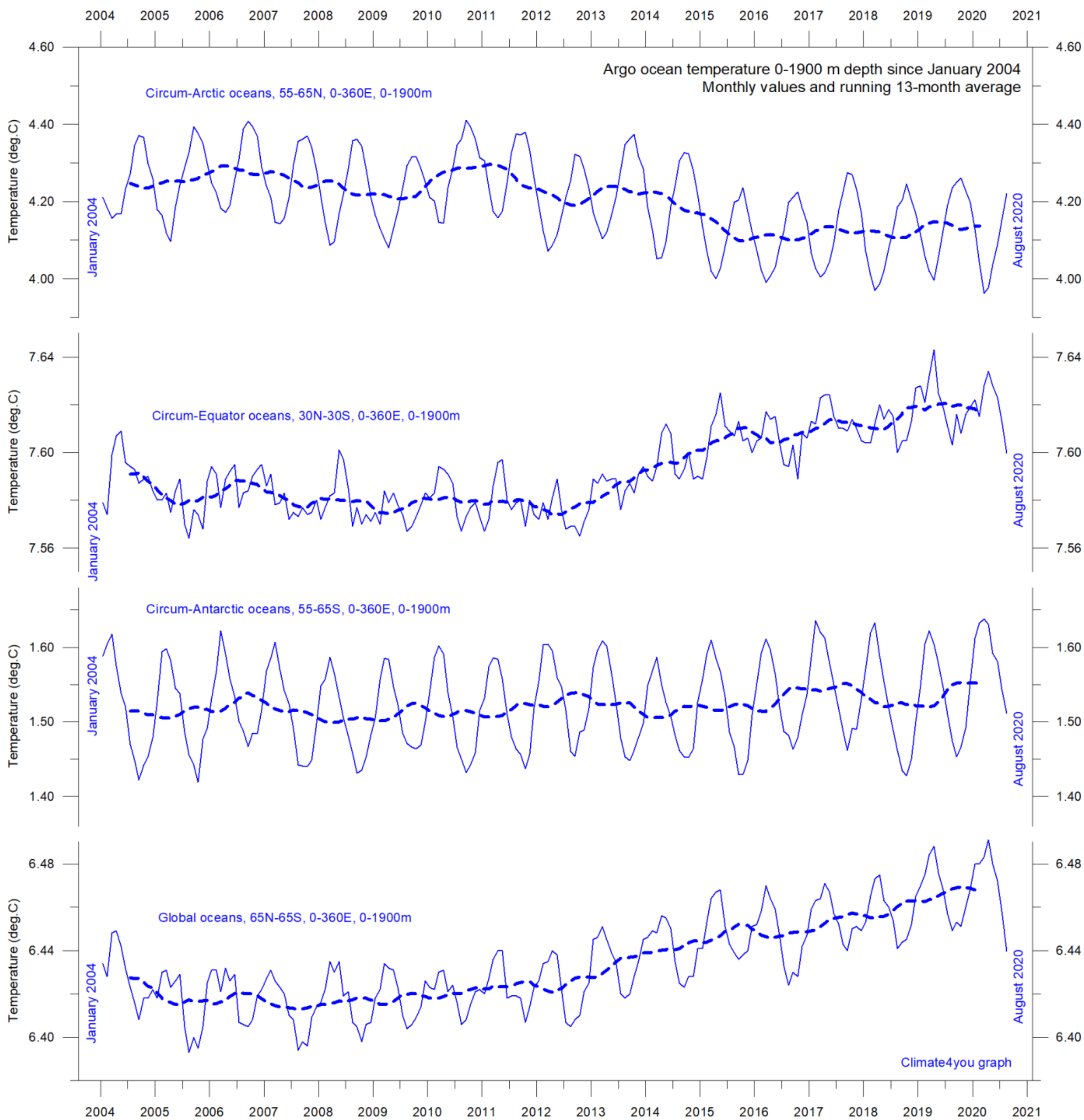

Summary of average temperature in uppermost 1900 m in different parts of the global oceans, using [Argo]-data. Source: [Global Marine Argo Atlas]. Additional information can be found in: Roemmich, D. and J. Gilson, 2009. The 2004-2008 mean and annual cycle of temperature, salinity, and steric height in the global ocean from the Argo Program. [Progress in Oceanography], 82, 81-100.

The global summary diagram above shows that, on average, the temperature of the global oceans down to 1900 m depth has been increasing since about 2011. It is also seen that this increase since 2013 dominantly is due to oceanic changes occurring near the Equator, between 30°N and 30°S. In contrast, for the circum-Arctic oceans north of 55°N, depth-integrated ocean temperatures have been decreasing since 2011. Near the Antarctic, south of 55°S, temperatures have essentially been stable. At most latitudes, a clear annual rhythm is seen.

Global ocean net temperature change since 2004 at different depths, updated to August 2020

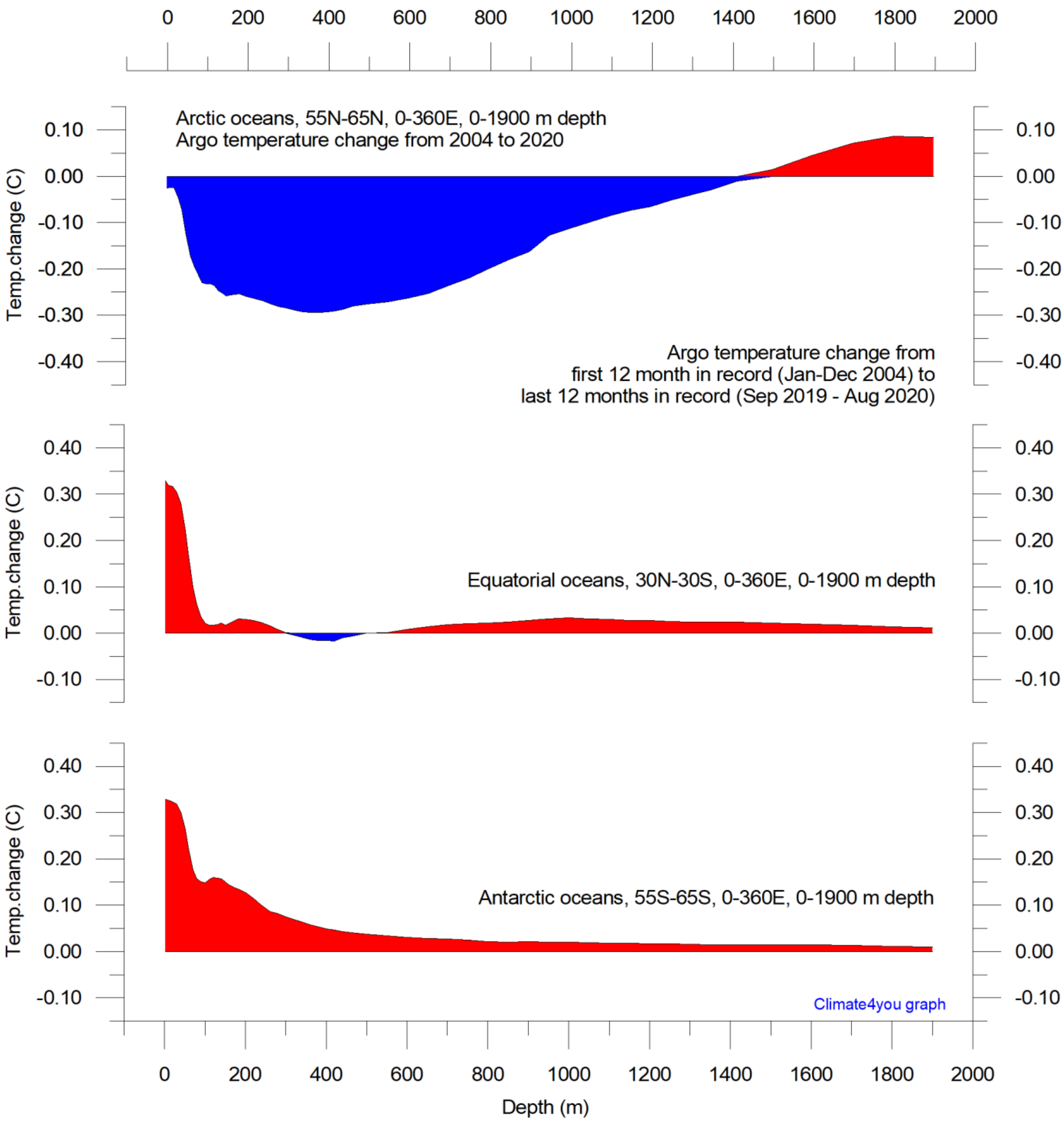

Net temperature change since 2004 from surface to 1900 m depth in different parts of the global oceans, using Argo-data. Source: Global Marine Argo Atlas. Additional information can be found in: Roemmich, D. and J. Gilson, 2009. The 2004-2008 mean and annual cycle of temperature, salinity, and steric height in the global ocean from the Argo Program. Progress in Oceanography, 82, 81-100. Please note that due to the spherical form of Earth, northern and southern latitudes represent only small ocean volumes, compared to latitudes near the Equator.

La Niña and El Niño episodes, Oceanic Niño Index (ONI), updated to August 2021

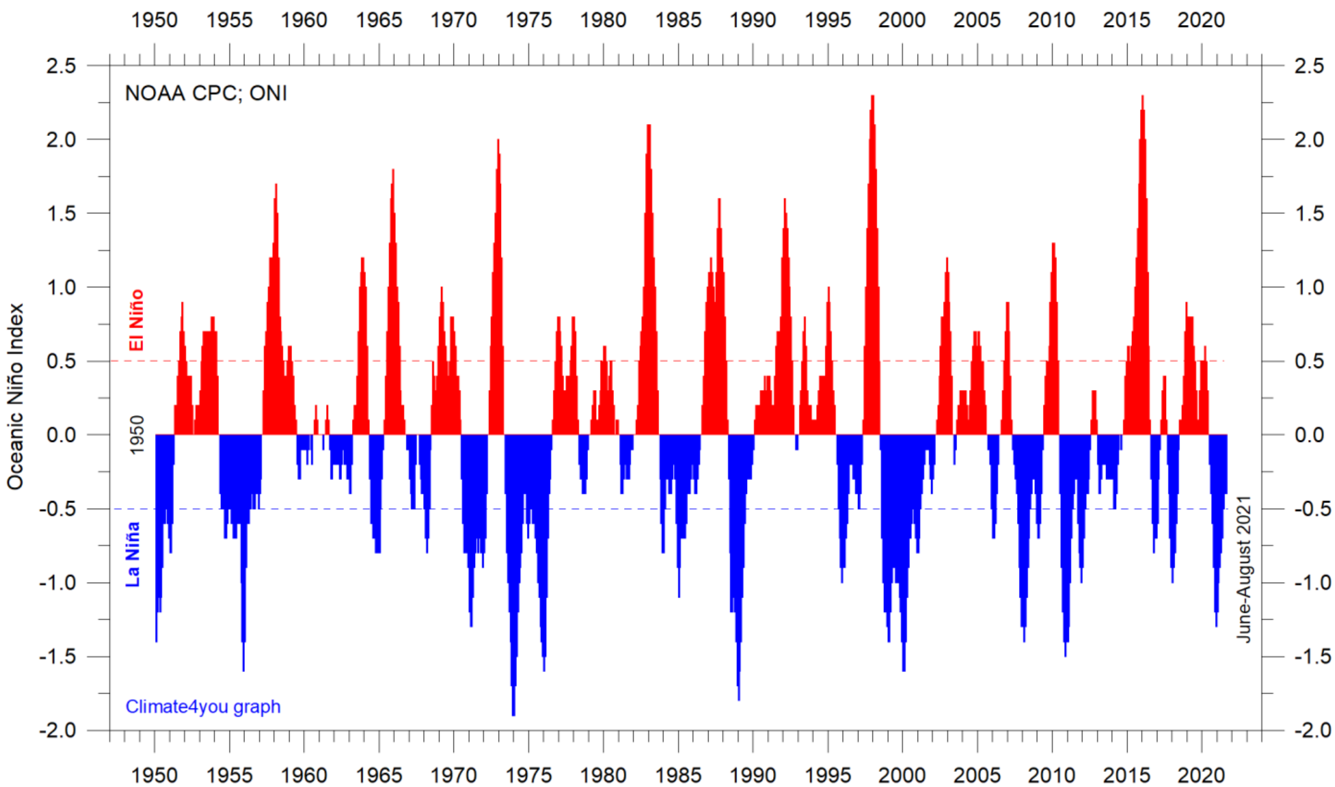

Warm (>+0.5°C) and cold (<0.5°C) episodes for the Oceanic Niño Index (ONI), defined as 3 month running mean of ERSSTv4 SST anomalies in the Niño 3.4 region (5°N-5°S, 120°-170°W)]. For historical purposes cold and warm episodes are defined when the threshold is met for a minimum of 5 consecutive over-lapping seasons. Anomalies are centred on 30-yr base periods updated every 5 years.

The subrecent 2015-16 El Niño episode is among the strongest since the beginning of the record in 1950. Considering the entire record, however, recent variations between El Niño and La Niña episodes do not appear abnormal in any way. See also diagrams on pages 43 and 52.

Zonal lower troposphere temperatures from satellites, updated to August 2021

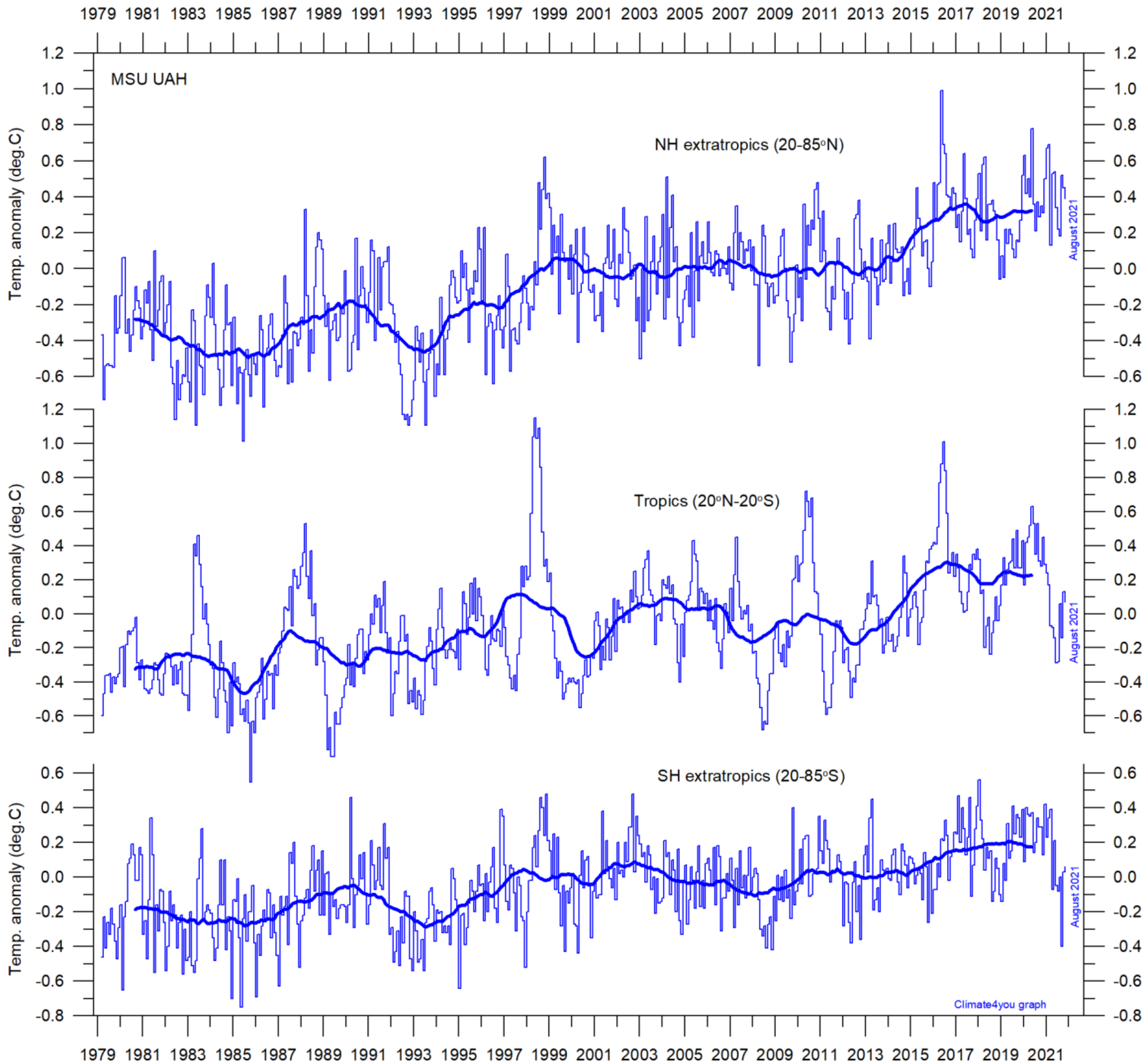

Global monthly average lower troposphere temperature since 1979 for the tropics and the northern and southern extratropics, according to University of Alabama at Huntsville, USA. Thin lines show the monthly temperature. Thick lines represent the simple running 37-month average, nearly corresponding to a running 3-year average. Reference period 1981-2010.

The overall warming since 1980 has dominantly been a northern hemisphere phenomenon, and mainly played out as a marked step change between 1994 and 1999. However, this rather rapid temperature change is influenced by the Mt. Pinatubo eruption 1992-93 and the subsequent 1997 El Niño episode. The diagram also shows the temperature effects of the strong Equatorial El Niño's in 1997 and 2015-16, as well as the moderate El Niño in 2019. Apparently, these effects were spreading to higher latitudes in both hemispheres with some delay.

Arctic and Antarctic lower troposphere temperature, updated to August 2021

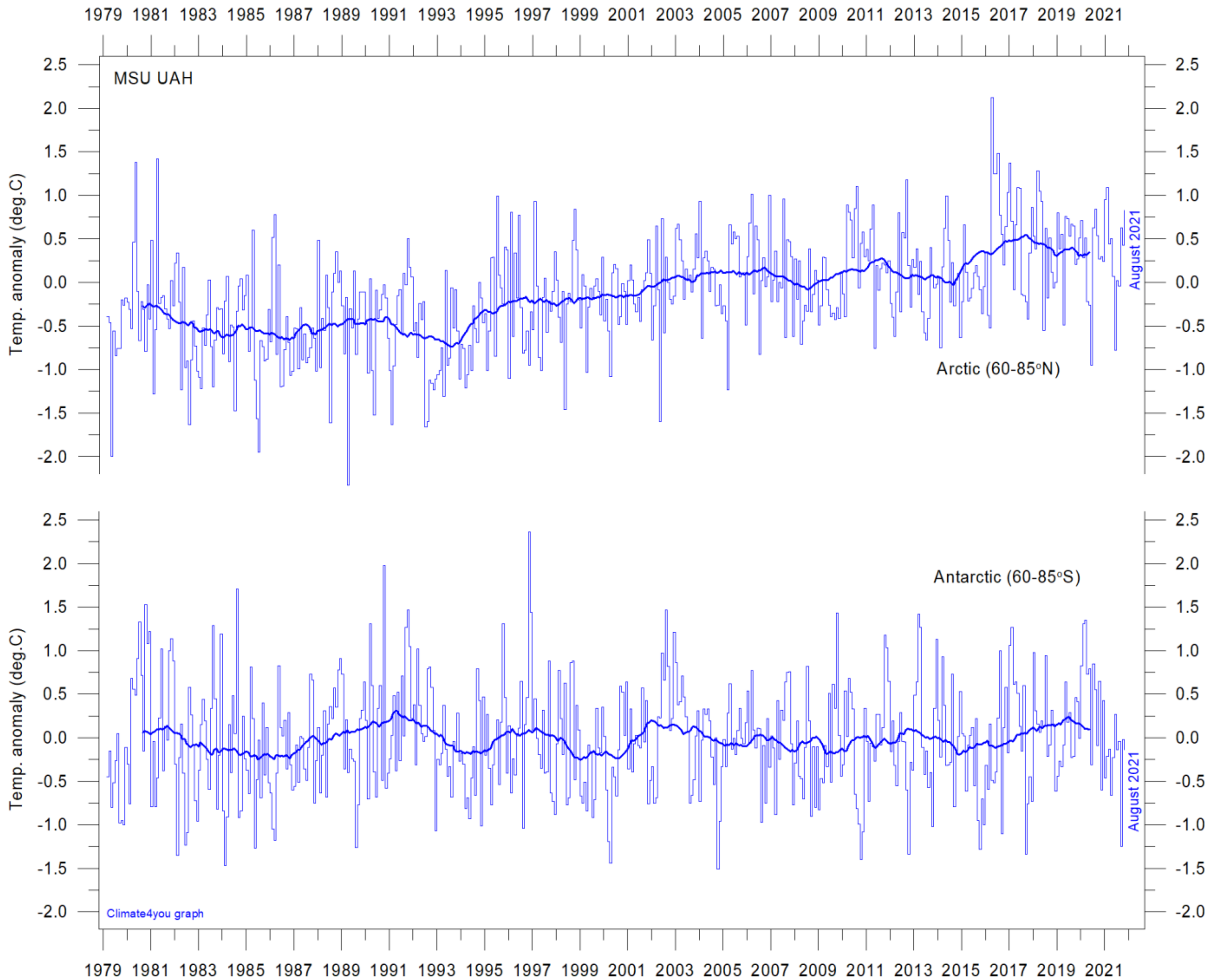

Global monthly average lower troposphere temperature since 1979 for the North Pole and South Pole regions, based on satellite observations (University of Alabama at Huntsville, USA). Thin lines show the monthly temperature. The thick line is the simple running 37-month average, nearly corresponding to a running 3-year average. Reference period 1991-2020.

In the Arctic region, warming mainly took place 1994-96, and less so subsequently. In 2016, however, temperatures peaked for several months, presumably because of oceanic heat given off to the atmosphere during the 2015-15 El Niño (see also figure on page 24) and subsequently advected to higher latitudes.

This underscores how Arctic air temperatures may be affected not only by variations in local conditions but also by variations playing out in geographically remote regions. A small overall temperature decrease has characterised the Arctic since the 2016 peak (see also diagrams on page 29-31).

In the Antarctic region, temperatures have basically remained stable since the onset of the satellite record in 1979. In 2016-17 a small temperature peak visible in the monthly record may be interpreted as the subdued effect of the recent El Niño episode.

Arctic and Antarctic surface air temperature, updated to June 2021

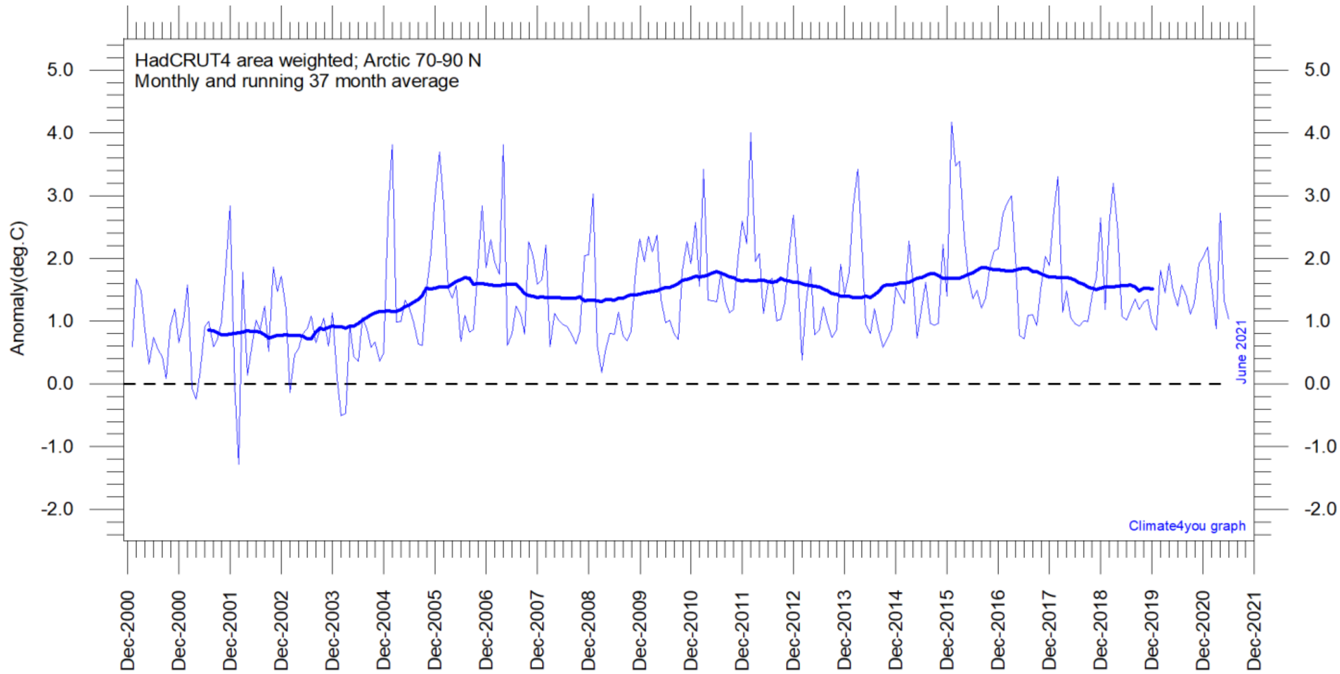

Diagram showing area weighted Arctic (70-90°N) monthly surface air temperature anomalies (HadCRUT4) since January 2000, in relation to the WMO normal period 1961-1990. The thin line shows the monthly temperature anomaly, while the thicker line shows the running 37-month (c. 3 year) average.

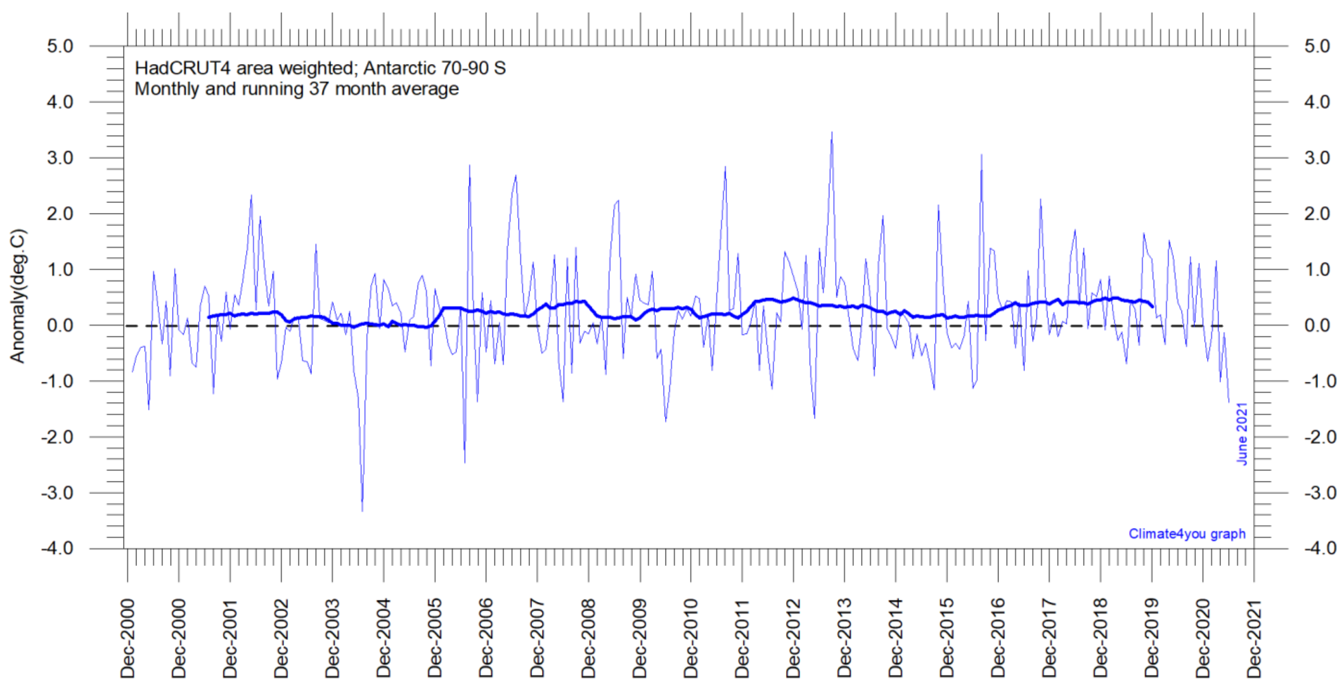

Diagram showing area weighted Antarctic (70-90°S) monthly surface air temperature anomalies (HadCRUT4) since January 2000, in relation to the WMO normal period 1961-1990. The thin line shows the monthly temperature anomaly, while the thicker line shows the running 37-month (c. 3 year) average.

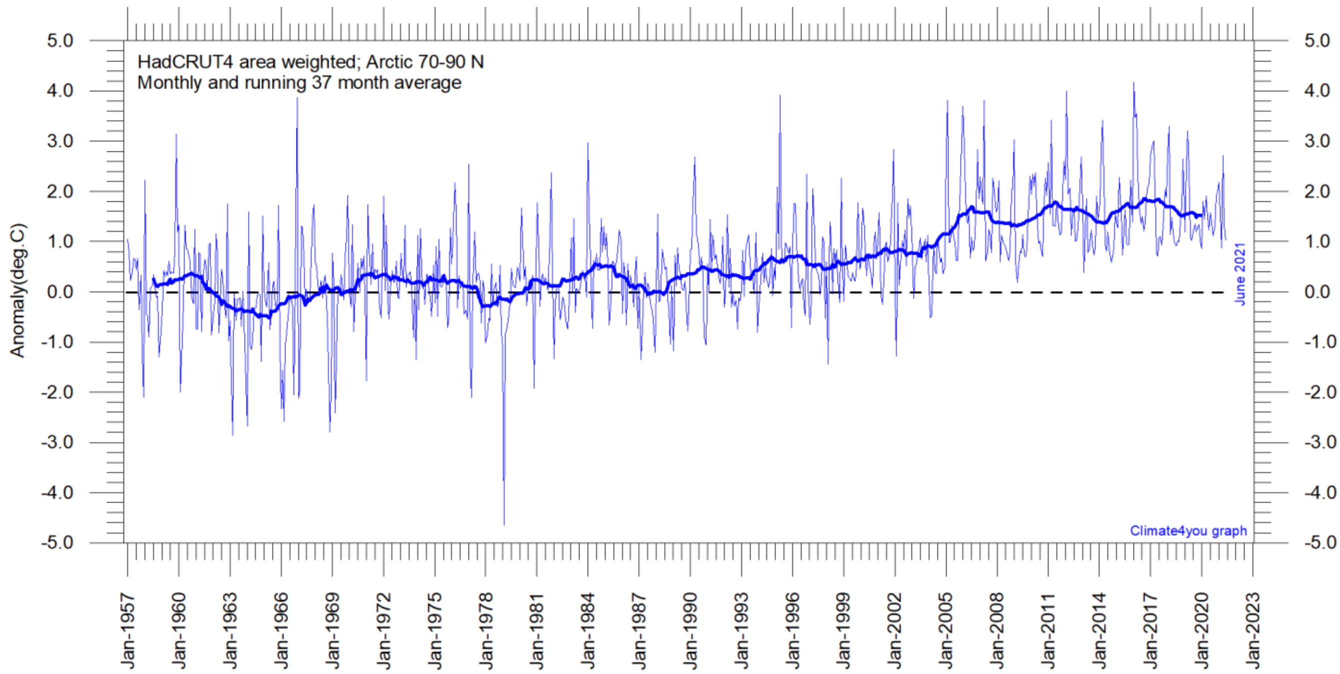

Diagram showing area weighted Arctic (70-90ºN) monthly surface air temperature anomalies ([HadCRUT4]) since January 1957, in relation to the WMO [normal period] 1961-1990. The thin line shows the monthly temperature anomaly, while the thicker line shows the running 37-month (c. 3 year) average.

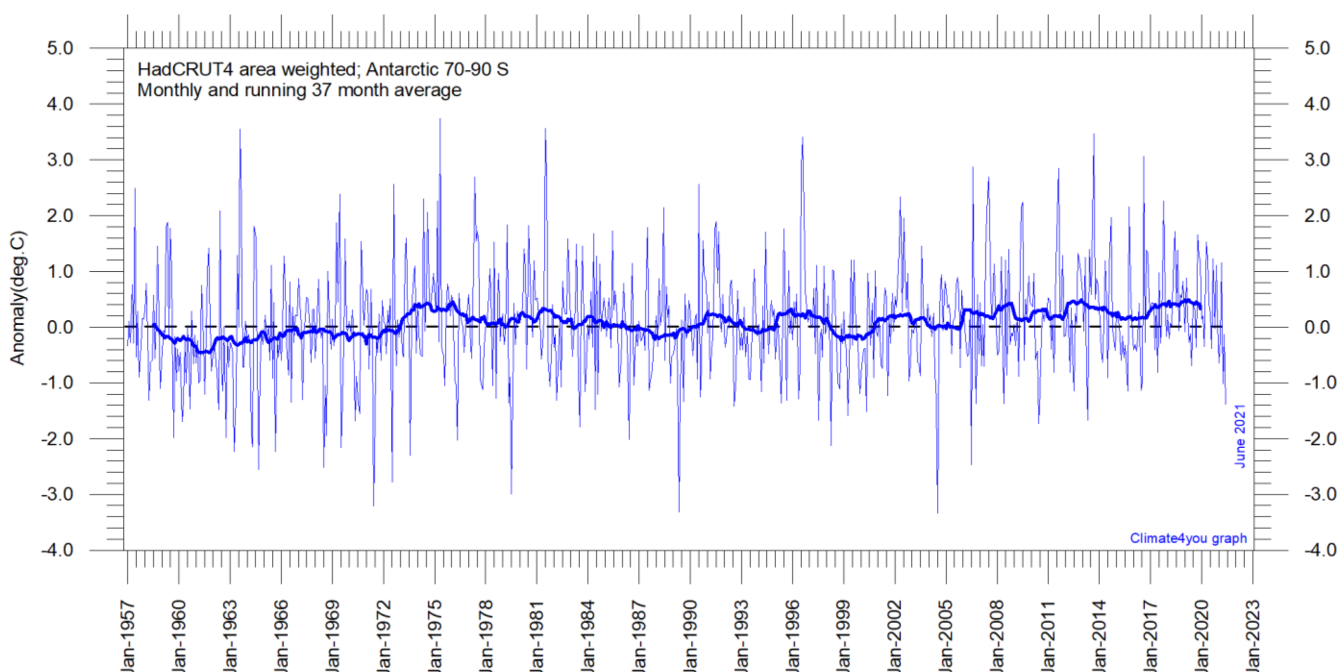

Diagram showing area weighted Antarctic (70-90ºS) monthly surface air temperature anomalies ([HadCRUT4]) since January 1957, in relation to the WMO [normal period] 1961-1990. The thin line shows the monthly temperature anomaly, while the thicker line shows the running 37-month (c. 3 year) average.

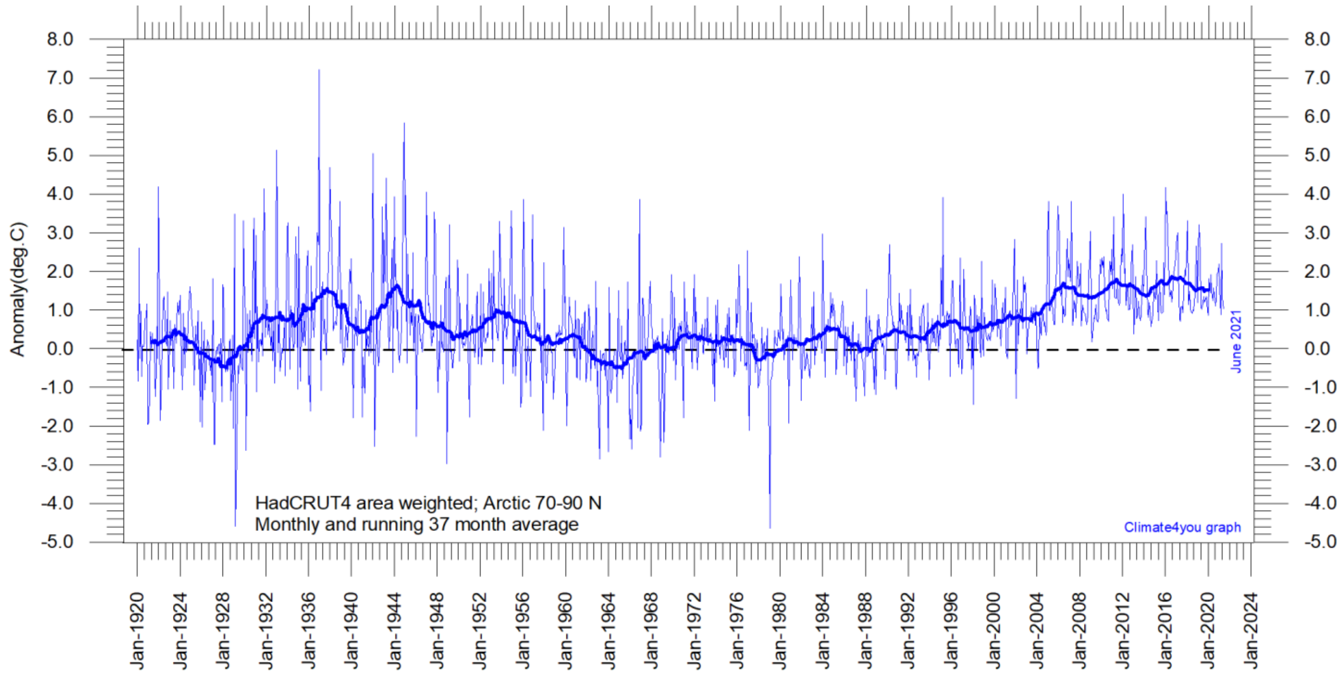

Diagram showing area-weighted Arctic (70-90°N) monthly surface air temperature anomalies ([HadCRUT4]) since January 1920, in relation to the WMO [normal period] 1961-1990. The thin line shows the monthly temperature anomaly, while the thicker line shows the running 37-month (c. 3 year) average.

Because of the relatively small number of Arctic stations before 1930, month-to-month variations in the early part of the Arctic temperature record 1920-2018 are bigger than later (diagram above).

The period from about 1930 saw the establishment of many new Arctic meteorological stations, first in Russia and Siberia, and following the 2nd World War, also in North America, explaining the above difference.

The period since 2005 is warm, about as warm as the period 1930-1940.

As the HadCRUT4 data series has improved high latitude coverage data coverage (compared to the HadCRUT3 series), the individual 5°x5° grid cells have been weighted according to their surface area. This area correction is especially important for polar regions, where longitudes converge rapidly. This approach differs from the approach used by Gillet et al. 2008, which calculated a simple average, with no correction for the substantial latitudinal surface area effect in polar regions.

The area weighted HadCRUT4 surface air temperature records (p.29-31) correspond rather well to the lower troposphere temperature records recorded by satellites (p.27).

Literature:

Gillett, N.P., Stone, D.A., Stott, P.A., Nozawa, T., Karpechko, A.Y.U., Hegerl, G.C., Wehner, M.F. and Jones, P.D. 2008. Attribution of polar warming to human influence. *Nature Geoscience* 1, 750-754.

Temperature over land versus over oceans, updated to August 2021

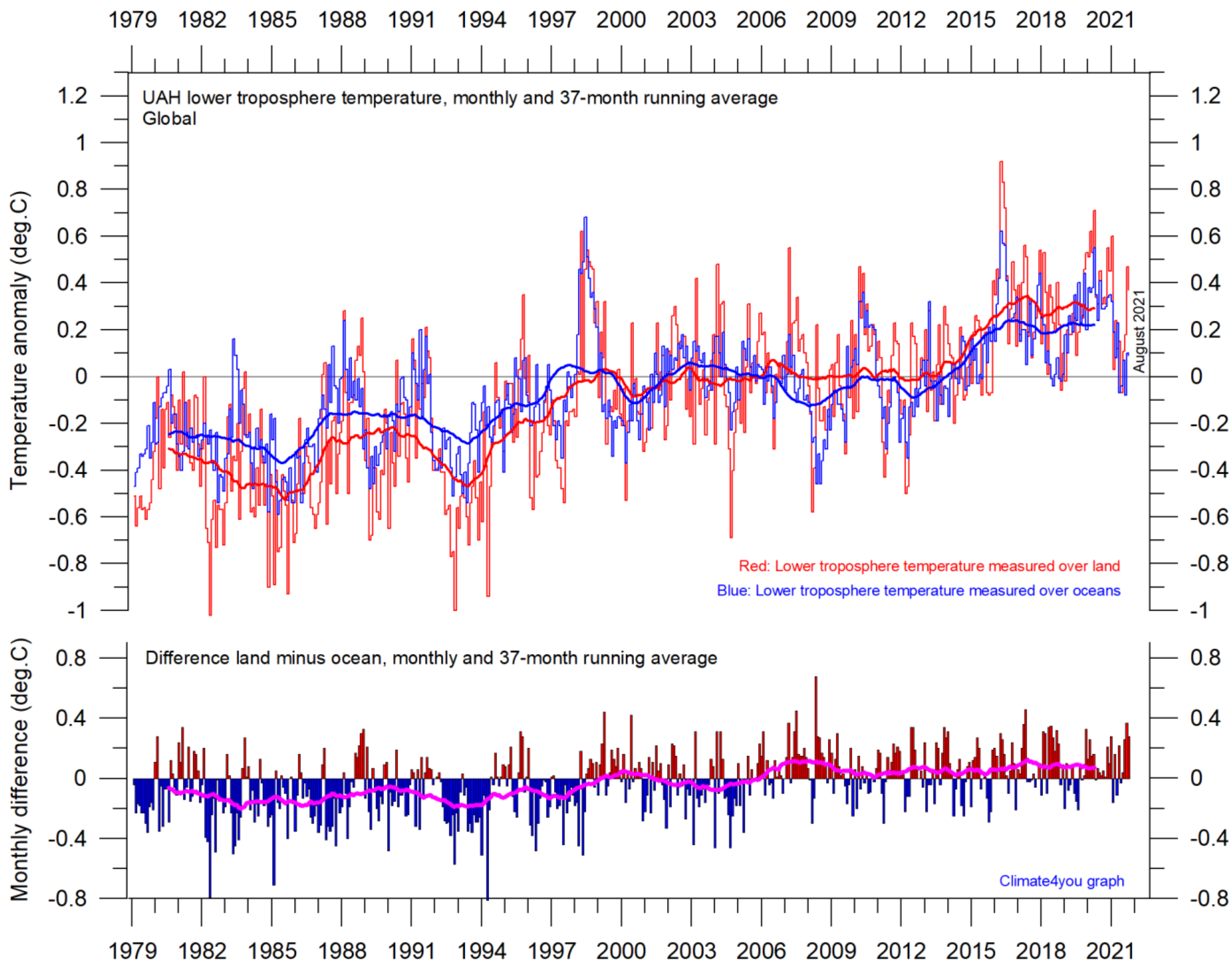

Global monthly average lower troposphere temperature since 1979 measured over land and oceans, respectively, according to University of Alabama at Huntsville, USA. Thick lines are the simple running 37-month average, nearly corresponding to a running 3-year average. Reference period 1991-2020.

Since 1979, the lower troposphere over land has warmed much more than over oceans, suggesting that the overall warming is derived mainly from incoming solar radiation. In addition, there may be supplementary reasons for this divergence, such as, e.g., variations in cloud cover and changes in land use.

Troposphere and stratosphere temperatures from satellites, updated to August 2021

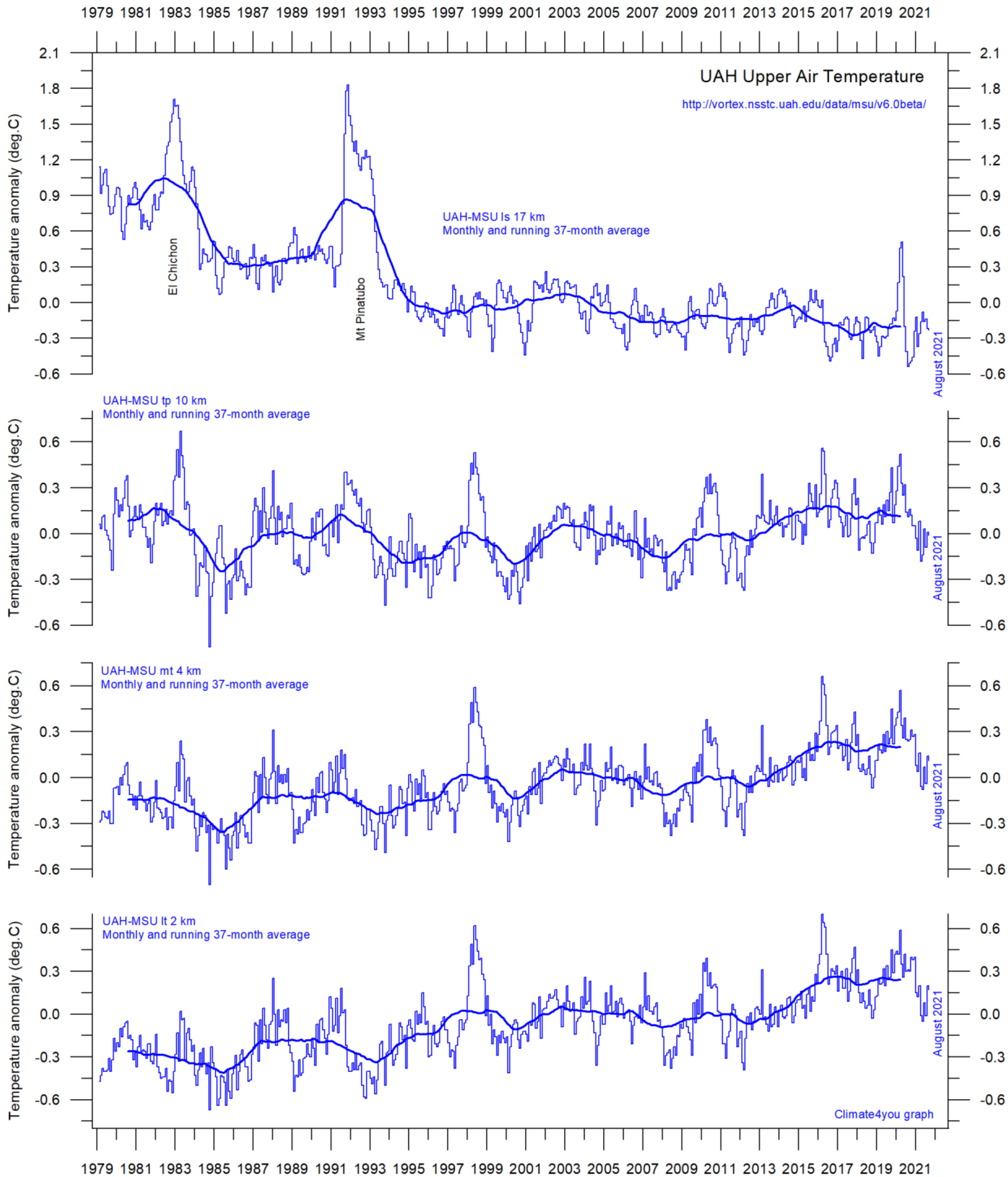

Global monthly average temperature in different according to University of Alabama at Huntsville, USA. The thin lines represent the monthly average, and the thick line the simple running 37-month average, nearly corresponding to a running 3-year average. Reference period 1991-2020.

Arctic and Antarctic sea ice, updated to August 2021

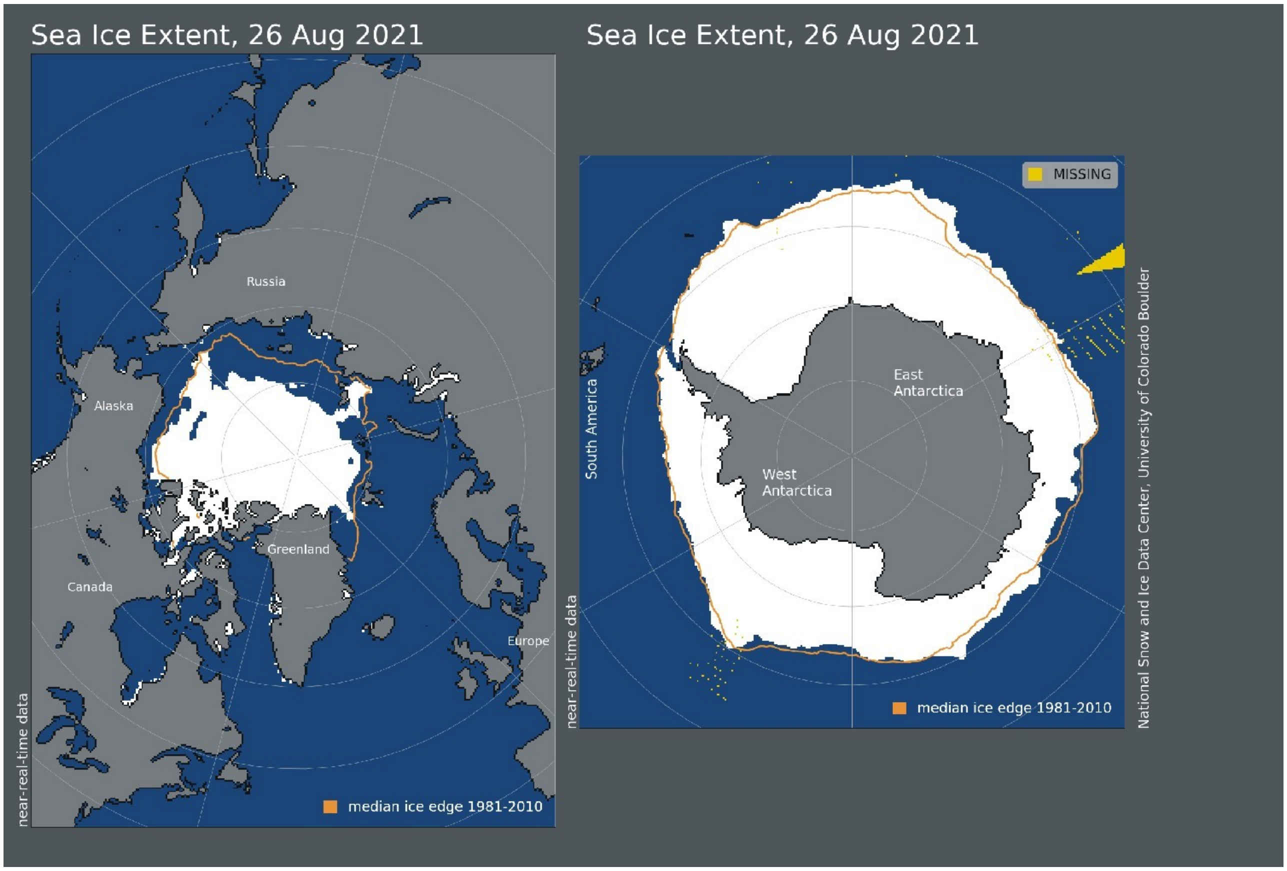

Sea ice extent 26 August 2021. The median limit of sea ice (orange line) is defined as 15% sea ice cover, according to the average of satellite observations 1981-2010 (both years included). Sea ice may therefore well be encountered outside and open water areas inside the limit shown in the diagrams above. Map source: National Snow and Ice Data Center (NSIDC).

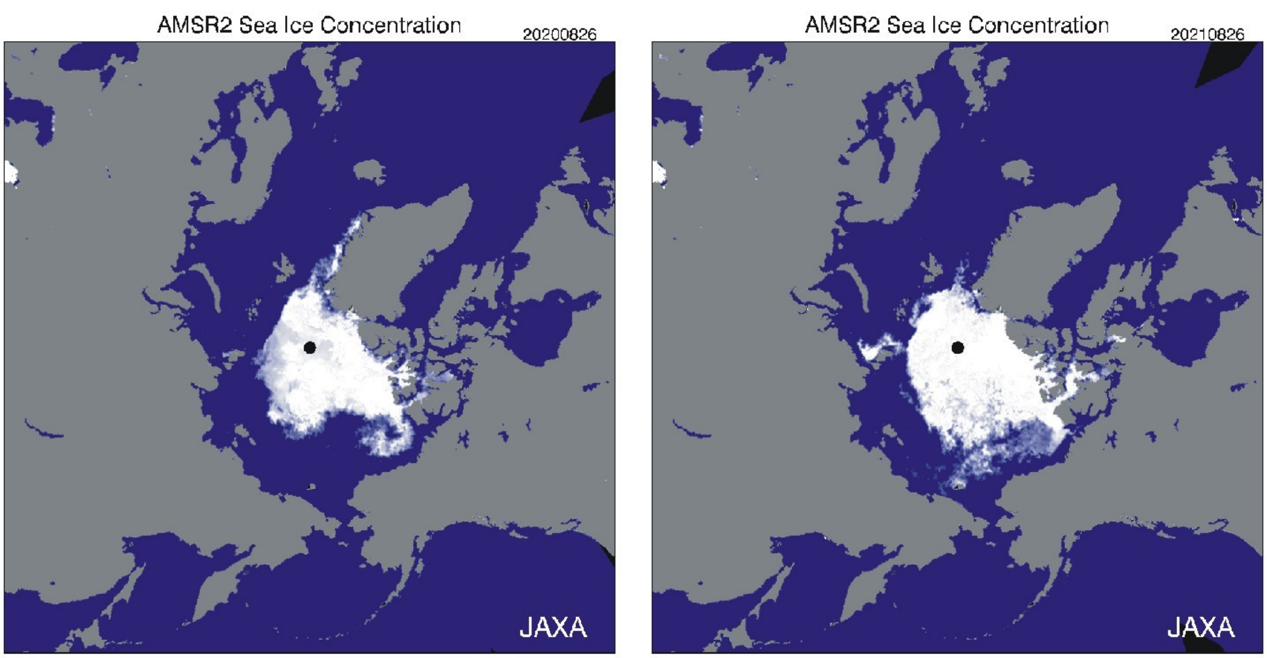

Diagrams showing Arctic sea ice extent and concentration 26 August 2020 (left) and 2021 (right), according to the Japan Aerospace Exploration Agency (JAXA).

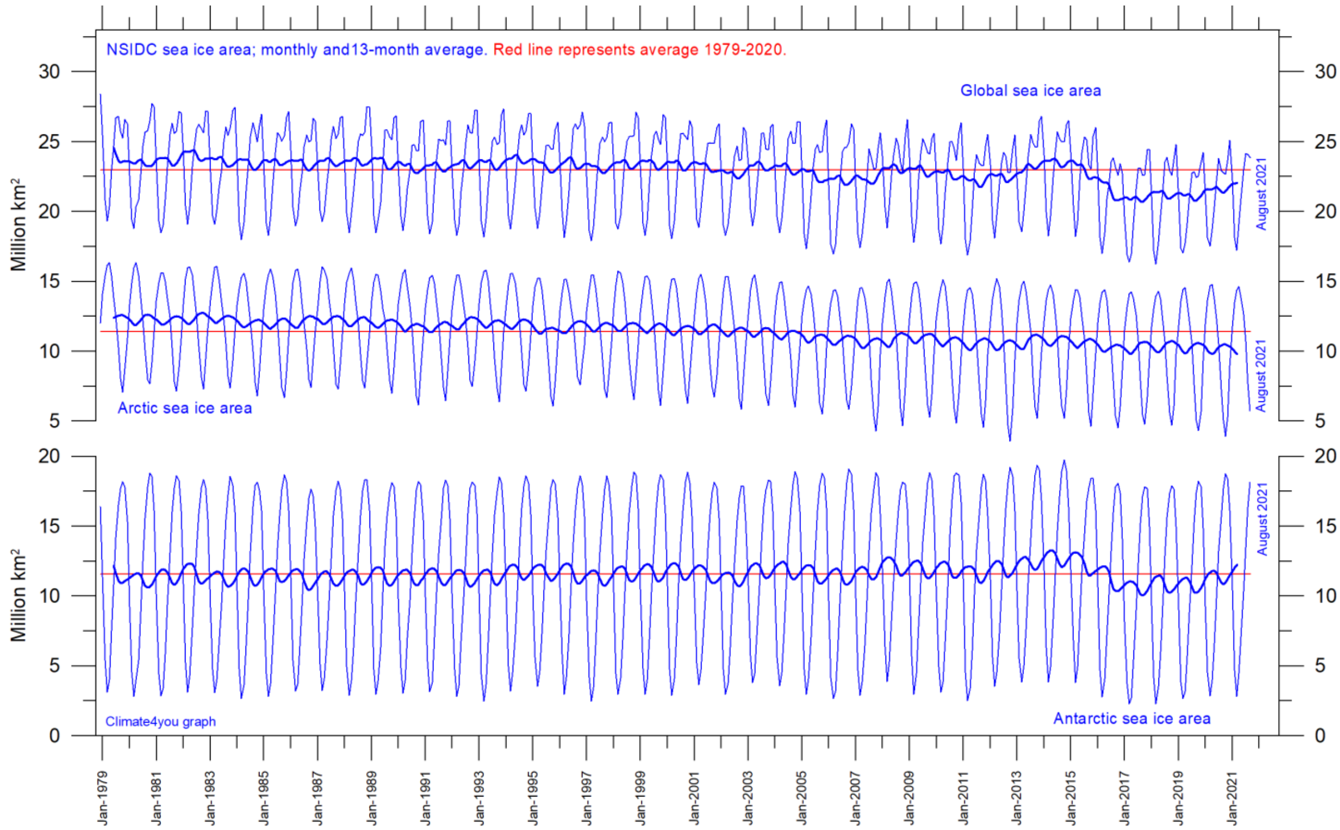

Graphs showing monthly Antarctic, Arctic, and global sea ice extent since November 1978, according to the [National Snow and Ice data Center](#) (NSIDC).

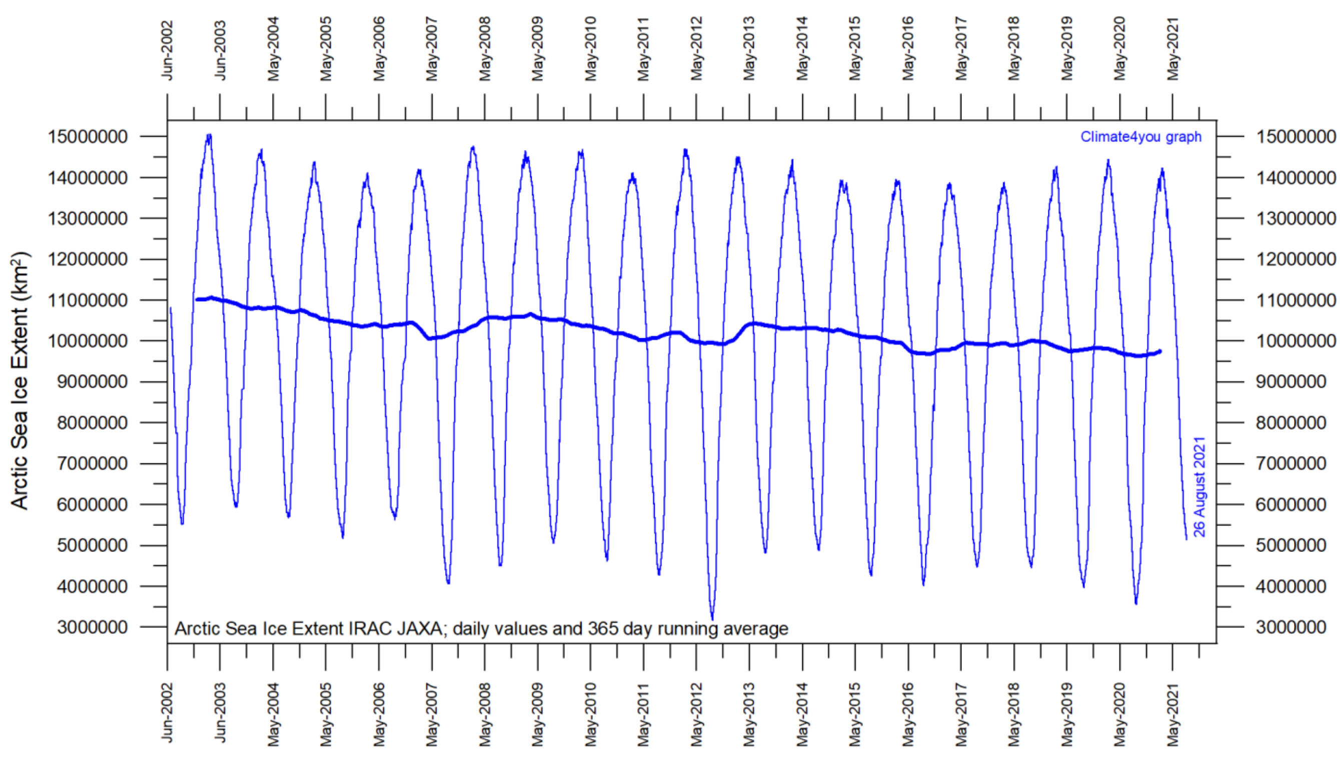

Diagram showing daily Arctic sea ice extent since June 2002, to 26 August 2021, by courtesy of [Japan Aerospace Exploration Agency](#) (JAXA).

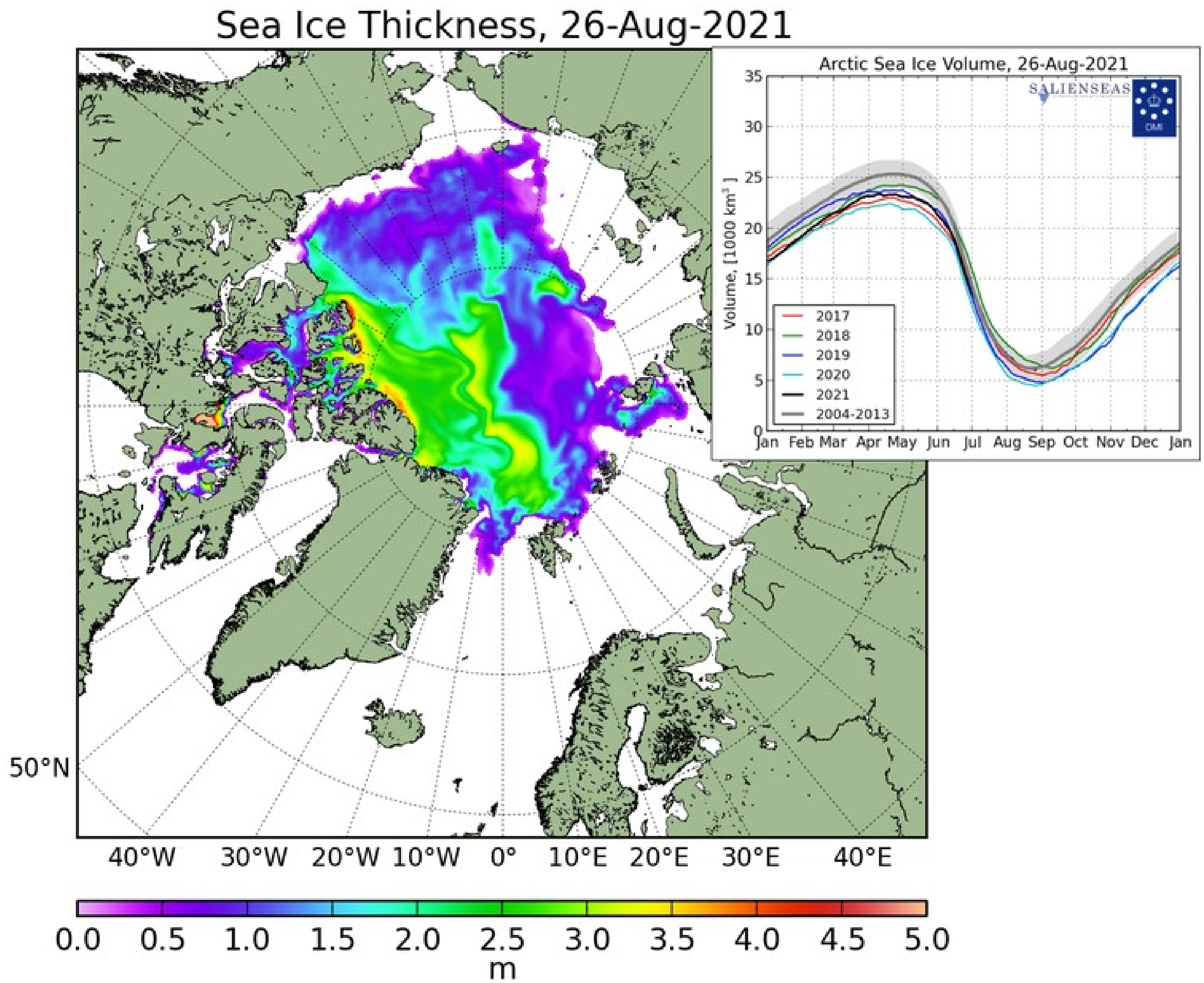

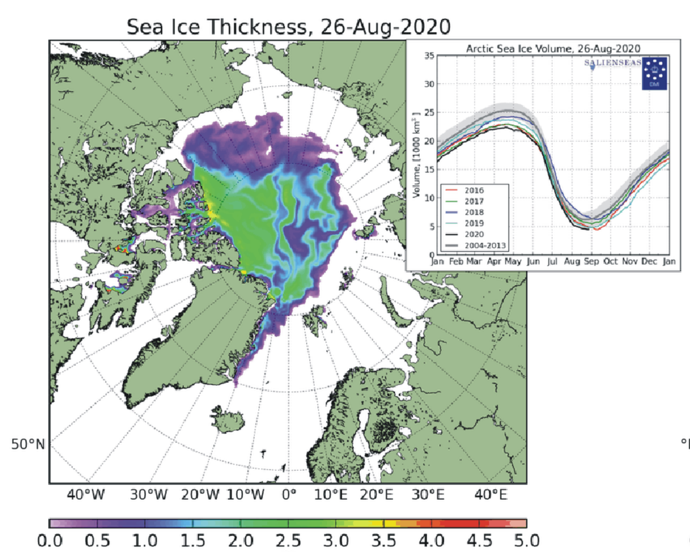

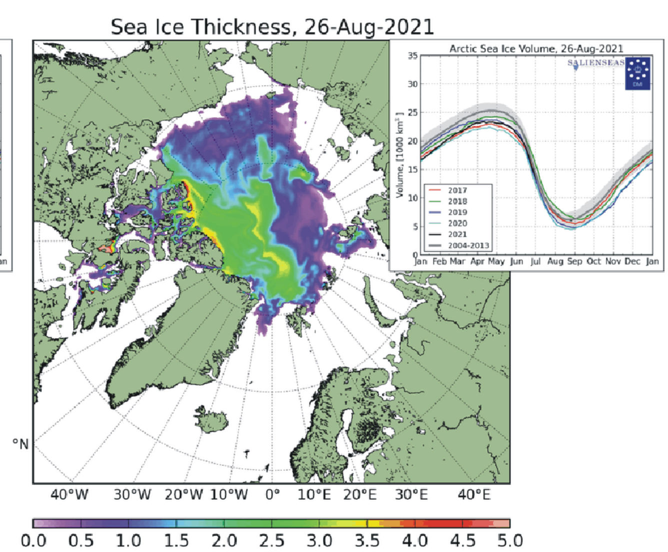

Diagrams showing Arctic sea ice extent and thickness 26 August 2020 (left) and 2021 (right and above) and the seasonal cycles of the calculated total arctic sea ice volume, according to [The Danish Meteorological Institute (DMI)](). The mean sea ice volume and standard deviation for the period 2004-2013 are shown by grey shading.

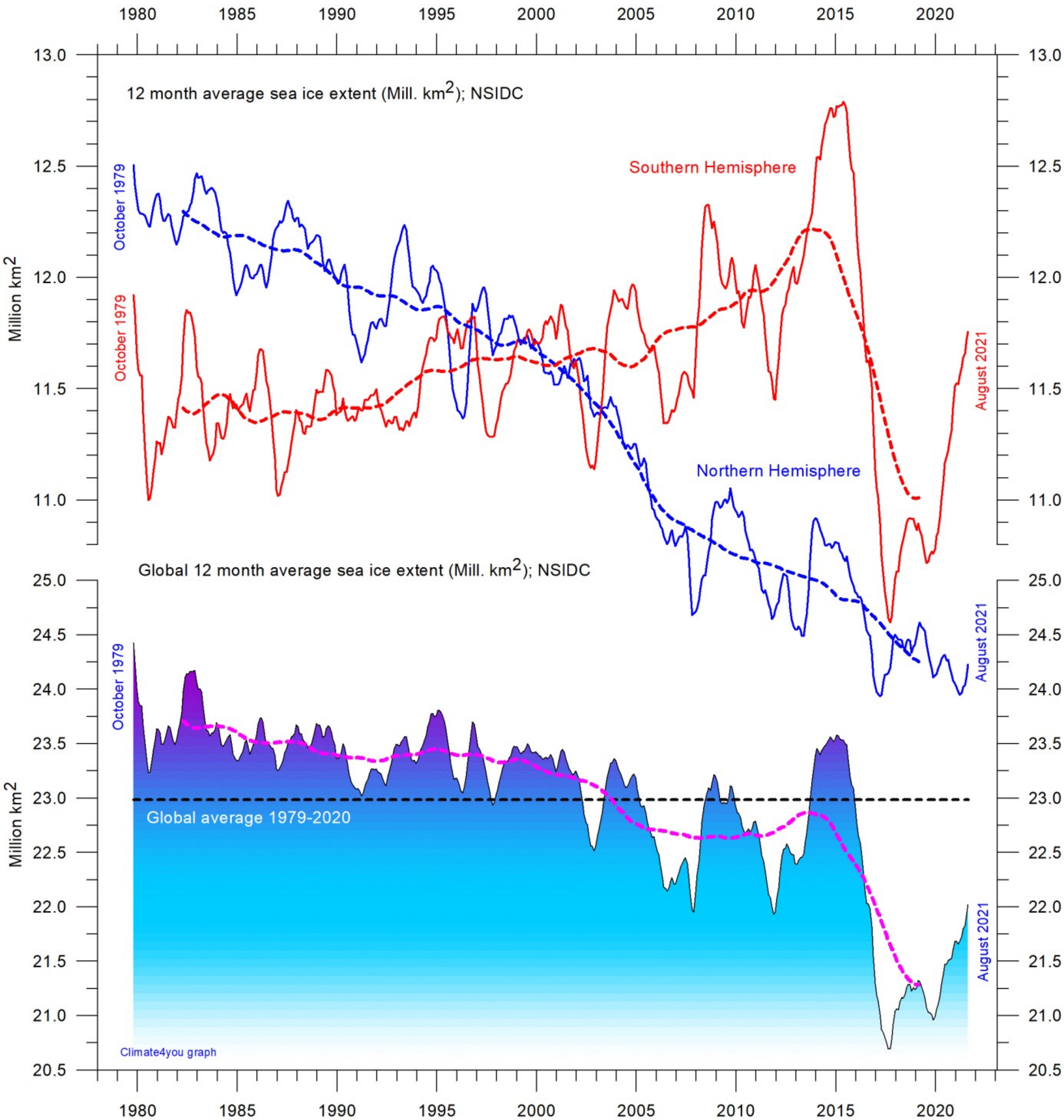

12 month running average sea ice extension, global and in both hemispheres since 1979, the satellite-era. The October 1979 value represents the monthly 12-month average of November 1978 - October 1979, the November 1979 value represents the average of December 1978 - November 1979, etc. The stippled lines represent a 61-month (ca. 5 years) average. Data source: National Snow and Ice Data Center (NSIDC).

Sea level in general

Global (or eustatic) sea-level change is measured relative to an idealised reference level, the geoid, which is a mathematical model of planet Earth's surface (Carter et al. 2014). Global sea-level is a function of the volume of the ocean basins and the volume of water they contain. Changes in global sea-level are caused by – but not limited to - four main mechanisms:

1. Changes in local and regional air pressure and wind, and tidal changes introduced by the Moon.
2. Changes in ocean basin volume by tectonic (geological) forces.
3. Changes in ocean water density caused by variations in currents, water temperature and salinity.
4. Changes in the volume of water caused by changes in the mass balance of terrestrial glaciers.

In addition to these there are other mechanisms influencing sea-level, such as storage of ground water, storage in lakes and rivers, evaporation, etc.

Mechanism 1 is controlling sea-level at many sites on a time scale from months to several years. As an example, many coastal stations show a pronounced annual variation reflecting seasonal changes in air pressures and wind speed. Longer-term climatic changes playing out over decades or centuries will also affect measurements of sea-level changes. Hansen et al. (2011, 2015) provide excellent analyses of sea-level changes caused by recurrent changes of the orbit of the Moon and other phenomena.

Mechanism 2 – with the important exception of earthquakes and tsunamis - typically operates over long (geological) time scales and is not significant on human time scales. It may relate to variations in the seafloor spreading rate, causing volume changes in mid-ocean mountain ridges, and to the slowly changing configuration of land and oceans. Another effect may be the slow rise of basins due to isostatic offloading by deglaciation after an ice age. The floor of the Baltic Sea and the Hudson Bay are presently rising, causing a slow net transfer of water from these basins into the adjoining oceans. Slow changes of excessively big glaciers (ice sheets) and movements in the mantle will affect the gravity field and thereby the vertical position of the ocean surface. Any increase of the total water mass as well as sediment deposition into oceans increase the load on their bottom, generating sinking by viscoelastic flow in the mantle below. The mantle flow is directed towards the surrounding land areas, which will rise, thereby partly compensating for the initial sea level increase induced by the increased water mass in the ocean.

Mechanism 3 (temperature-driven expansion) only affects the uppermost part of the oceans on human time scales. Usually, temperature-driven changes in density are more important than salinity-driven changes. Seawater is characterised by a relatively small coefficient of expansion, but the effect should however not be overlooked, especially when interpreting satellite altimetry data. Temperature-driven expansion of a column of seawater will not affect the total mass of water within the column considered and will therefore not affect the potential at the top of the water column. Temperature-driven ocean water expansion will therefore not in itself lead to any lateral displacement of water, but only locally lift the ocean surface. Near the coast, where people are living, the depth of water approaches zero, so no measurable temperature-driven expansion will take place here (Mörner 2015). Mechanism 3 is for that reason not important for coastal regions.

Mechanism 4 (changes in glacier mass balance) is an important driver for global sea-level changes along coasts, for human time scales. Volume changes of floating glaciers – ice shelves – has no influence on the global sea-level, just like volume changes of floating sea ice has no influence. Only the mass-balance of grounded or land-based glaciers is important for the global sea-level along coasts.

Summing up: Presumably, mechanism 1 and 4 are the most important for understanding sea-level changes along coasts.

References:

Carter R.M., de Lange W., Hansen, J.M., Humlum O., Idso C., Kear, D., Legates, D., Mörner, N.A., Ollier C., Singer F. & Soon W. 2014. Commentary and Analysis on the Whitehead& Associates 2014 NSW Sea-Level Report. Policy Brief, NIPCC, 24. September 2014, 44 pp. http://climatechangereconsidered.org/wp-content/uploads/2014/09/NIPCC-Report-on-NSW-Coastal-SL-9z-corrected.pdf

Hansen, J.-M., Aagaard, T. and Binderup, M. 2011. Absolute sea levels and isostatic changes of the eastern North Sea to central Baltic region during the last 900 years. Boreas, 10.1111/j.1502-3885.2011.00229.x. ISSN 0300–9483.

Hansen, J.-M., Aagaard, T. and Huijpers, A. 2015. Sea-Level Forcing by Synchronization of 56- and 74-YearOscillations with the Moon's Nodal Tide on the Northwest European Shelf (Eastern North Sea to Central Baltic Sea). Journ. Coastal Research, 16 pp.

Mörner, Nils-Axel 2015. Sea Level Changes as recorded in nature itself. Journal of Engineering Research and Applications, Vol.5, 1, 124-129.

Global sea level from satellite altimetry, updated to September 2020

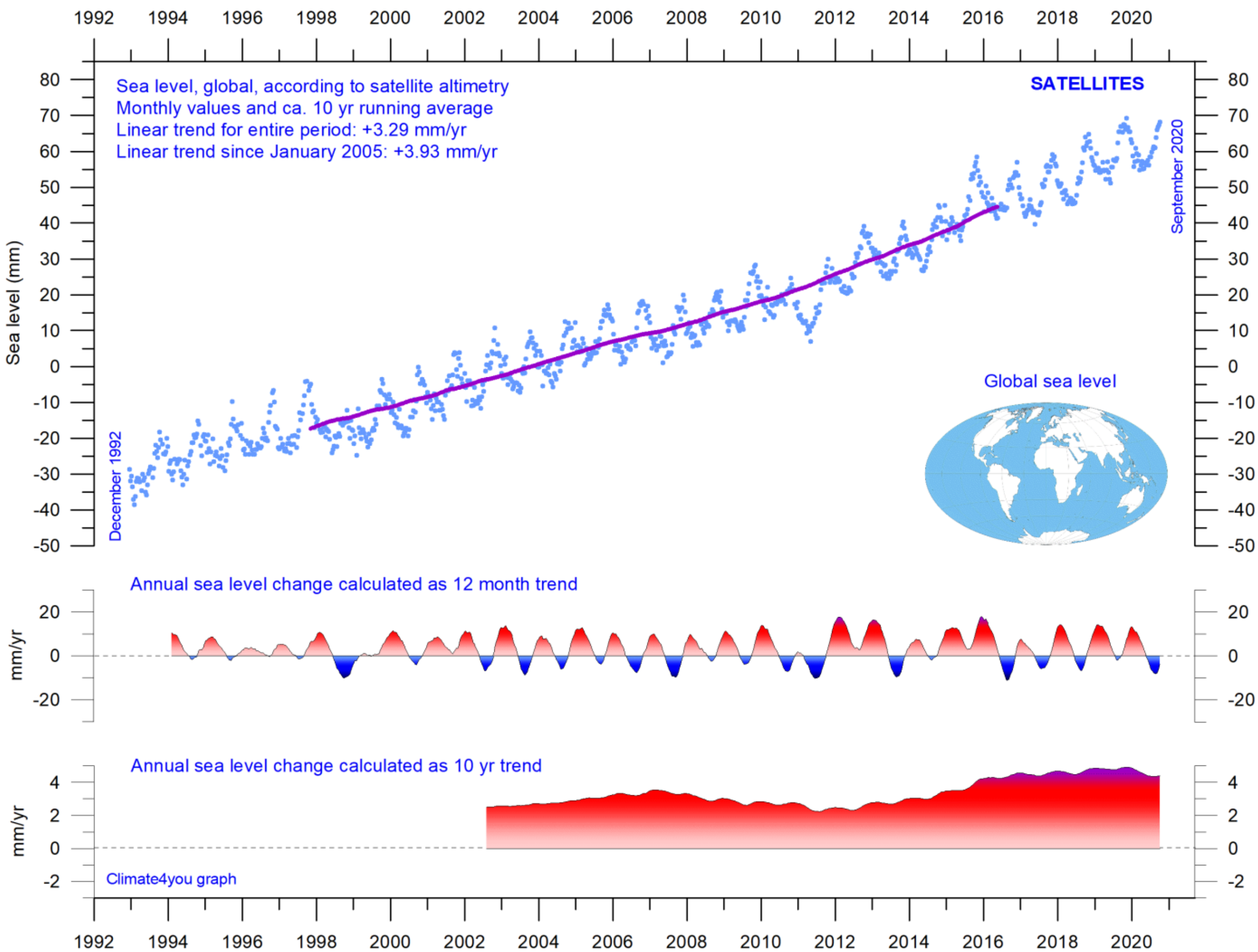

Global sea level since December 1992 according to the Colorado Center for Astrodynamics Research at University of Colorado at Boulder. The blue dots are the individual observations, and the purple line represents the running 121-month (ca. 10 year) average. The two lower panels show the annual sea level change, calculated for 1 and 10-year time windows, respectively. These values are plotted at the end of the interval considered.

Ground truth is a term used in various fields to refer to information provided by direct observation as opposed to information provided by inference, such as, e.g., by satellite observations.

In remote sensing using satellite observations, ground truth data refers to information collected on location. Ground truth allows the satellite data to be related to real features observed on the planet surface. The collection of ground truth data enables calibration of remote-sensing data, and aids in the interpretation and analysis of what is being sensed or recorded by satellites. Ground truth sites allow the remote sensor operator to correct and improve the interpretation of satellite data.

For satellite observations on sea level ground true data are provided by the classical tide gauges (example diagram on next page), that directly measures the local sea level many places distributed along the coastlines on the surface of the planet.

Global sea level from tide-gauges, updated to December 2018

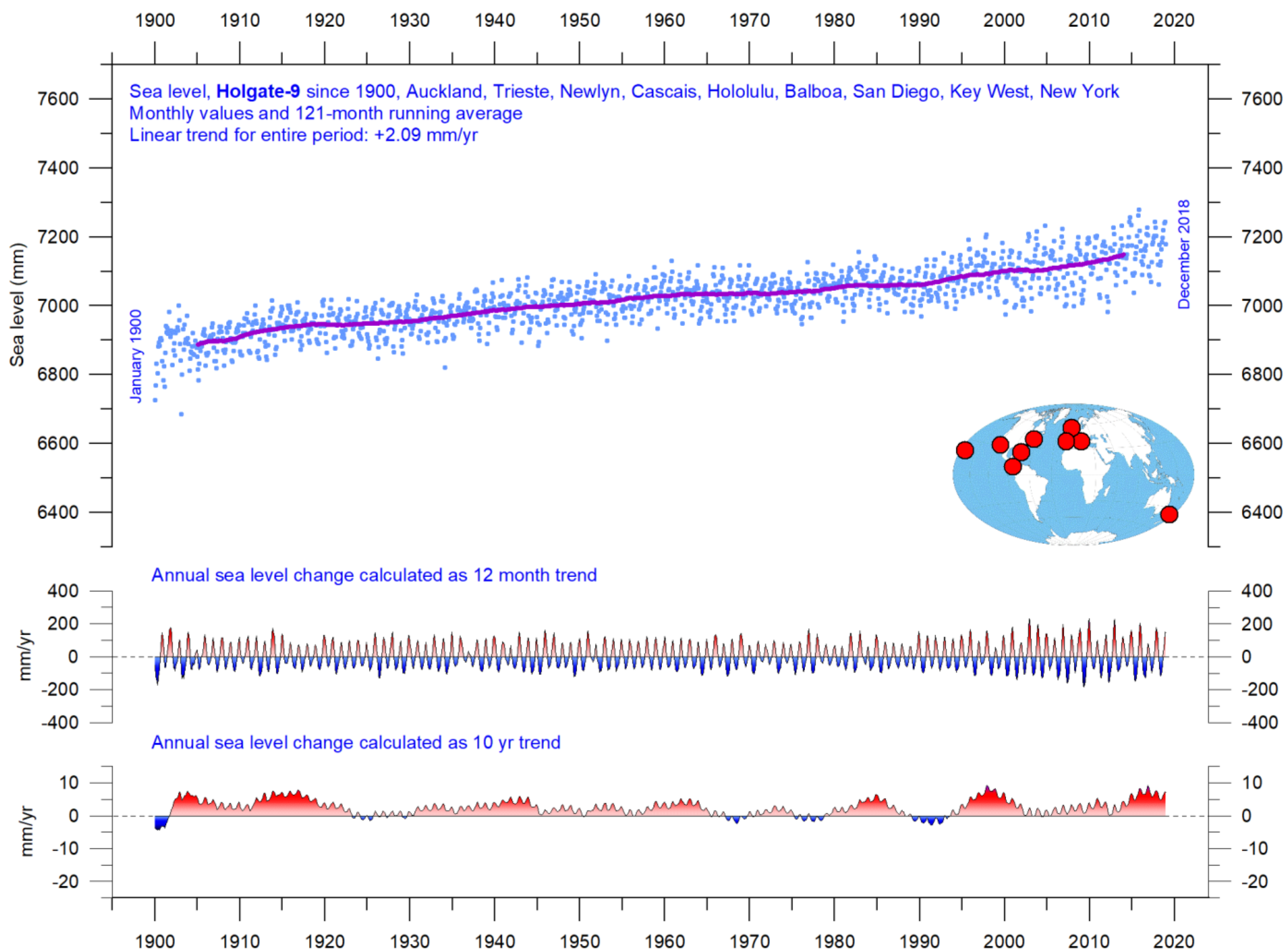

Holgate-9 monthly tide gauge data from PSMSL Data Explorer. Holgate (2007) suggested the nine stations listed in the diagram to capture the variability found in a larger number of stations over the last half century studied previously. For that reason, average values of the Holgate-9 group of tide gauge stations are interesting to follow, even though Auckland (New Zealand) has not reported data since 2000, and Cascais (Portugal) not since 1993. Unfortunately, by this data loss the Holgate-9 series since 2000 is underrepresented with respect to the southern hemisphere and should therefore not be overinterpreted. The blue dots are the individual average monthly observations, and the purple line represents the running 121-month (ca. 10 year) average. The two lower panels show the annual sea level change, calculated for 1 and 10-year windows, respectively. These values are plotted at the end of the interval considered.

Data from tide-gauges all over the world suggest an average global sea-level rise of 1-2 mm/year, while the satellite-derived record (page 37) suggest a rise of about 3.3 mm/year, or more. The noticeable difference (about 1:2) between the two data sets is remarkable but has no generally accepted explanation. It is however known that satellite observations are facing several complications in areas near the coast. Vignudelli et al. (2019) provide an updated overview of the current limitations of classical satellite altimetry in coastal regions.

References:

Holgate, S.J. 2007. On the decadal rates of sea level change during the twentieth century. Geophys. Res. Letters, 34, L01602, doi:10.1029/2006GL028492

Vignudelli et al. 2019. Satellite Altimetry Measurements of Sea Level in the Coastal Zone. *Surveys in Geophysics, Vol.* 40, p. 1319–1349. https://link.springer.com/article/10.1007/s10712-019-09569-1

Northern Hemisphere weekly and seasonal snow cover, updated to August 2021

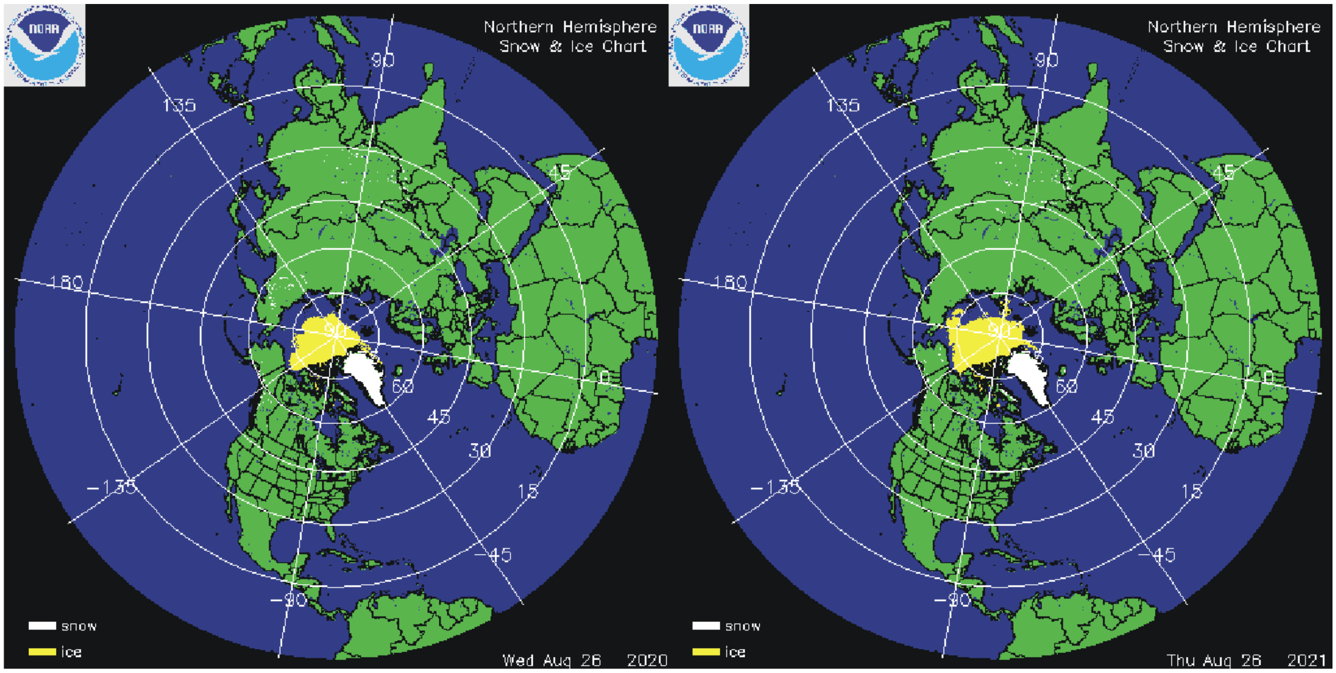

Northern hemisphere snow cover (white) and sea ice (yellow) 26 August 2020 (left) and 2021 (right). Map source: [National Ice Center](#) (NIC).

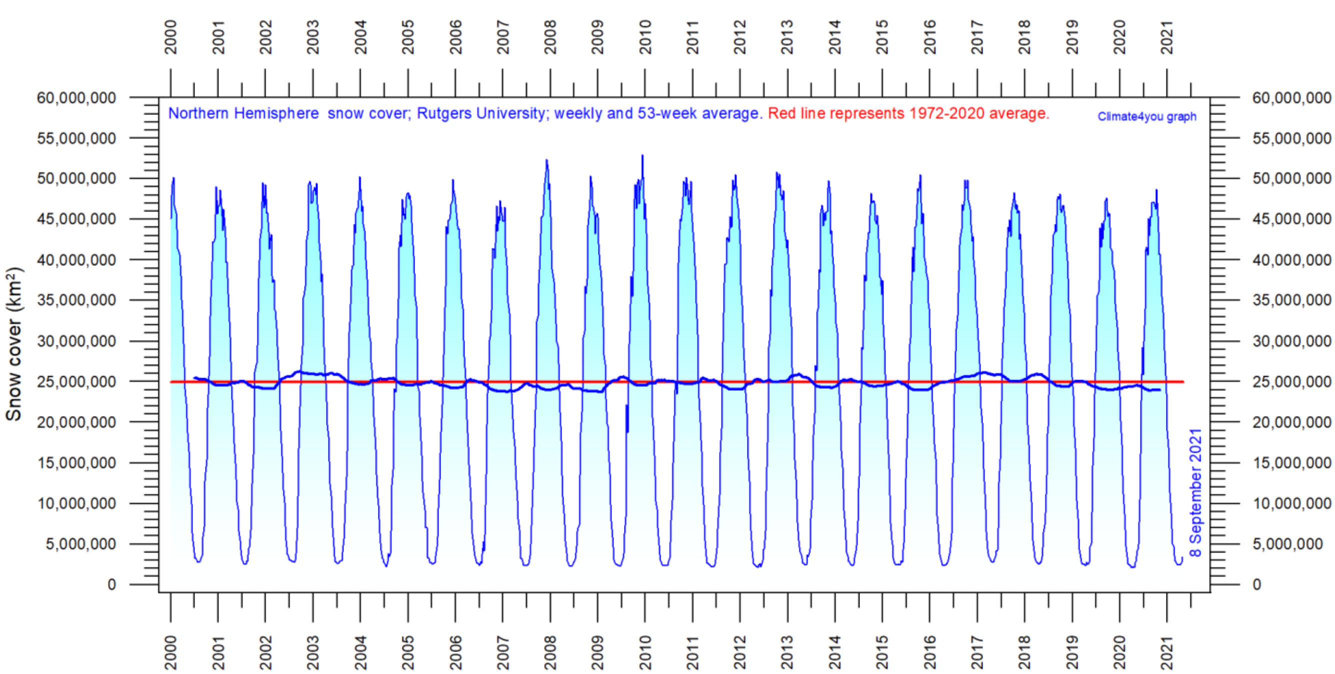

Northern hemisphere weekly snow cover since January 2000 according to Rutgers University Global Snow Laboratory. The thin blue line is the weekly data, and the thick blue line is the running 53-week average (approximately 1 year). The horizontal red line is the 1972-2020 average.

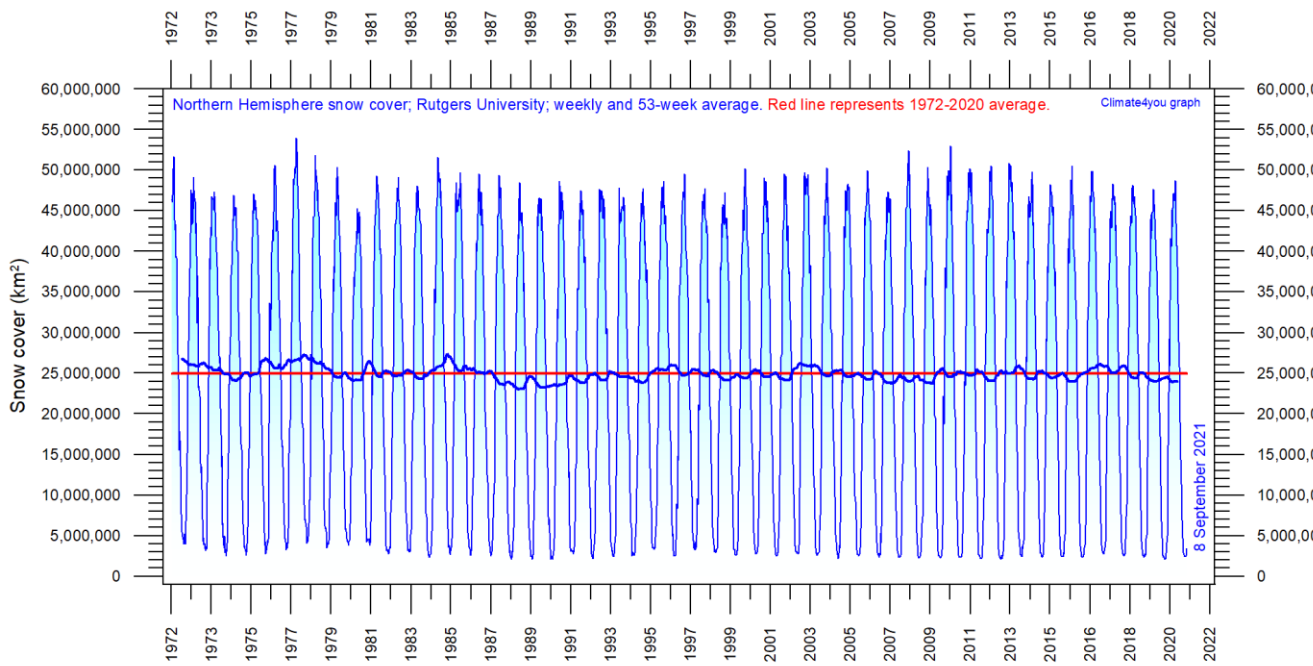

Northern hemisphere weekly snow cover since January 1972 according to Rutgers University Global Snow Laboratory. The thin blue line is the weekly data, and the thick blue line is the running 53-week average (approximately 1 year). The horizontal red line is the 1972-2020 average.

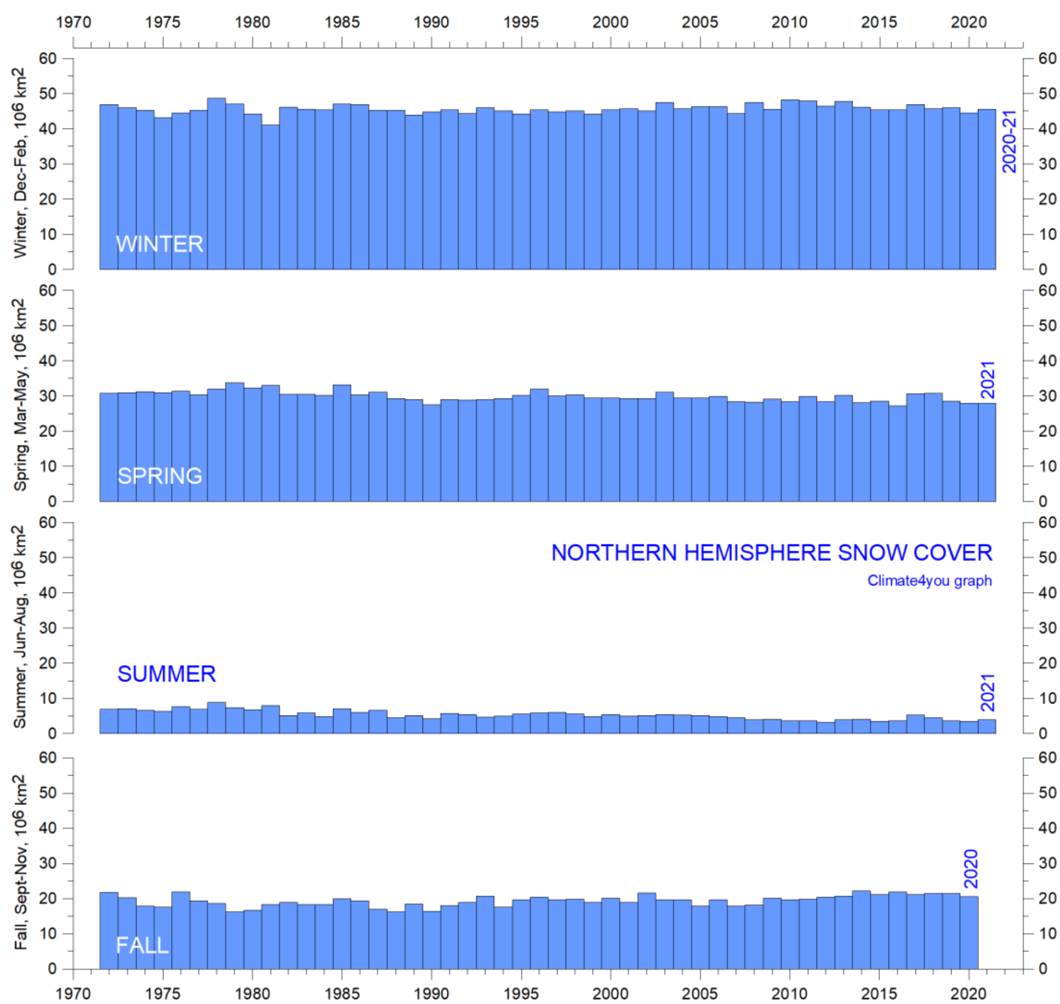

Northern hemisphere seasonal snow cover since January 1972 according to Rutgers University Global Snow Laboratory.

Atmospheric specific humidity, updated to August 2021

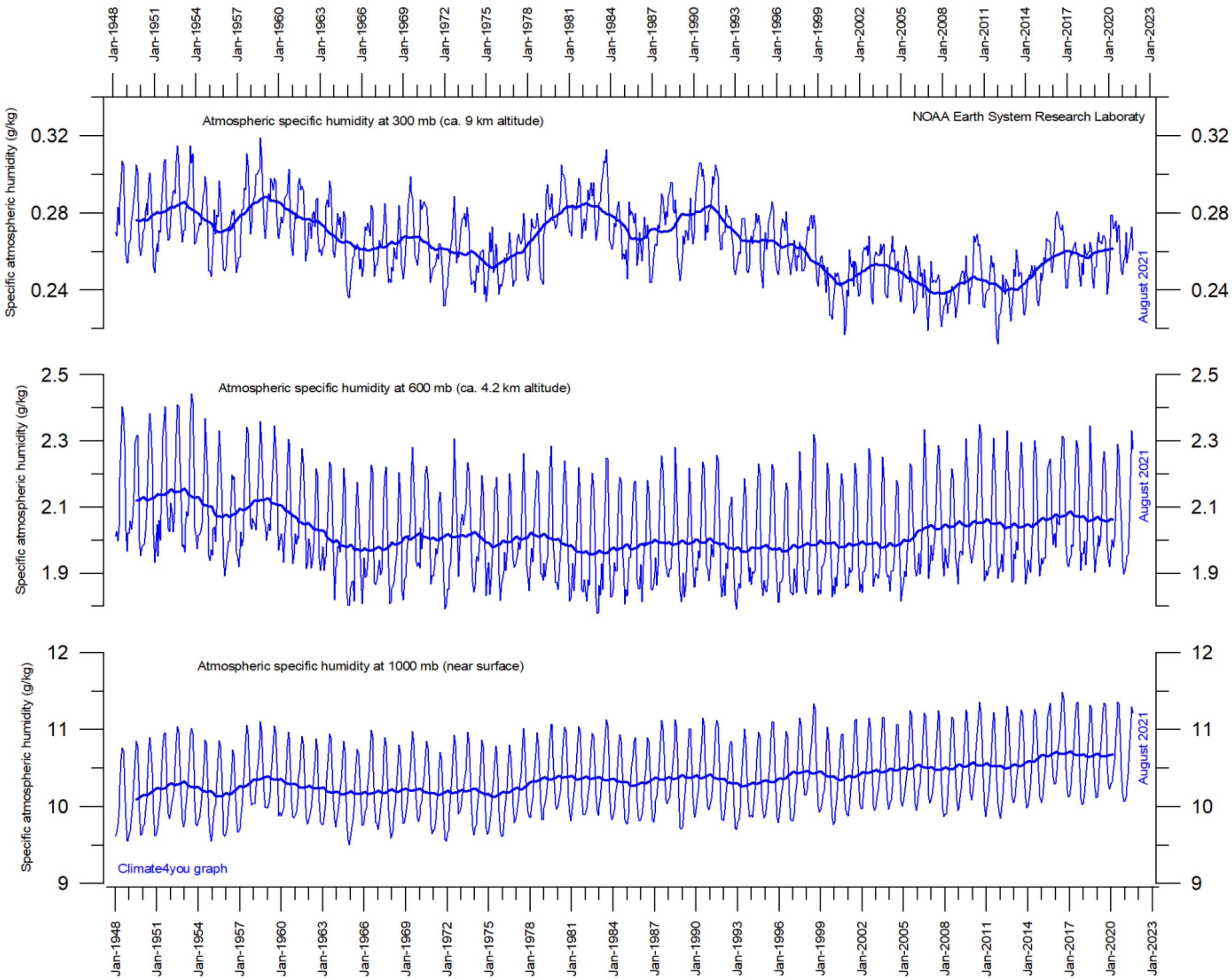

Specific atmospheric humidity (g/kg) at three different altitudes in the lower part of the atmosphere (the Troposphere) since January 1948 (Kalnay et al. 1996). The thin blue lines show monthly values, while the thick blue lines show the running 37-month average (about 3 years). Data source: Earth System Research Laboratory (NOAA).

Water vapor is the most important greenhouse gas in the Troposphere. The highest concentration is found within a latitudinal range from 50°N to 60°S. The two polar regions of the Troposphere are comparatively dry.

The diagram above shows the specific atmospheric humidity to be stable or slightly increasing up to about 4-5 km altitude. At higher levels in the Troposphere (about 9 km), the specific humidity has been decreasing for the duration of the record (since 1948), but with shorter variations superimposed on the falling trend. A Fourier frequency analysis (not shown here) shows these variations to be influenced especially by a periodic variation of about 3.7-year duration.

The persistent decrease in specific humidity at about 9 km altitude is particularly noteworthy, as this altitude roughly corresponds to the level where the theoretical temperature effect of increased atmospheric CO_2 is expected initially to play out.

Atmospheric CO_2, updated to August 2021

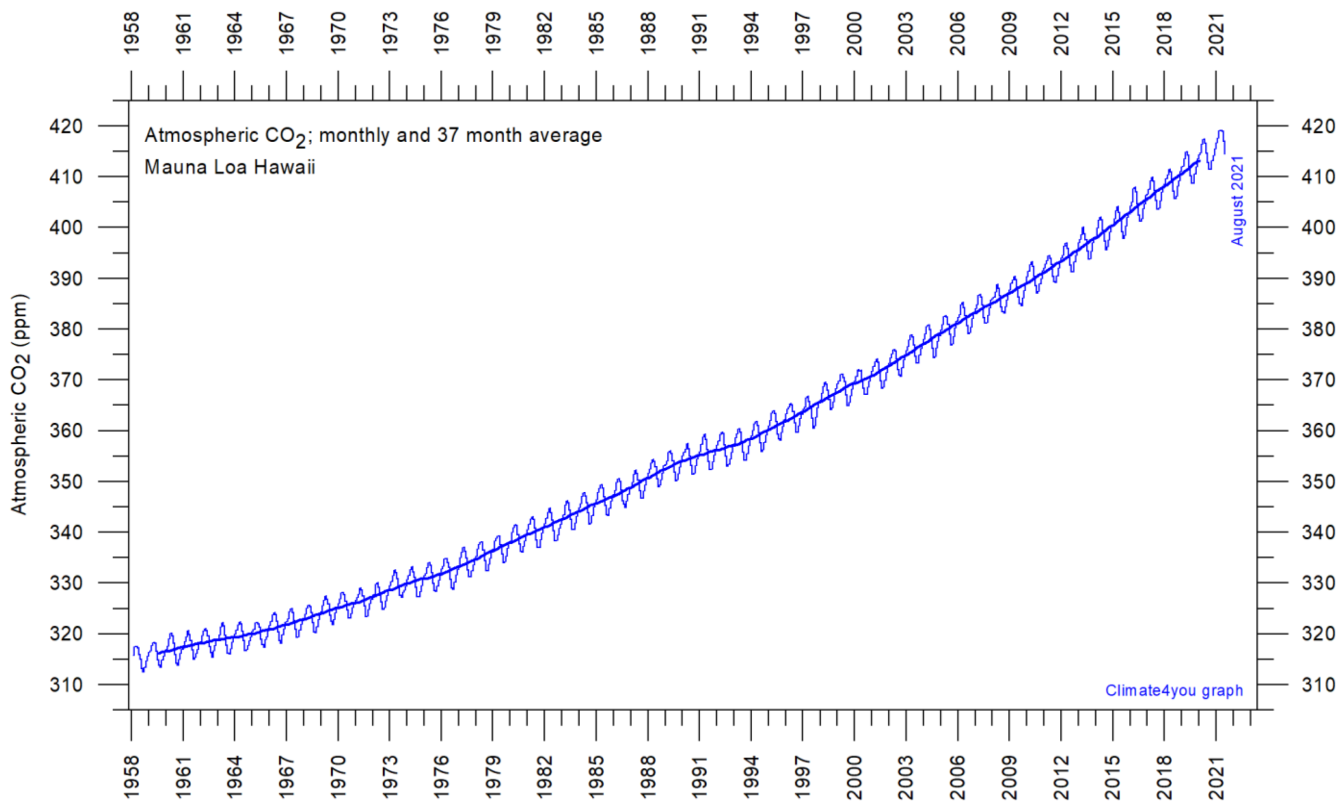

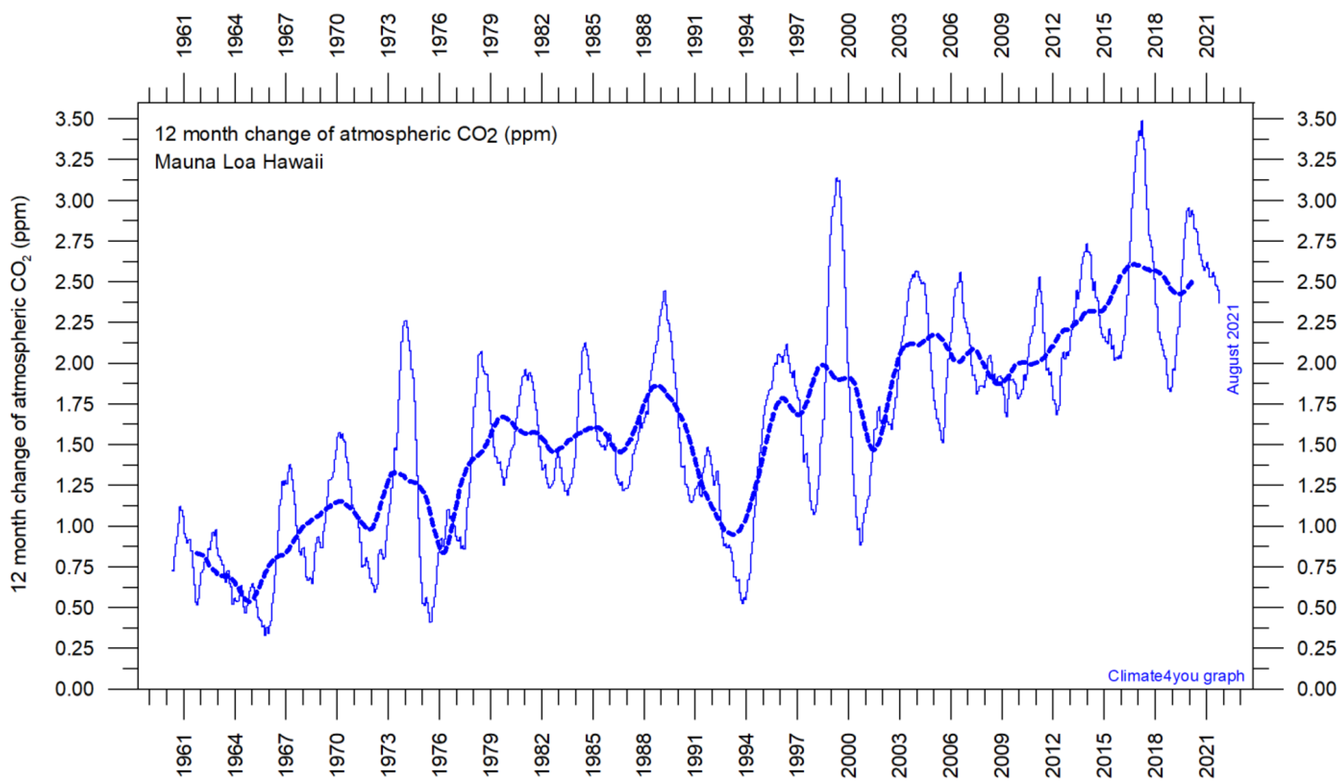

Monthly amount of atmospheric CO_2 (upper diagram) and annual growth rate (lower diagram); average last 12 months minus average preceding 12 months, thin line) of atmospheric CO_2 since 1959, according to data provided by the [Mauna Loa Observatory](), Hawaii, USA. The thick, stippled line is the simple running 37-observation average, nearly corresponding to a running 3-year average. A Fourier frequency analysis (not shown here) shows the 12-month change of Tropospheric CO2 to be influenced especially by periodic variations of 2.5- and 3.8-years' duration.

The relation between annual change of atmospheric CO_2 and La Niña and El Niño episodes, updated to August 2021

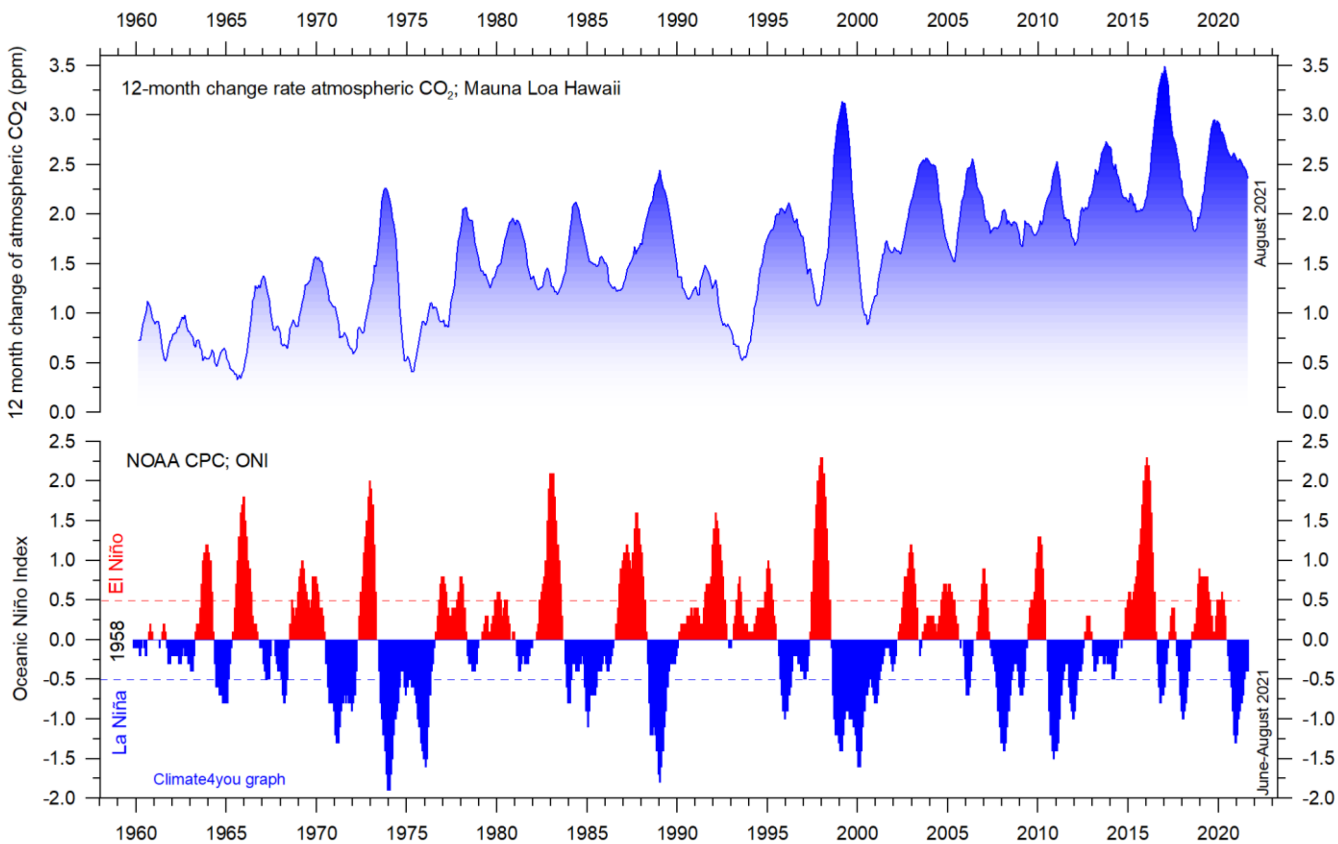

Visual association between annual growth rate of atmospheric CO_2 (upper panel) and Oceanic Niño Index (lower panel). See also diagrams on page 40 and 22, respectively.

Changes in the global atmospheric CO_2 is seen to vary roughly in concert with changes in the Oceanic Niño Index. The typical sequence of events is that changes in the global atmospheric CO_2 to a certain degree follows changes in the Oceanic Niño Index, but clearly not in all details. Many processes, natural as well as anthropogenic, controls the amount of atmospheric CO_2, but oceanographic processes are clearly particularly important (see also diagram on next page).

Atmospheric CO_2 and the present coronavirus pandemic

Modern political initiatives usually assume the human influence (mainly the burning of fossil fuels) to represent the core reason for the observed increase in atmospheric CO_2 since 1958 (diagrams on page 42).

The coronavirus pandemic since January 2020 resulted in a marked reduction in the global consumption of fossil fuels. It is therefore enlightening to follow the effect of this reduction on the amount of atmospheric CO_2.

However, there is still no clear effect to be seen of the above reduction in release of CO_2 from fossil fuels. Presumably, the main explanation for this is that the human contribution is too small compared to the numerous natural sources and sinks for atmospheric CO_2 to appear in diagrams showing the amount of atmospheric CO_2 (see, e.g., the diagrams on p. 42-44).

The phase relation between atmospheric CO_2 and global temperature, updated to June 2021

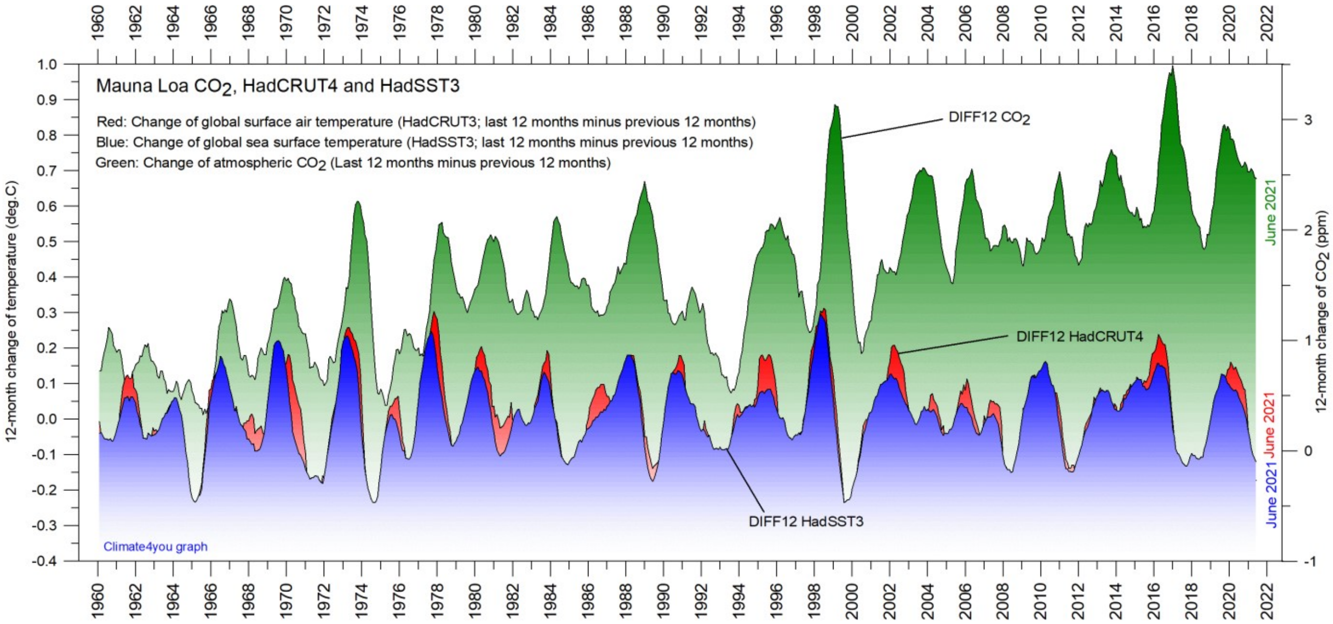

12-month change of global atmospheric CO_2 concentration (Mauna Loa; green), global sea surface temperature (HadSST3; blue) and global surface air temperature (HadCRUT4; red dotted). All graphs are showing monthly values of DIFF12, the difference between the average of the last 12 month and the average for the previous 12 months for each data series.

The typical sequence of events is seen to be that changes in the global atmospheric CO_2 follow changes in global surface air temperature, which again follow changes in global ocean surface temperatures. Thus, changes in global atmospheric CO_2 are lagging 9.5–10 months behind changes in global air surface temperature, and 11–12 months behind changes in global sea surface temperature.

References:

Humlum, O., Stordahl, K. and Solheim, J-E. 2012. The phase relation between atmospheric carbon dioxide and global temperature. Global and Planetary Change, August 30, 2012.
http://www.sciencedirect.com/science/article/pii/S0921818112001658?v=s5

Global air temperature and atmospheric CO_2, updated to August 2021

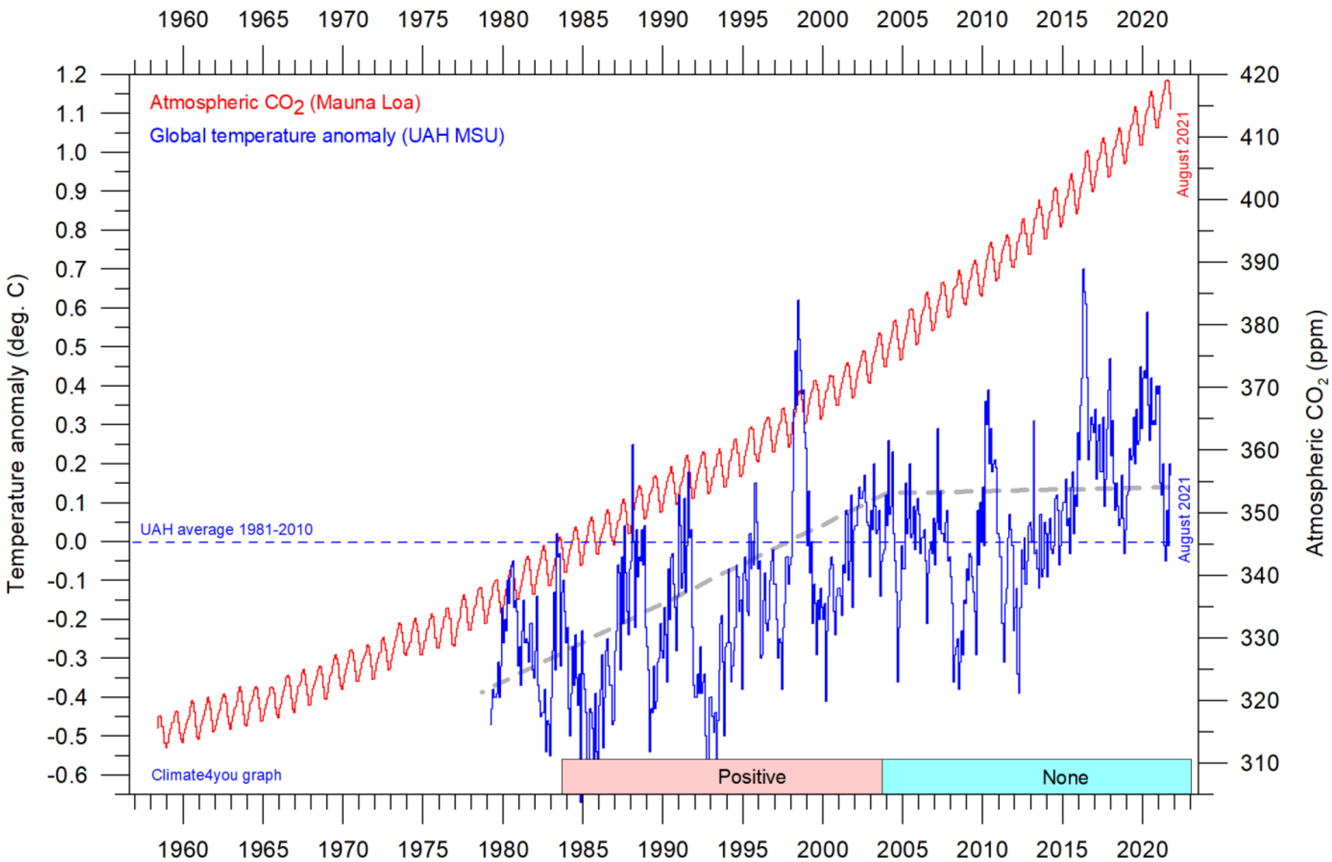

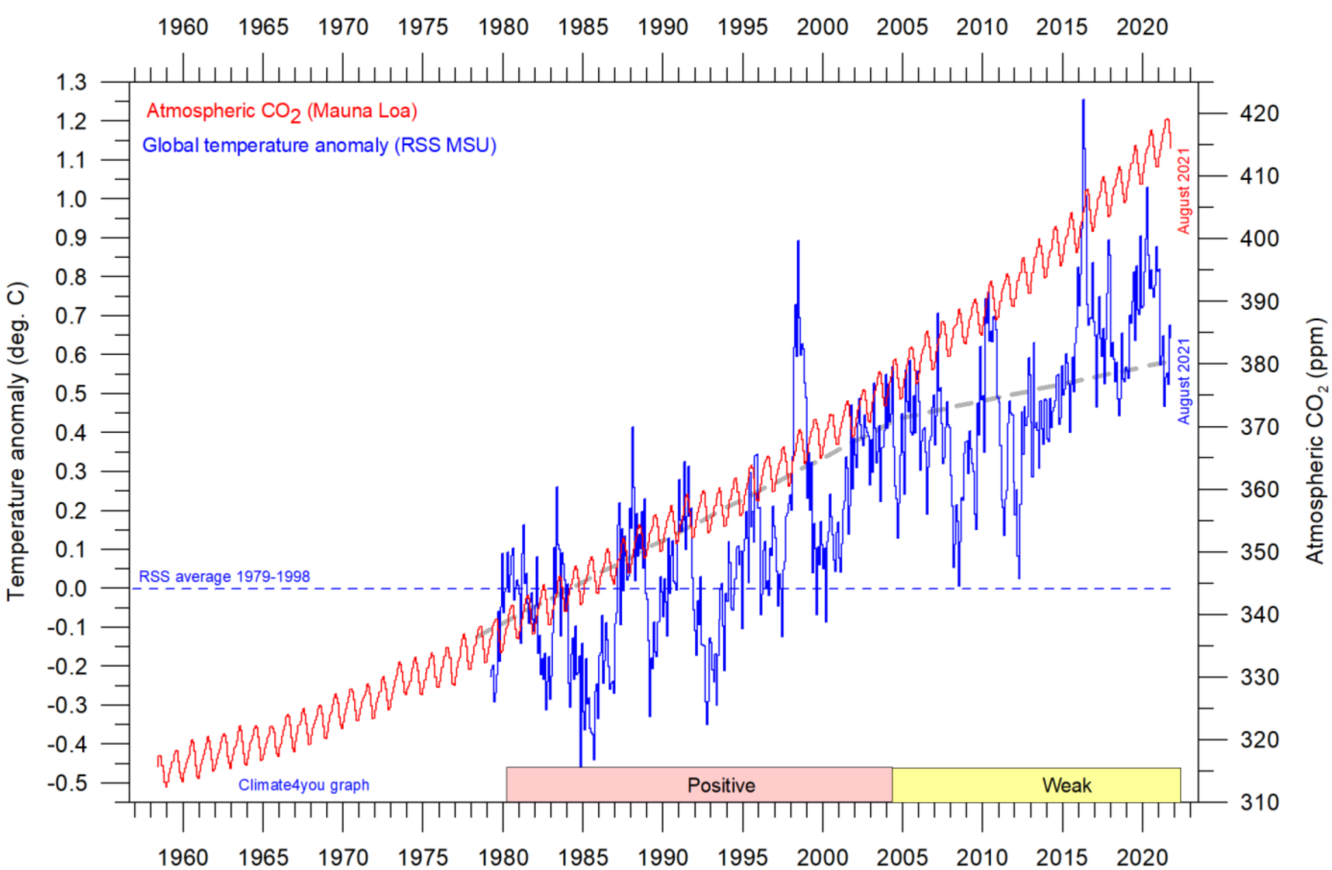

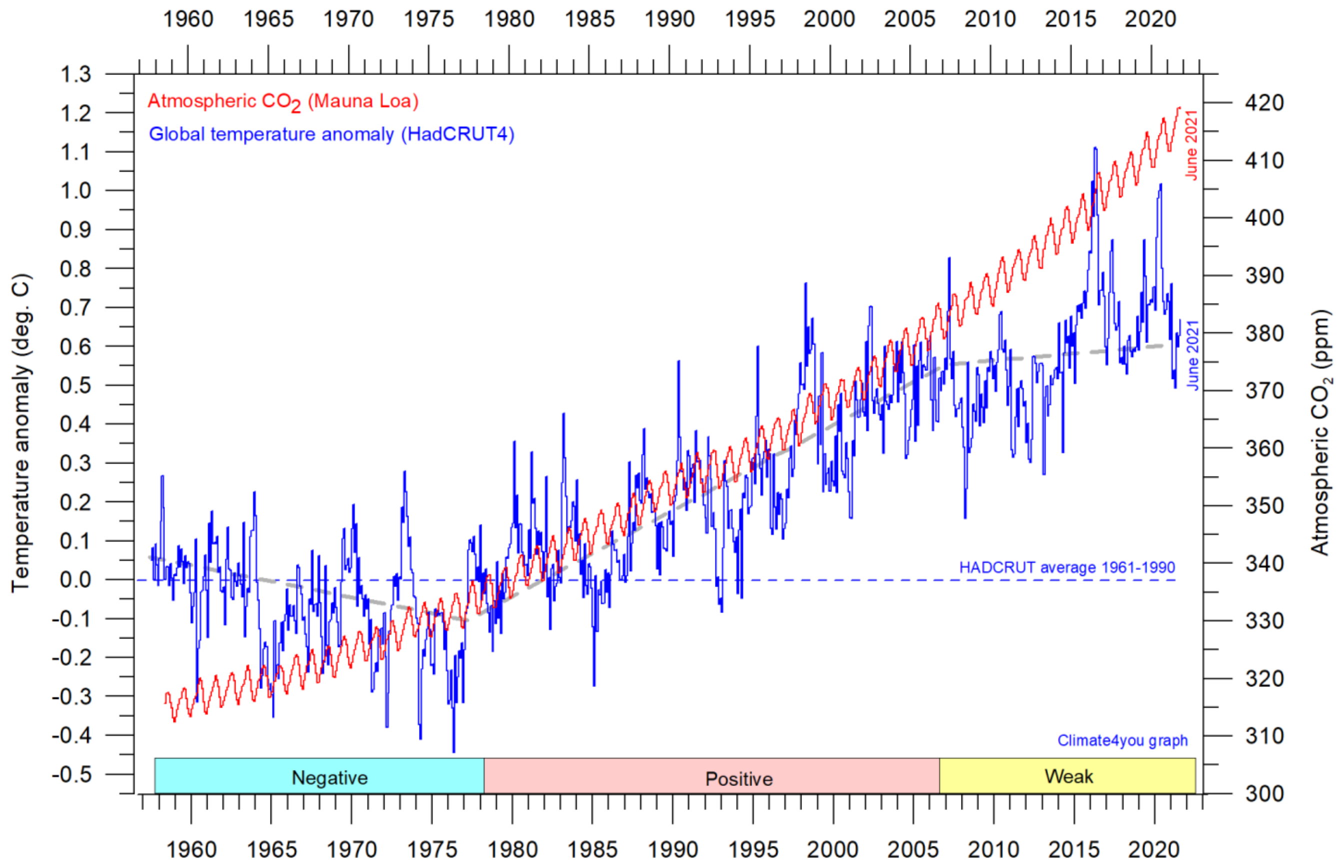
Atmospheric CO2 (Mauna Loa)
Global temperature anomaly (HadCRUT4)
Temperature anomaly (deg. C)
Atmospheric CO2 (ppm)
June 2021
June 2021
HADCRUT average 1961-1990
Climate4you graph
Negative
Positive
Weak

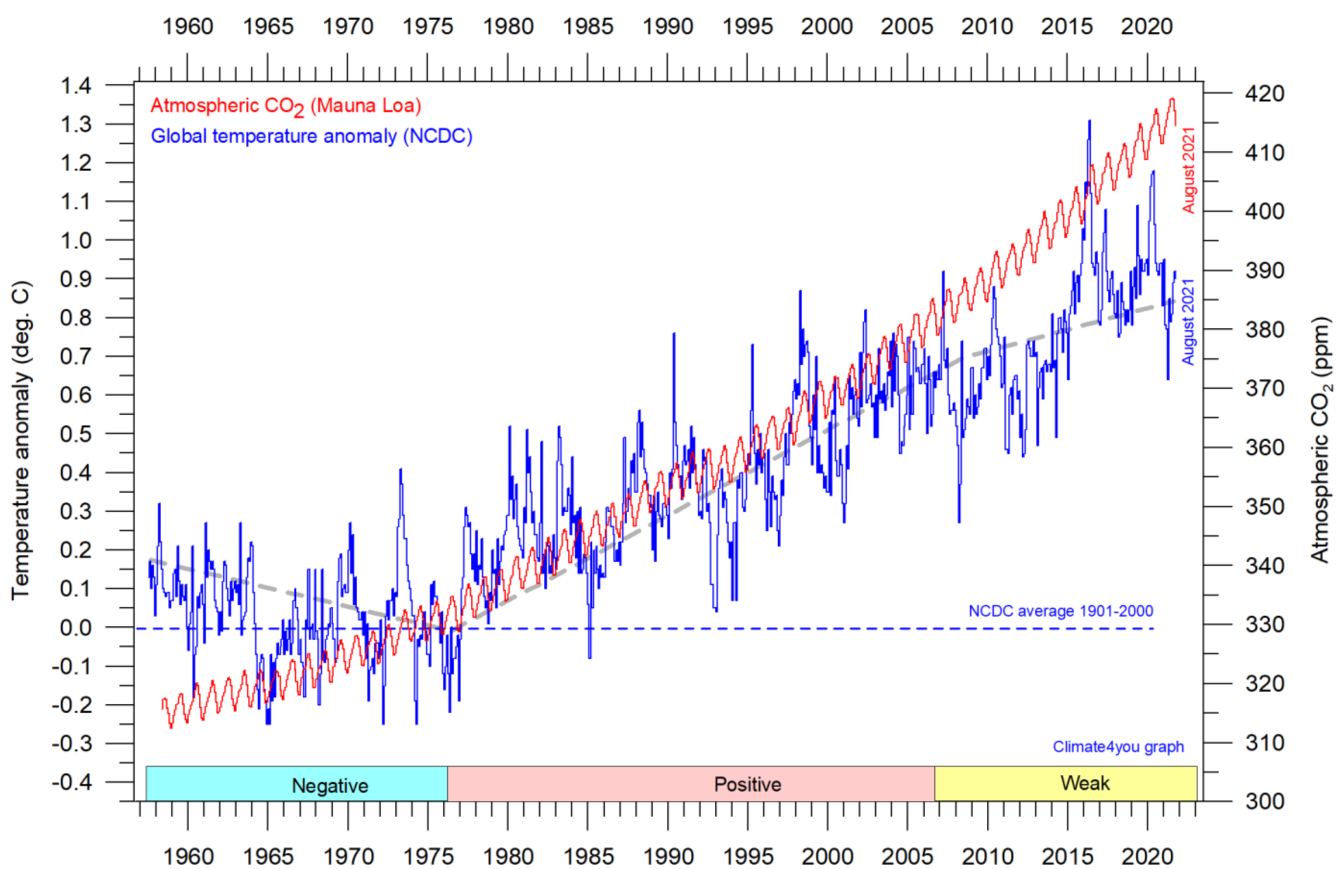
Atmospheric CO2 (Mauna Loa)
Global temperature anomaly (NCDC)
Temperature anomaly (deg. C)
Atmospheric CO2 (ppm)
August 2021
August 2021
NCDC average 1901-2000
Climate4you graph
Negative
Positive
Weak

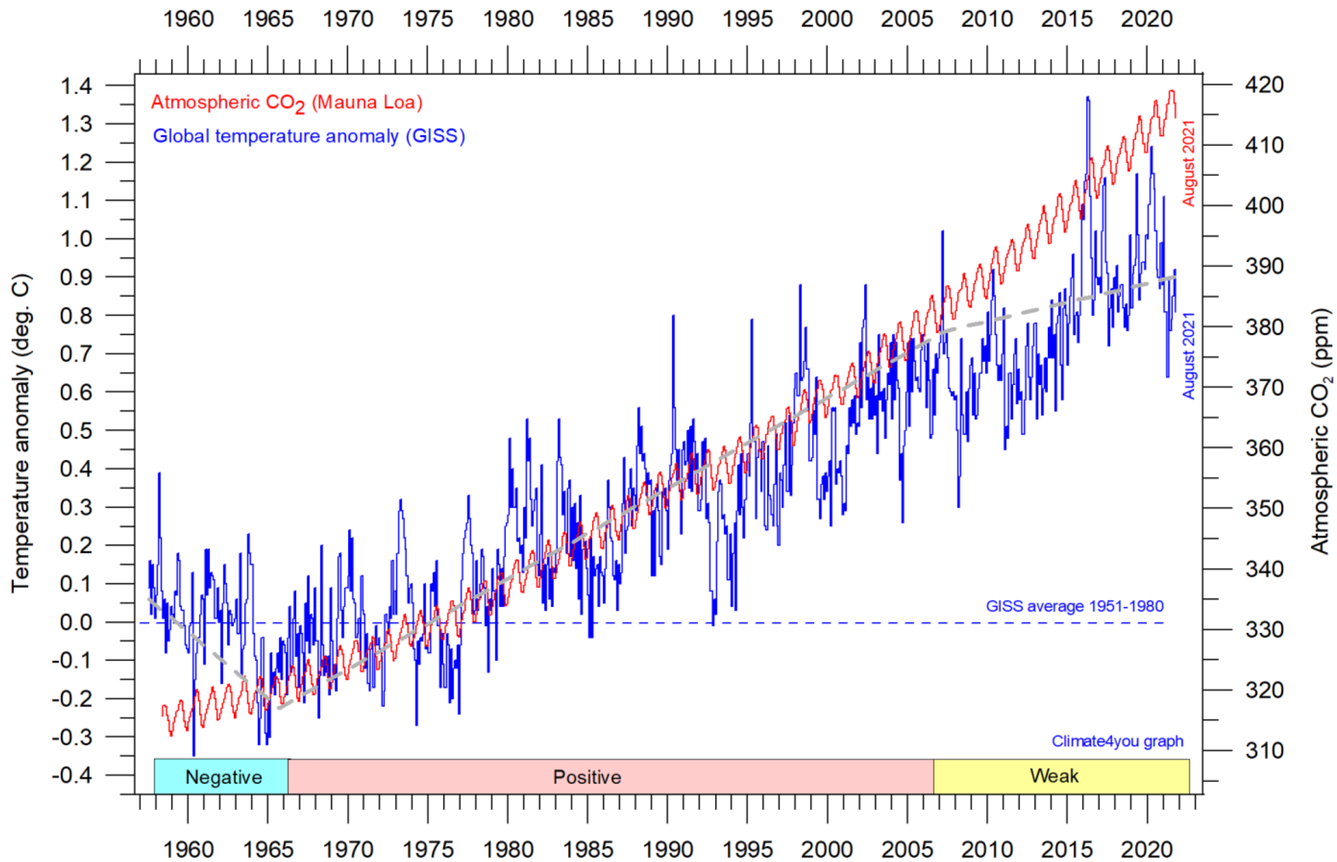

Diagrams showing UAH, RSS, HadCRUT4, NCDC and GISS monthly global air temperature estimates (blue) and the monthly atmospheric CO_2 content (red) according to the [Mauna Loa Observatory](), Hawaii. The Mauna Loa data series begins in March 1958, and 1958 was therefore chosen as starting year for all diagrams above. Reconstructions of past atmospheric CO_2 concentrations (before 1958) are not incorporated in this diagram, as such past CO_2 values are derived by other means (ice cores, stomata, or older measurements using different methodology), and therefore are not directly comparable with direct atmospheric measurements. The dotted grey line indicates the approximate linear temperature trend, and the boxes in the lower part of the diagram indicate the relation between atmospheric CO_2 and global surface air temperature, negative or positive.

Most climate models are programmed to give the greenhouse gas carbon dioxide CO_2 significant influence on the calculated global air temperature. It is therefore relevant to compare different air temperature records with measurements of atmospheric CO_2, as shown in the diagrams above.

Any comparison, however, should not be made on a monthly or annual basis, but for a longer time, as other effects (oceanographic, cloud cover, etc.) may override the potential influence of CO_2 on short time scales such as just a few years.

It is of cause equally inappropriate to present new meteorological record values, whether daily, monthly, or annual, as demonstrating the legitimacy of the hypothesis ascribing high importance of atmospheric CO_2 for global air temperatures. Any such meteorological record value may well be the result of other phenomena. Unfortunately, many media repeatedly fall into this trap.

What exactly defines the critical length of a relevant period length to consider for evaluating the alleged importance of CO_2 remains elusive and still represents a theme for discussions.

Nonetheless, the length of the critical period must be inversely proportional to the temperature sensitivity of CO_2, including feedback effects. Thus, if the net temperature effect of atmospheric CO_2 is strong, the critical period will be short, and vice versa.

However, past climate research history provides some clues as to what has traditionally been considered the relevant length of period over which to compare temperature and atmospheric CO_2.

After about 10 years of concurrent global temperature- and CO_2-increase, IPCC was established in 1988. For obtaining public and political support for the CO_2-hyphotesis the 10-year warming period leading up to 1988 most likely was considered important. Had the global temperature instead been decreasing at that time, politic support for the hypothesis probably would have been difficult to obtain in 1988.

Based on the previous 10 years of concurrent temperature- and CO_2-increase, many climate scientists in 1988 presumably felt that their understanding of climate dynamics was enough to conclude about the importance of CO_2 for affecting observed global temperatures.

Thus, it may with confidence be concluded that 10 years in 1988 was considered a period long enough to demonstrate the effect of increasing atmospheric CO_2 on global temperatures. The 10-year period is also basis for the anomality diagrams shown on page 2.

Adopting this approach as to critical time length (at least 10 years), the varying relation (positive or negative) between global temperature and atmospheric CO_2 has been indicated in the lower panels of the diagrams above.

Latest 20-year QC1 global monthly air temperature changes, updated to August 2021

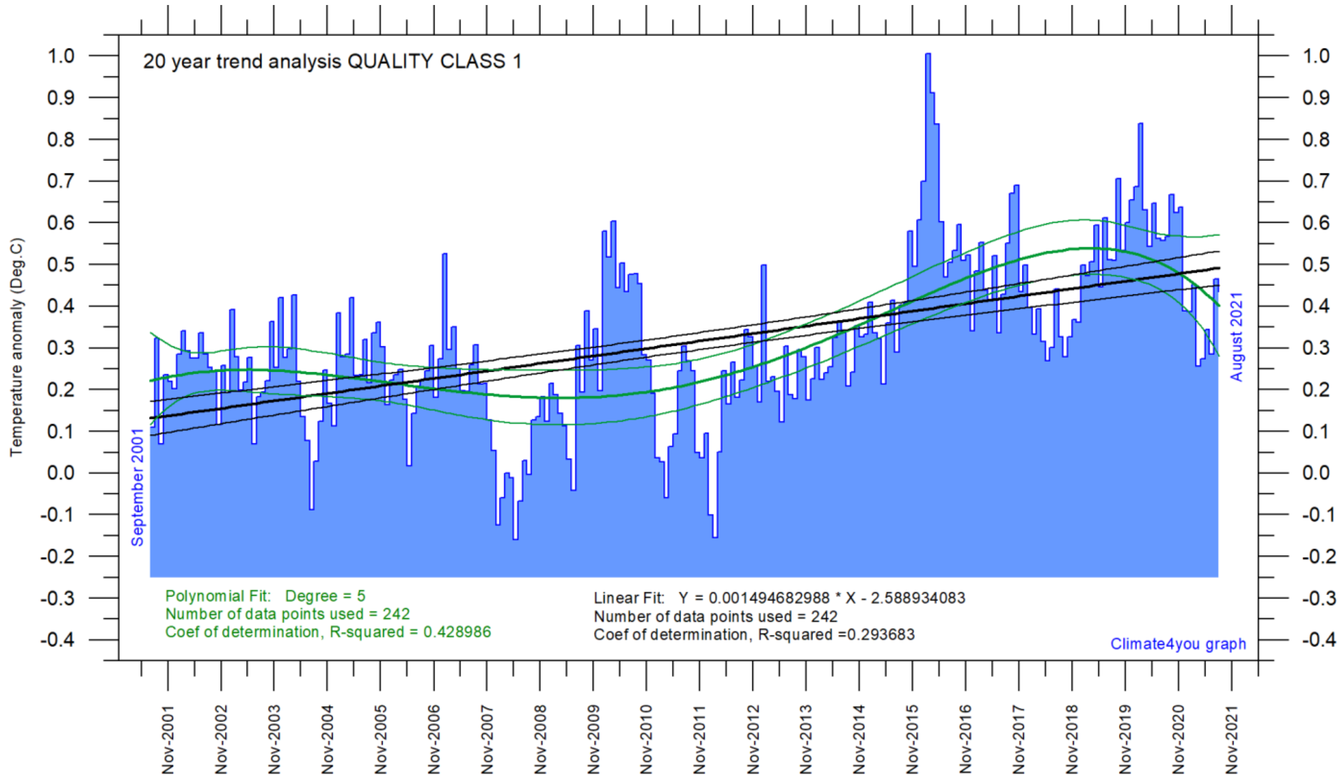

Last 20 years' global monthly average air temperature according to Quality Class 1 (UAH and RSS; see p.6 and 9) global monthly temperature estimates. The thin blue line represents the monthly values. The thick black line is the linear fit, with 95% confidence intervals indicated by the two thin black lines. The thick green line represents a 5-degree polynomial fit, with 95% confidence intervals indicated by the two thin green lines. A few key statistics are given in the lower part of the diagram (please note that the linear trend is the monthly trend).

In the enduring scientific climate debate, the following question is often put forward: Is the surface air temperature still increasing or has it basically remained without significant changes during the last 15-16 years?

The diagram above may be useful in this context and demonstrates the differences between two often used statistical approaches to determine recent temperature trends. Please also note that such fits only attempt to describe the past, and usually have small, if any, predictive power.

In addition, before using any linear trend (or other) analysis of time series a proper statistical model should be chosen, based on statistical justification.

For global temperature time series, there is no *a priori* physical reason why the long-term trend should be linear in time. In fact, climatic time series often have trends for which a straight line is not a good approximation, as is clearly demonstrated by several of the diagrams shown in the present report.

For an commendable description of problems often encountered by analyses of temperature time series analyses, please see Keenan, D.J. 2014: Statistical Analyses of Surface Temperatures in the IPCC Fifth Assessment Report.

See also diagrams on page 12.

Sunspot activity (SIDC) and QC1 average satellite global air temperature, updated to August 2021

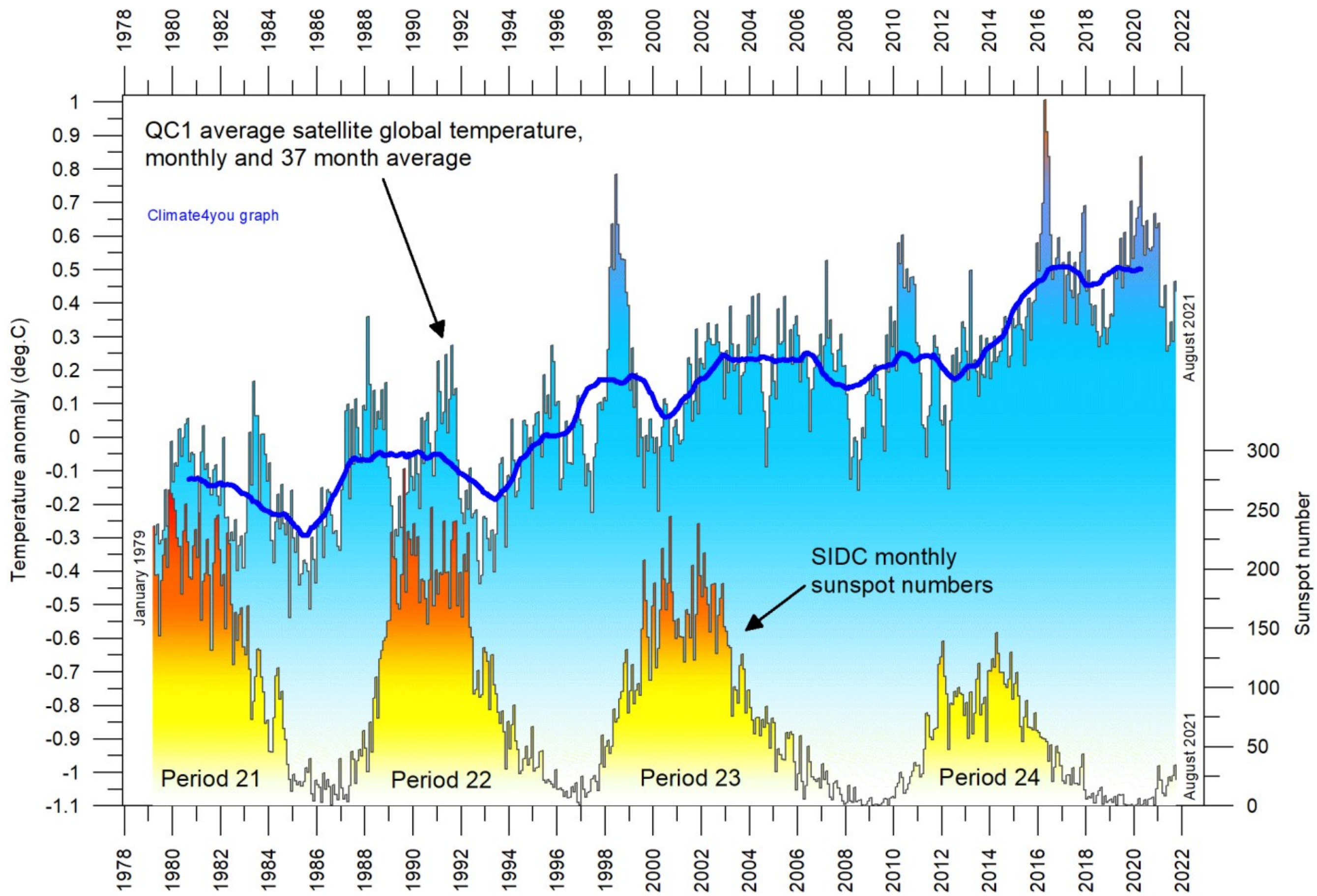

Variation of global monthly air temperature according to Quality Class 1 (UAH and RSS; see p.4) and observed sunspot number as provided by the Solar Influences Data Analysis Center (SIDC), since 1979. The thin lines represent the monthly values, while the thick line is the simple running 37-month average, nearly corresponding to a running 3-year average. The asymmetrical temperature 'bump' around 1998 is influenced by the oceanographic El Niño phenomenon in 1998, as is the case also for 2015-16. Temperatures in year 2019-20 was influenced by a moderate El Niño.

.

Monthly sunspot activity (SIDC) and average neutron counts (Oulu, Finland), updated to August 2021

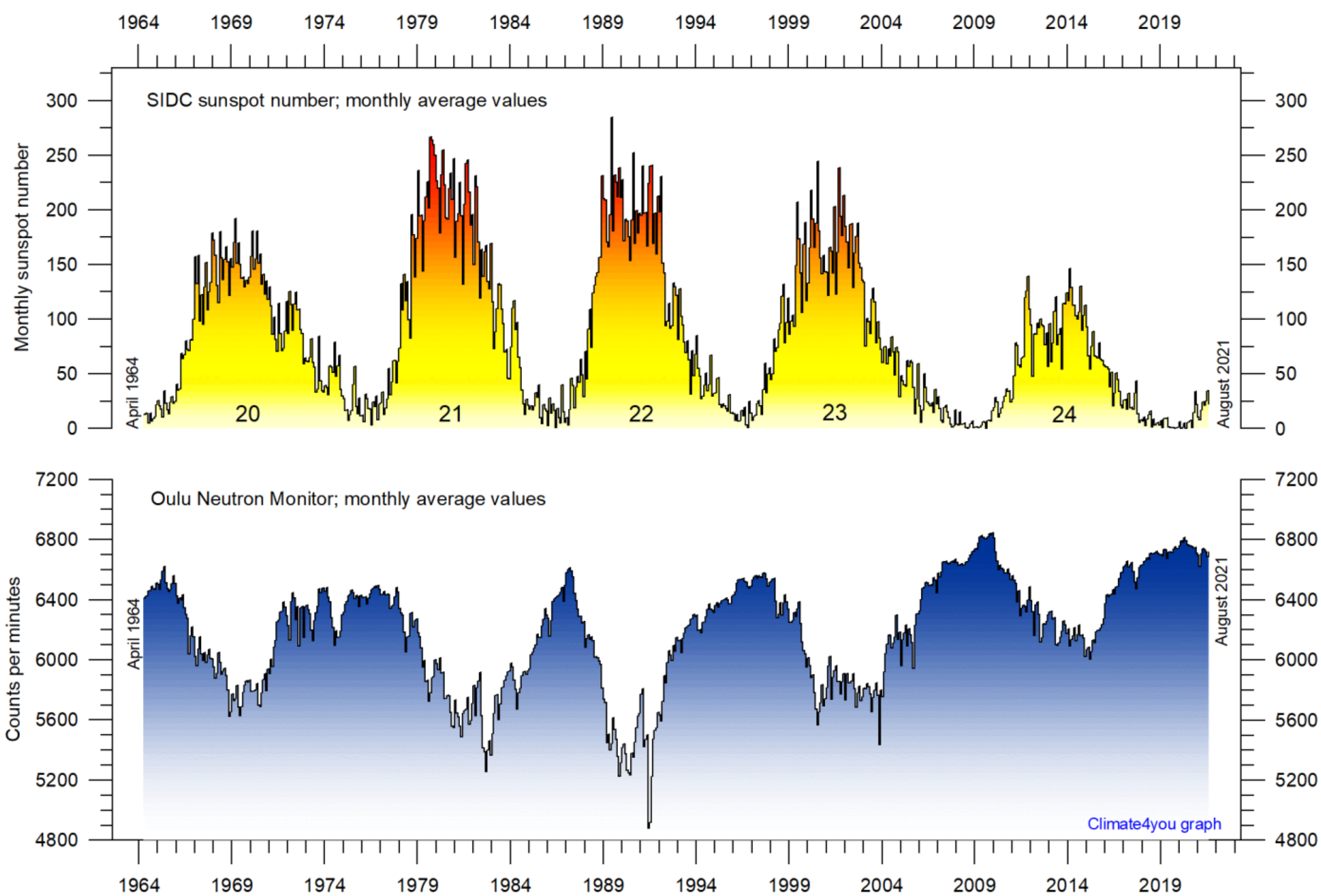

Observed monthly sunspot number (Solar Influences Data Analysis Center (SIDC) since April 1964, and (lower panel) monthly average counts of the Oulu (Finland) neutron monitor, adjusted for barometric pressure and efficiency.

Monthly sunspot activity (SIDC), Oceanic Niño Index (ONI), and change rates of atmospheric CO2 and specific humidity, updated to August 2021

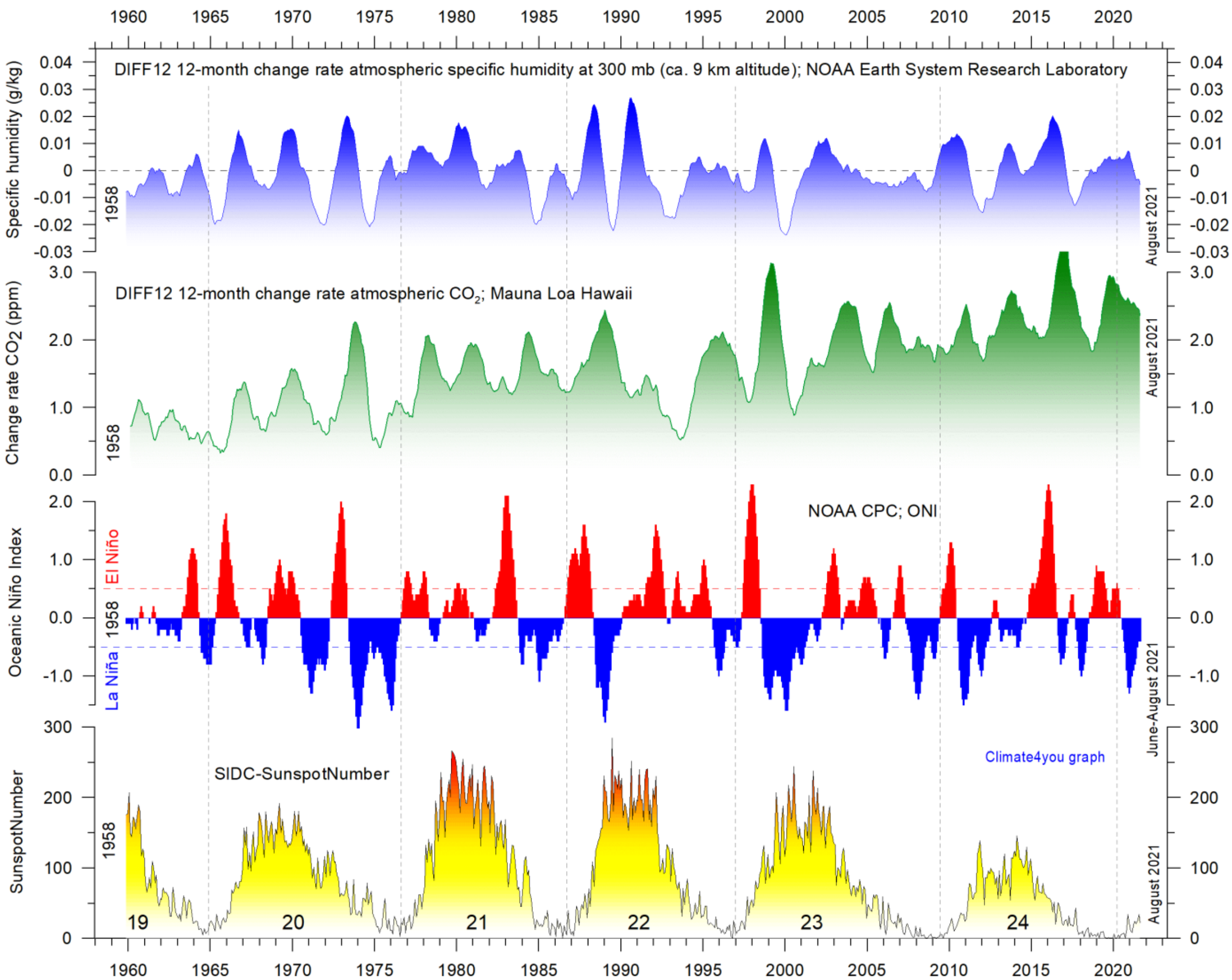

Visual association since 1958 between (from bottom to top) Sunspot Number, Oceanic Niño Index (ONI) and annual change rate of atmospheric CO2. and specific humidity at 300 mb (ca. 9 km altitude). Upper two panels: Annual (12 month) change rate of atmospheric CO2 and specific humidity at 300 mb since 1959, calculated as the average amount of atmospheric CO2/humidity during the last 12 months, minus the average for the preceding 12 months (see also diagrams on page 43+44). Niño index panel: Warm (>+0.5°C) and cold (<0.5°C) episodes for the Oceanic Niño Index (ONI), defined as 3 month running mean of ERSSTv4 SST anomalies in the Niño 3.4 region (5°N-5°S, 120°-170°W)]. For historical purposes cold and warm episodes are defined when the threshold is met for a minimum of 5 consecutive over-lapping seasons. Anomalies are centred on 30-yr base periods updated every 5 years. Thin vertical stippled lines indicate the visually estimated timing of sunspot minima. The typically sequence following a sunspot minimum appears to be a warm El Niño episode followed by a cold La Niña episode. Effects on change rates of atmospheric CO_2 and atmospheric specific humidity are visually apparent, with ONI variations being followed by changes in first humidity, and then (last) by CO_2.

The above diagram is inspired by the Leamon et al. 2021 publication: *Robert J. Leamon, Scott W. McIntosh, Daniel R. Marsh. Termination of Solar Cycles and Correlated Tropospheric Variability. Earth and Space Science, 2021; 8 (4) DOI: [10.1029/2020EA001223](10.1029/2020EA001223)*

Monthly lower troposphere temperature (UAH) and global cloud cover, updated to April 2021

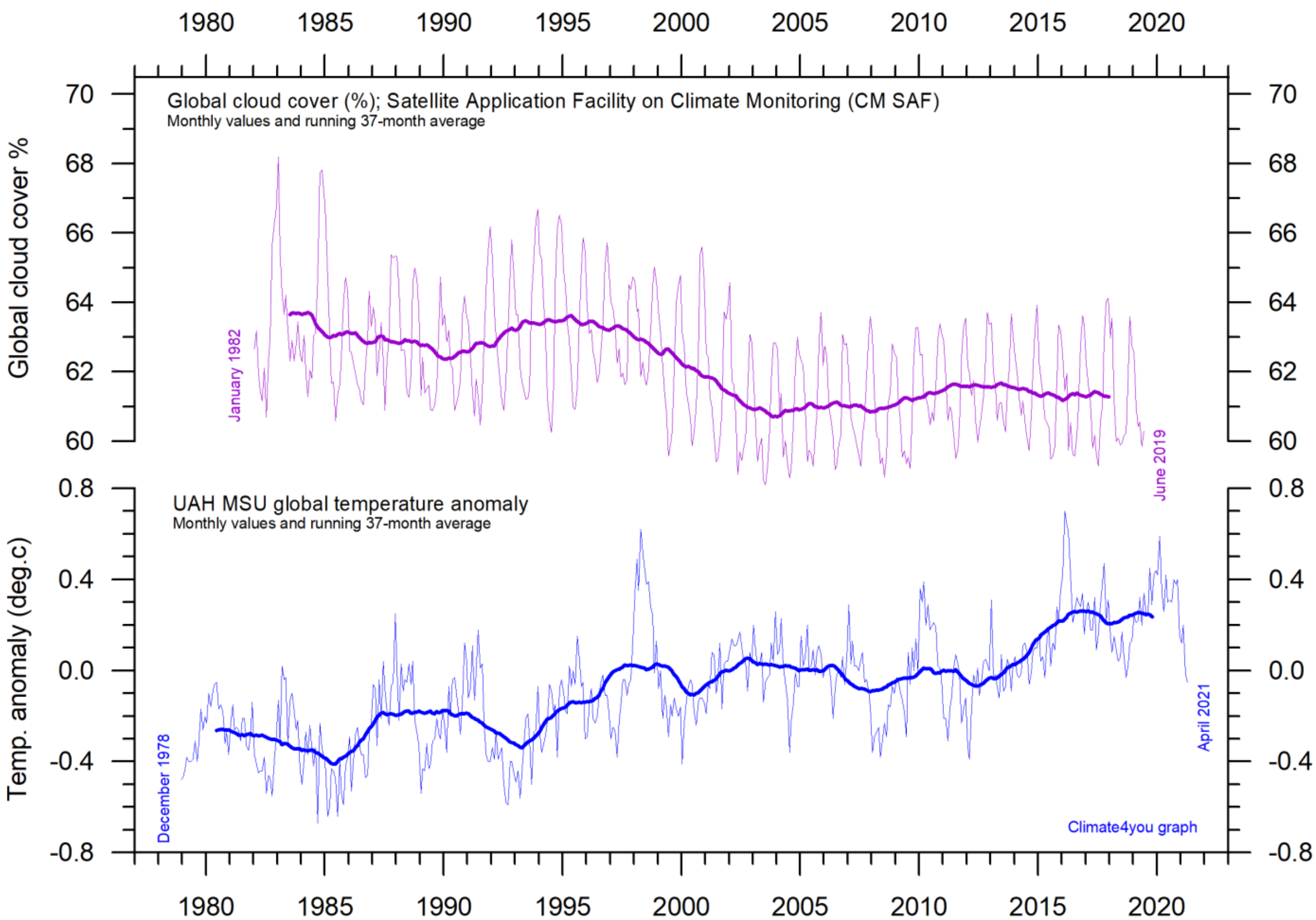

Lower tropospheric air temperature and global cloud cover. Upper panel: Global cloud cover according to Satellite Application Facility on Climate Monitoring. Lower panel: Global monthly average lower troposphere temperature (thin line) since 1979 according to [University of Alabama](#) at Huntsville, USA. The thick lines represent the simple running 37-month average. Reference period for UAH is 1991-2020.

Cloud cover data citation: Karlsson, Karl-Göran; Anttila, Kati; Trentmann, Jörg; Stengel, Martin; Solodovnik, Irina; Meirink, Jan Fokke; Devasthale, Abhay; Kothe, Steffen; Jääskeläinen, Emmihenna; Sedlar, Joseph; Benas, Nikos; van Zadelhoff, Gerd-Jan; Stein, Diana; Finkensieper, Stephan; Håkansson, Nina; Hollmann, Rainer; Kaiser, Johannes; Werscheck, Martin (2020): CLARA-A2.1: CM SAF cLoud, Albedo and surface RAdiation dataset from AVHRR data - Edition 2.1, Satellite Application Facility on Climate Monitoring, DOI:10.5676/EUM_SAF_CM/CLARA_AVHRR/V002_01, https://doi.org/10.5676/EUM_SAF_CM/CLARA_AVHRR/V002_01.

Climate and history; one example among many

1694: The Culbin Sands disaster in northeast Scotland

Scotland with location of Culbin Sands indicated by red arrow (left). Satellite picture and air photo showing Culbin Sands, today covered by forest (dark green, right). The rivers Nairn and Findhorn are seen to the left and right, respectively. The geometry of the coastal barriers (white due to lack of vegetation) shows the net coastal transport to be from NE towards SW (left). This suggests the river Findhorn to be the main sediment source for the sand now accumulated in the Culbin Sands. The picture covers 20 km from east to west. North is upward to the right, parallel to the border between the two types of pictures. Picture source: Google Earth.

Little more than 300 years ago there was a very fertile and well-cultivated estate on the southern shore of the Moray Firth in northeastern Scotland. It was known as the barony of Culbin. Amidst the various farms of which the property was composed, stood a well-built mansion in which the owner dwelt; and close by was an extensive orchard, rich in fruit-bearing trees. The Kinnaird family then in possession was distinguished among the gentry of the neighbourhood, and was connected, by blood or marriage, with some of the leading nobility of Scotland. Surrounded by flourishing tenants on smaller farms and rejoicing in a fair estate of many hundred acres, it seemed as if nothing could be more secure than the position which the family of Culbin was privileged to enjoy.

In many respects, this part of Scotland enjoys a mild and pleasant climate, sheltered as it is by mountains both to the west and to the south. The number of warm summer days with sun from a clear sky is relatively high due to this topographic setting, and during winter the nearby North Sea ensures that air temperatures seldom drop more than a few degrees below freezing. The mountains also protect against winter storms with westerly wind direction The area, however, has one climatic weakness: It has little protection against strong winds from N and

NW, wind directions often accompanying travelling weather systems (cyclones) on their backside. In combination with huge amounts of sand eroded from glacial deposits inland and being deposited on the coast west and east of the area by the rivers Nairn and Findhorn, this lack of protection against north-westerly winds was to be the background for the major storm disaster in 1694.

Culbin Sands near Kintessack, looking NW on June 2, 2008. The forest in the background delimits the southernmost part of of the sand dune field which extends 2-3 km inland from the coast. The houses in the middle ground are located on the small remnants of the fertile farming areas which barely escaped destruction during the 1694 storm.

The precise data of the 1694 storm is not known, but presumably it was late October or early November, as reports from the frigate S/S Packan at that time indicate a very severe storm with force 11 suggested. In addition, London reported an unbroken 10-day period of N and NW winds with frequent frost, snow and sleet leading up to the end of October 1694. Stavanger in Norway on 31 October reported snow and hail showers, while Copenhagen in Denmark had frost (Lamb 1991).

By the 1694 storm 16 fertile farms and farmland with a total area of 20-30 km^2 were overwhelmed by moving sand within the Culbin area. The whole area and the buildings were buried with depths of up to 30 m loose sand. Presumably this was not the first storm with problems derived from moving sand, and there has been discussions on the extent of the sand dunes before the disaster. There apparently was another severe episode of blowing sand in the Culbin area on 21 April 1663, and in the autumn of 1676 a NW storm buried the harvest on the westernmost Culbin farms with up to 50-60 cm of sand (Lamb 1991).

Before the 1694 disaster, Culbin was shown on a 17th century map as being on a peninsula between two bays (Edlin 1976). It was at that time a prosperous area, known as '*the Garden*', or alternatively '*the Granary*', of the county of Moray.

Reports of the disaster tell that it came during the barley harvest, which in the cool summers of the 1690s was probably late, most likely in late October. In upland parts of Scotland, the largely failed harvests of that decade (including 1694) were generally cut later than late October, but presumably in the fertile lowlands along the south shore of Moray Firth the overall situation was more favourable.

Edlin (1976) and Lamb (1991) cites the following accounts from the event: 'At first only fields were invaded by the sand. A ploughman had to leave his plough, while reapers left their stocks of barley. When the returned, both plough and barley were buried forever. The drift advanced upon the village, engulfing cottages, and the laird's mansion. The storm continued through the night, and the next morning some of the cottars had to break through the backs of their houses to get out. On the second day of the storm, the people freed their cattle and fled with their belongings to safer ground. Their flight (downwind, towards SE) was obstructed by the river Findhorn: since its mouth had been blocked by the drifting sand, its waters rose until it could force a new passage to the sea'. When this eventually happened, the water masses swept away the ancient town and harbour of Findhorn on the east bank of the river, shifting the river's month nearly 2 miles eastward to its present position (Chambers 1861). When the population of Culbin returned after the storm, no traces of their houses were to be seen.

Sand dunes near Wellhill, Culbin Sands, looking upwind (NW) on June 2, 2008. The sand dunes in the area are typically 5-25 m high, and extends 12 km parallel to the coast, and to a maximum distance of 3 km inland. The old fertile farmland and farms are still buried beneath the 28 km^2 sand cover.

Many stories, the product of naturally curious and superstitious minds, developed in the time following the disaster. How could such a disaster befall the once wealthy lands and families of Culbin? Women were accused of witchcraft and put to death by the Laird who, in turn, was accused of playing cards with the Devil with his estates at stake. To make things worse, this was reported to have taken place on a Sunday.

For over a hundred years the Culbin Sands remained a sand desert. The land was sold several times and divided into smaller estates. It was, however, not until 1839 that anything was successfully grown on it. Then, Grant of Kincorth, growing marram grass to stabilise the sand planted the first shelter belt to be successful. In 1842 Grigor of Forres, a tree nurseryman, planted 300 acres on Moy Estate. He introduced the technique of '*thatching*' to tree planting in Culbin, which turned out to be the key to the ultimate success of planting trees on sand dunes. Branches and tops of trees cut for thinning were laid on the ground, the tree seedlings being planted through the branches. These dead branches remained, holding the sand, protecting the small trees from wind slowing down the evaporation of moisture from the soil. Between 1922 and 1945 the estates constituting Culbin were acquired by the forestry Commission who, over a period of 32 years, planted over 9000 acres of trees. They stabilised the mobile sand by first planting marram grass whose plexus of spreading roots bound the sand. This was successful on the less hilly terrain but the thatching system, pioneered by Grigor in 1841, was found to be necessary for holding the larger sand dunes. Most of Culbin sands today is afforested.

Proximal (upwind) side of 10-15 m high sand dune in central Culbin Sands, looking E on June 2, 2008. The trees on top of the dune provide the scale.

During the 2nd World War, the extensive tidal flats north of Culbin Sands were considered a possible landing area for airplanes and gliders, should Germany attempt an invasion of the British Isles. To prevent this, many wooden poles were dug into the tidal flats. Many of these poles can still be seen. Later in the war, a large part of Culbin and adjacent coastal areas were commandeered by the British Army for manoeuvres in preparation for the D-Day landings. 'Lost' shells and rockets have been found during planting and in 1986 a wrecked aircraft was discovered, having lain undisturbed for 40 years within the dune field.

1966 the Nature Conservancy Council (forerunner of Scottish Natural Heritage) designated the Culbin area a Site of Special Scientific Interest. It also now forms part of a Ramsar site, a Special Protection Area. This unique region is now frequently visited and studied by geologists, botanists and zoologists and other interested parties from around the world.

Lamb (1991) carried out an analysis of the likely meteorological situation leading to the storm destroying the Culbin area, citing, among others, Willis (1986). It is concluded that the fatal 1694 storm winds indeed were blowing from the NW, exposing pre-existing coastal sand dunes to the full force of the wind. At low tide, also the extensive sandy tidal flats (see satellite picture above) beyond the coast would have been exposed to wind erosion, generating additional amounts of wind-blown sand. Finally, excessive plucking of the marram grass on the coastal dunes may have contributed to exposing their surface for wind erosion. That this may have been a contributing factor is indicated by an Act of the Scottish parliament in 1695 (the year after the disaster) forbidding the pulling of marram grass for thatching. However, Lamb (1991) concludes that the winds associated with the 1694 NW storm must have been exceptionally strong, and presumably lasted for about 30 hours without interruption. Gust wind speeds during the storm are estimated to have reached 50-65 m/s, while the mean wind speed may have been around 25-30 m/s.

Edlin (1976) concluded that the new landscape produced by the 1694 storm, today known as the Culbin Sands, probably represents one of the greatest wind-borne deposits formed anywhere in Britain in recent geological time.

Lamb (1991) further draws attention to the fact that this was the time during the Little Ice Age, where the polar pack ice expanded farthest south into the North Atlantic, surrounding Iceland completely by the end of the year. Although the polar waters had long extended further south than what has been normal during the 20th century, the reported swift advance of the polar ice-pack limit between October and December 1694 must have required continual northerly strong winds over much of the North Atlantic north of Iceland. The Culbin Sands may thus be perceived as the geomorphological result of a climatic situation with the oceanic Polar Front taking a very southerly position, in the vicinity of northern Scotland.

References

Chambers, N. 1861. *Domestic Annals of Scotland*, vol. iii., pp. 119-120.

Edlin, H.L. 1976. *The Culbin Sands*. In Environment and Man, vol.4, Reclamation (Edited by J. Leniham and W.W. Fletcher), Glasgow and Edinburgh, pp. 1-13.

Lamb, H.H. 1991. *Historical Storms of the North Sea, British Isles and Northwest Europe*. Cambridge University Press, Cambridge, 204 pp.

Willis, D.P. 1986. *Sand and silence - lost villages of the North (Forvie, Rattray, Culbin and Skara Brae*). Aberdeen University Centre for Scottish Studies, Aberdeen.

*****

All diagrams in this report, along with any supplementary information, including links to data sources and previous issues of this newsletter, are freely available for download on www.climate4you.com

Yours sincerely,

Ole Humlum (Ole.Humlum@gmail.com)

Arctic Historical Evaluation and Research Organisation, Longyearbyen, Svalbard

18 September 2021.